CHAPTER SIX

SIMULATION RESULTS

6.1 CHAPTER OVERVIEW

THIS chapter commences with extensive investigations into the operation of the complex flat and multipath fading channel simulator structures, proposed in *Section* 2.6.2.3 and *Section* 2.6.3.2, respectively. Numerous simulation results verify accurate functioning of the complex channel simulators. Included are detailed time and frequency domain analyses of the output signals generated by these complex channel simulators. Studies into the statistical behaviours of the proposed simulators are also given.

Next, *Chapter* 6 focusses on the narrowband complex QPSK and wideband complex DSSS/MA QPSK communication systems, presented in *Section* 5.2 and *Section* 5.3, respectively. The functioning of these narrowband and wideband communication systems are scrutinised in perfect and fading channel conditions. A multitude of time signals, measured at crucial system interfaces, are presented and extensively analysed. The frequency characteristics of the output signals generated by the narrowband and wideband communication systems' transmitter structures are also investigated.

Chapter 5 presented multi-functional AWGN (see *Section* 5.4.1), flat fading (see *Section* 5.4.2) and multipath fading (see *Section* 5.4.3) simulation platforms, built around the narrowband complex QPSK and wideband complex DSSS/MA QPSK communication systems (described in *Section* 5.2 and *Section* 5.3, respectively), as well as the novel complex flat and multipath fading channel simulators (proposed in *Section* 2.6.2.3 and *Section* 2.6.3.2, respectively). These simulation platforms were used to obtain the large number of simulated AWGN, flat fading and multipath fading channel BER performance results, presented in the remainder of *Chapter* 6. Simulated BER performance results are given for uncoded narrowband and wideband systems, as well as communication systems employing various VA decoded convolutional and linear block coding schemes. Convolutional codes considered include binary 4-state, rate $R_c = 1/2$ NSC codes (see *Section* 3.2.1.3.1), binary 8-state, rate $R_c = 2/3$ RSC codes (see *Section* 3.2.1.3.2) and punctured (see *Section* 3.2.4) binary 4-state, rate $R_c = 1/2$ RSC codes. VA decoded binary linear block codes (see *Chapter* 4) investigated include Hamming $(7, 4, 3)$ codes (see *Section* 3.2.2.3.1), cyclic $(5, 3, 2)$ linear block codes (see *Section* 3.2.2.2), interleaved (see *Section* 3.2.3) Hamming $(7, 4, 3)$ codes and punctured BCH $(15, 7, 5)$ codes (see *Section* 3.2.2.3.2). In the case of the binary cyclic $(5, 3, 2)$ block code, VA decoding using original and reduced BCJR trellis structures are compared. The only VA decoded non-binary linear block

code considered in this study, with and without interleaving, is the RS $(7, 5, 3)$ code (see *Section* 3.2.2.3.3). BER performance improvements observed due to the inclusion of fading amplitude CSI during the VA decoding of the convolutional and linear block codes investigated in this study, receive special attention.

The simulation platforms of *Chapter* 5, as well as the VA decoded convolutional and block coding schemes considered in this study, were developed in a C++ environment using an OOP approach. A large number of Matlab scripts and functions, primarily responsible for the creation and evaluation of filters, pulse shapes, power delay profiles, interleavers and block code generator matrices, were also developed. The BER performance results presented in this chapter were obtained through command-line driven executable applications, compiled using *Intel*'s *ICC* and *GNU is Not Unix*'s (GNU) *G++* compilers for *Linux* platforms. In order to minimise simulation execution times, theses applications' computational load were distributed over multiple workstations in the *University of Pretoria*'s *I-percube*, donated by *Intel*. The *I-percube* is an HPC cluster, which consists of seventeen 2.4 GHz *Pentium* 4 stations, each station running a *Mandrake Linux Operating System* (OS). *Fast Ethernet* connections are used to interconnect the seventeen drone stations in the HPC cluster. *Open Mosix* for *Linux* is responsible for transparent process migration and message handling between the stations. *Appendix E* supplies an index of the simulation software scripts, function, classes and compiled applications developed during this study. Upon request, a *Compact Disc Read Only Memory* (CD-ROM) containing the simulation software modules listed in *Appendix E* can be obtained from the author.

6.2 VALIDATION OF THE COMPLEX MOBILE CHANNEL SIMULATOR MODELS

The following subsections present simulation results obtained during the testing and validation of the novel complex flat and multipath fading channel simulators, presented in *Section* 2.6.2.3 and *Section* 2.6.3.2, respectively.

6.2.1 COMPLEX FLAT FADING CHANNEL SIMULATOR

In order to verify the correctness of its operation, three simulation tests were performed on the complex implementation of *Clarke*'s flat fading channel simulator, shown in *Fig.* 2.5. These tests include the measurement of output signals' envelope PDFs, phase PDFs and Doppler spectra for the different channel configurations, stated in *Table* 5.3. All simulation results were obtained using the complex exponential simulator input signal $u_i(t) = \exp(j.2\pi.f_c.t)$, with the carrier frequency chosen as $f_c = 2$ kHz.

6.2.1.1 MEASURED ENVELOPE PROBABILITY DENSITY FUNCTION RESULTS

Fig. 6.1 shows measured envelope PDFs, obtained using the complex flat fading channel simulator, configured for Rician factors of $K_i = -100$ dB, $K_i = 0$ dB and $K_i = 6$ dB. These simulation results were acquired by calculating the PDFs of the fading amplitude experienced by the simulator output signal $b_i(t)$, for each of the different Rician factor scenarios. The fading amplitude information was extracted directly from the complex flat fading channel simulator using *Eq.* (2.56). Although it is of no real consequence, it can be noted that the channel simulator was configured for a maximum Doppler spread of $B_{D,i} = 100$ Hz during the execution of these tests.

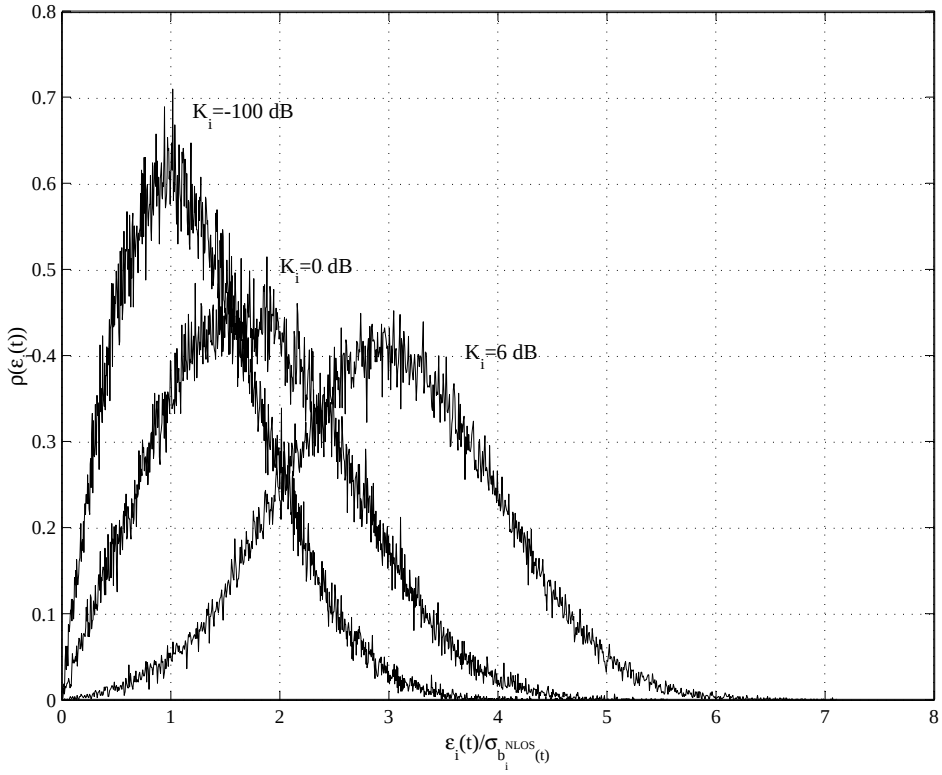

Figure 6.1: Measured Complex Flat Fading Channel Simulator Output Signal Envelope PDF Results for Rician Factors of $K_i = -100$ dB, $K_i = 0$ dB and $K_i = 6$ dB

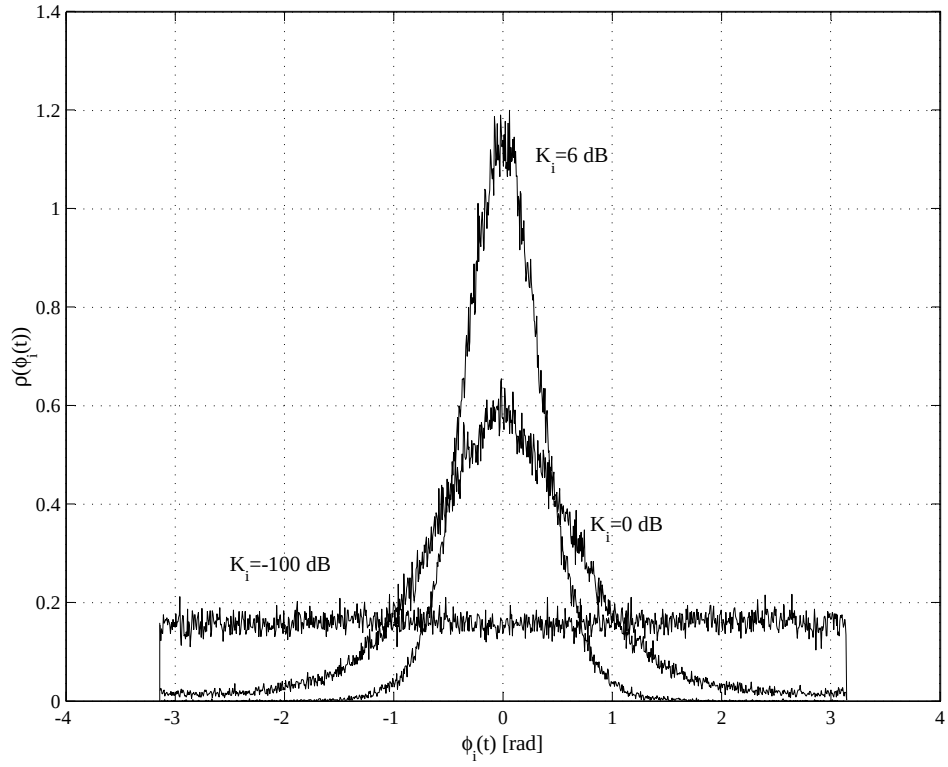

Figure 6.2: Measured Complex Flat Fading Channel Simulator Output Signal Phase PDF Results for Rician Factors of $K_i = -\infty$ dB (Rayleigh), $K_i = 0$ dB (Rician) and $K_i = 6$ dB ($\approx$ Gaussian)

6.2.1.2 MEASURED PHASE PROBABILITY DENSITY FUNCTION RESULTS

With the complex flat fading channel simulator once again configured for a maximum Doppler spread of $B_{D,i} = 100$ Hz and Rician factors of $K_i = -100$ dB, $K_i = 0$ dB and $K_i = 6$ dB, the measured phase PDFs shown in *Fig.* 6.2 were obtained as follows: Firstly, the instantaneous phase variation $\phi_i(t)$ experienced by the simulator output signal $b_i(t)$ was extracted directly from the complex flat fading channel simulator, using *Eq.* (2.57). The results shown in *Fig.* 6.2 were then obtained by calculating the PDF of the output signal's phase variations for the different Rician factors.

6.2.1.3 MEASURED DOPPLER SPECTRA RESULTS

In order to determine whether the novel complex flat fading channel simulator produces valid Doppler spectral characteristics, the simulator output signal's PSD was measured for $B_{D,i} = 33$ Hz, $B_{D,i} = 67$ Hz and $B_{D,i} = 100$ Hz. During these simulation tests, a Rician factor of $K_i = -100$ dB was chosen, i.e. almost no LOS signal component was present in the simulator output signal $b_i(t)$. *Fig.* 6.3 shows the measured output signal PSD results obtained for the above mentioned channel configuration parameters.

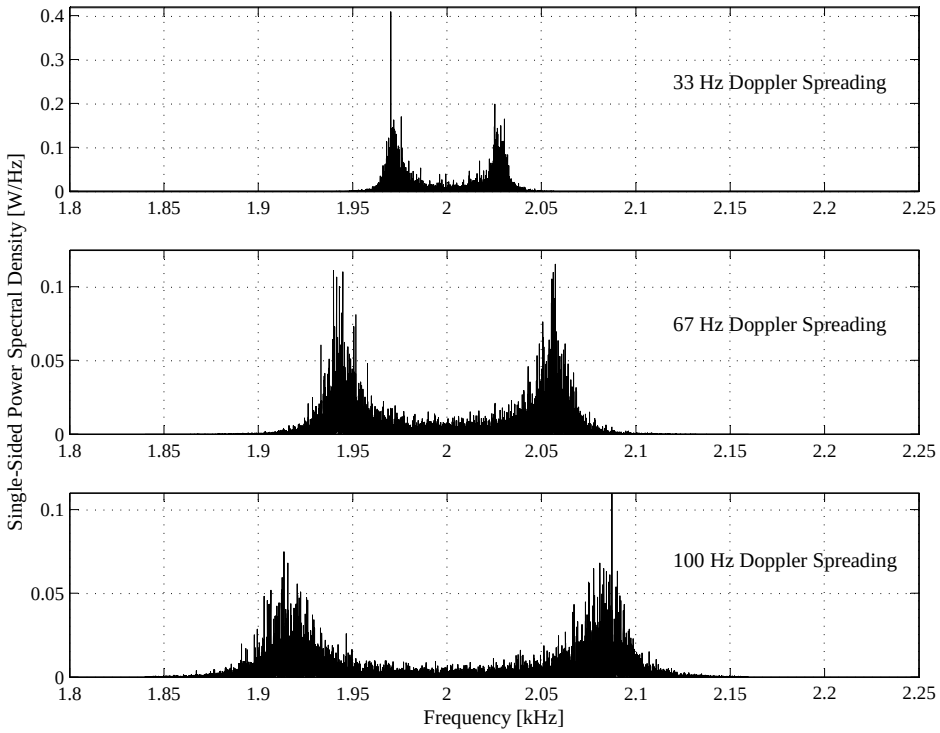

Figure 6.3: Measured Complex Flat Fading Channel Simulator Output Signal PSD Results for Maximum Doppler Spreads of $B_{D,i} = 33$ Hz, $B_{D,i} = 67$ Hz and $B_{D,i} = 100$ Hz

6.2.1.4 DISCUSSION OF THE SIMULATION RESULTS

From the measured complex flat fading channel simulator results presented in the preceding three subsections, the following conclusions can be made:

- By comparing *Fig.* 2.2 and *Fig.* 6.1, it is clear that the novel complex flat fading channel simulator is capable of producing Rayleigh and Rician fading envelope PDFs that closely match the mathematical models, discussed in *Section* 2.5.2.

- The theoretical flat fading channel phase distributions shown in *Fig.* 2.3 and the measured complex flat fading channel simulator output signal phase PDFs shown in *Fig.* 6.2 are comparable. Thus, the simulator is also capable of creating realistic flat fading channel phase distortions.
- Although the Doppler spectra presented in *Fig.* 6.3 do not match the theoretical PSD shown in *Fig.* 2.1 to a tee, it is close enough to ensure that the simulator output signal's fading envelope and phase exhibit acceptable temporal characteristics. Using higher order IIR Doppler filters will deliver improved results, but at the cost of higher channel simulator complexity.

6.2.2 COMPLEX MULTIPATH FADING CHANNEL SIMULATOR

Temporal and spectral simulation results, substantiating the satisfactory operation of the novel complex multipath fading channel simulator, presented in *Fig.* 2.8 of *Section* 2.6.3.2, is presented in the following subsection. These results were obtained using a complex exponential simulator input signal $s(t) = \exp(j.2\pi.f_c.t)$, with a carrier frequency of $f_c = 126$ kHz. Furthermore, the simulation tests were performed on a complex multipath fading channel simulator configured according to user-1's channel parameters, as given by *Table* 5.5.

6.2.2.1 MEASURED PATH DELAYS AND POWER SPECTRAL DENSITIES

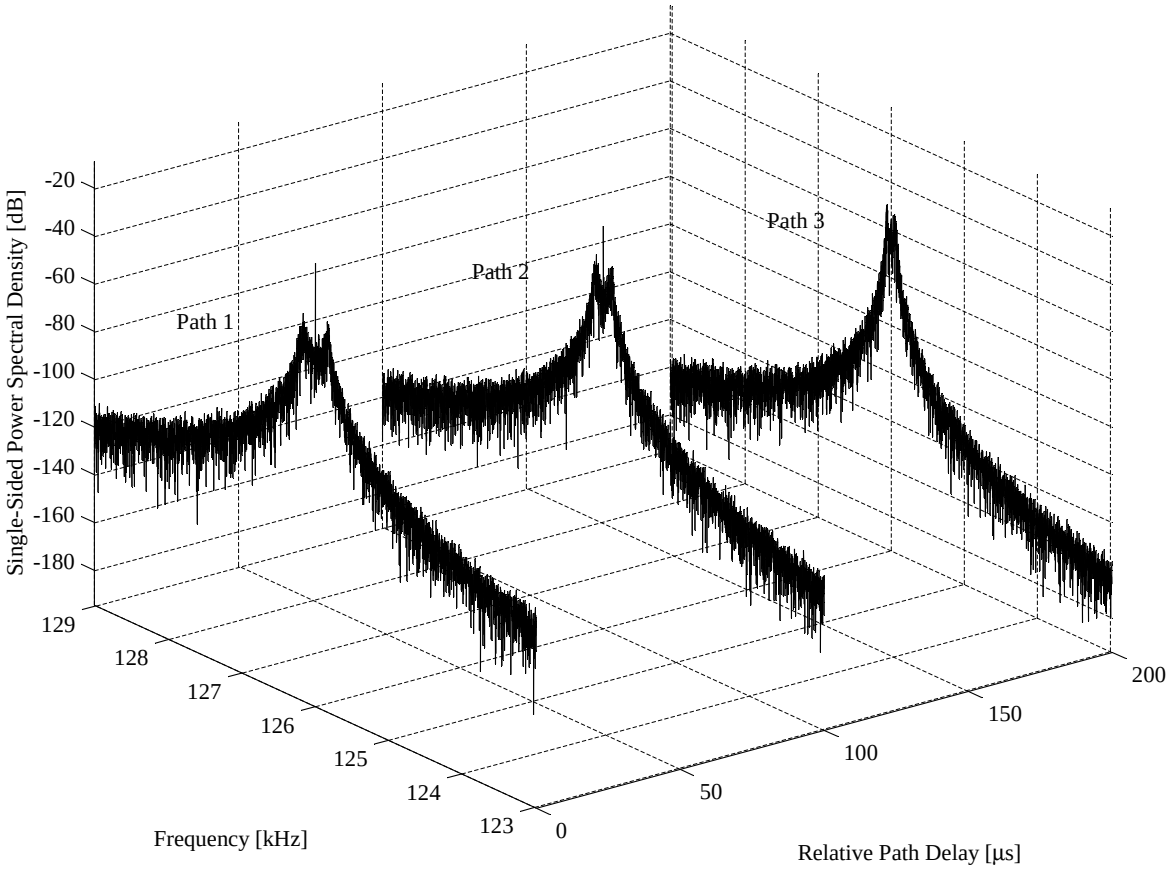

Figure 6.4: Measured Path Delays and PSDs Created by User-1's Complex Multipath Fading Channel Simulator

Each of the three flat faded paths, created by the complex multipath fading channel simulator for the complex input signal $s(t)$, were observed for a large number of samples. From the time signals

obtained for each path, relative path delays and PSDs were determined. *Fig.* 6.4 summarises these findings.

6.2.2.2 DISCUSSION OF THE SIMULATION RESULTS

From *Fig.* 6.4 it is clear that the first, second and third paths exhibit maximum Doppler spreads of 100 Hz, 67 Hz and 33 Hz, respectively. The PSDs of the first and second paths also show different, but noticeable LOS signal components, i.e. carrier components at 126 kHz. Thus, these paths are predominantly Rician distributed. The third path, however, experiences Rayleigh flat fading, since no LOS component is present. In summary, the following conclusions can be drawn from *Fig.* 6.4:

- The novel complex multipath fading channel simulator is capable of generating a variable number of statistically independent flat faded paths. Each path can be configured with its own maximum Doppler spread and Rician factor.
- The relative path delays and average path powers can be configured to exhibit realistic power delay profiles. In this study, exponential decay power delay profiles (see *Section* 2.6.3.3) were employed.
- Only fixed relative path delays are supported by the complex multipath fading channel simulator. Thus, the channel simulator can only mimic time invariant, or wide sense stationary multipath channels (see *Section* 2.4.1).

6.3 EVALUATION OF THE NARROWBAND COMPLEX QPSK COMMUNICATION SYSTEM

The general operation of the narrowband complex QPSK communication system (described in *Section* 5.2), used during the BER performance evaluation tests performed in AWGN and flat fading channel conditions, is evaluated in the following subsections. The complex QPSK transmitter and receiver structures were configured according to *Table* 5.1 and *Table* 5.2, respectively. Furthermore, no AWGN was included during the tests presented in the following subsections.

6.3.1 MEASURED TIME SIGNALS

Several I-channel and Q-channel narrowband complex QPSK receiver (see *Section* 5.2.2) time signals, including the matched filter and averaged fading amplitude outputs, were measured in noiseless, flat fading channel conditions in order to ensure the receiver's error-free operation. A complex flat fading channel simulator (see *Section* 2.6.2.3) configuration, consisting of a 9 dB Rician factor and 33 Hz Doppler spread, were chosen for these tests. Time signals measured in the receiver, together with the transmitter's original I-channel and Q-channel input symbol streams (prior to square-root Nyquist pulse shaping), are shown in *Fig.* 6.5. Note that the same symbols are present on the I-channel and Q-channel, since the system was configured for balanced operation.

From this figure, it is clear that there is a time lag of approximately 10 symbols between the transmitter's symbol streams (prior to pulse shaping) and the receiver's demodulated streams. This is the result of the time delays induced by the pulse shaping filters, elliptic receive filters (see *Fig.* 5.7) and matched filters. Note that this delay can be reduced by employing asymmetrically matched square-root Nyquist pulse shaping filtered in the transmitter and receiver [44]. Even with this time delay, which is compensated for during the BER performance measurements, the receiver functions satisfactorily (i.e. without any bit errors). Furthermore, it is clear that the average fading amplitude calculation, accomplished by implementing *Eq.* (5.13) in the receiver, was also successful, since it tracks the average changes in the symbol amplitudes perfectly.

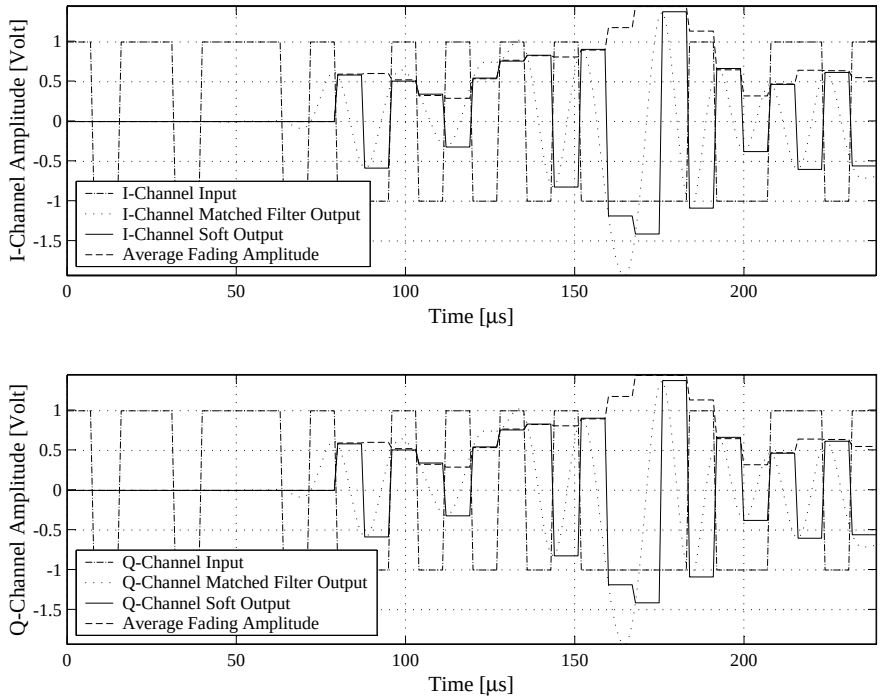

Figure 6.5: Measured Narrowband Complex QPSK Receiver's I-Channel and Q-Channel Time Signals

6.3.2 MEASURED EYE DIAGRAMS

Ensuring the correct operation of the I-channel and Q-channel square-root Nyquist pulse shaping filters (see *Eq.* (5.48)), employed in the narrowband complex QPSK transmitter (see *Section* 5.2.1), entailed obtaining the eye diagrams of their outputs. *Fig.* 6.6 shows that the eyes created by the transmitter's pulse shaping filters are not open, which was to be expected for square-root Nyquist pulse shaping.

Similar eye diagram results were obtained for the I-channel and Q-channel matched filter outputs in the narrowband complex QPSK receiver, which are shown in *Fig.* 6.7. From inspection it is clear that the receiver's eye diagrams are completely open at the appropriate sampling instances. This was to be expected, since the square-root Nyquist pulse shaping in the transmitter and matched filtering in the receiver combine to give overall Nyquist filtering with open eye diagrams [44]. Note that a noiseless channel, without any fading effects, were used to obtain these results.

6.3.3 MEASURED POWER SPECTRAL DENSITIES

PSDs were calculated for several of the critical time signals present in the narrowband complex QPSK communication system. These included PSDs for the transmitter's I-channel and Q-channel symbol streams, before and after square-root Nyquist pulse shaping, as well as PSDs for the outputs of the I-channel and Q-channel AWGN limiting elliptic receive filters. A perfect channel, without any AWGN or flat fading effects, was used to obtain these PSDs. From these results, depicted in *Fig.* 6.8, it is clear the square-root Nyquist pulse shaping limited the transmitter's effective output signal bandwidth from 1000 Hz to 750 Hz, as predicted by *Eq.* (5.49). Furthermore, the PSDs for the outputs of the I-channel and Q-channel elliptic receive filters show significant reductions in the frequency components above 750 Hz, without causing major distortions in the amplitude spectra of the information carrying frequency band from 0 Hz to 750 Hz.

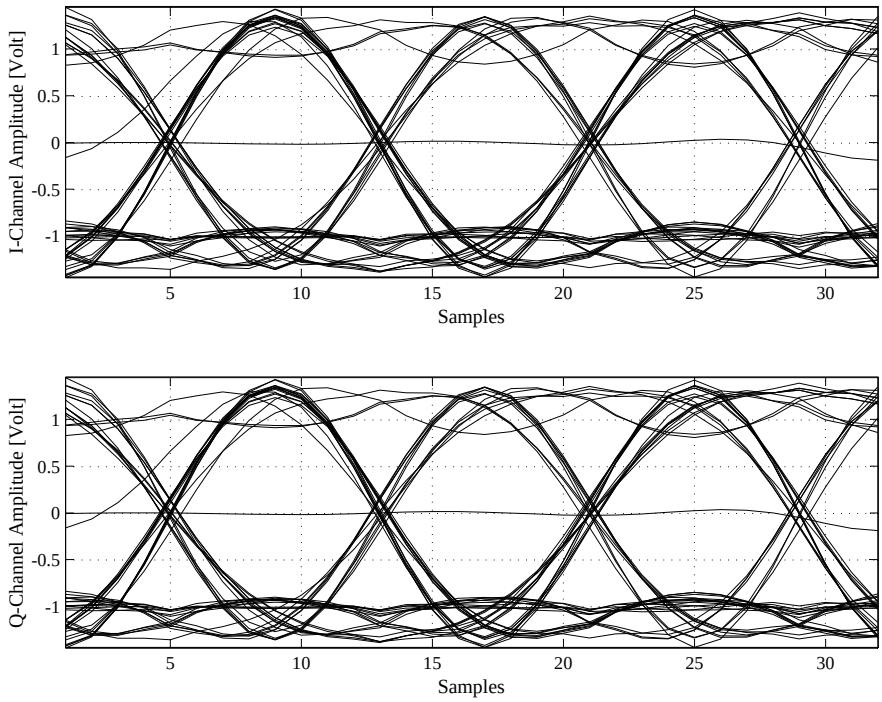

Figure 6.6: Measured Eye Diagrams of the Narrowband Complex QPSK Transmitter's I-Channel and Q-Channel Pulse Shaping Filter Outputs

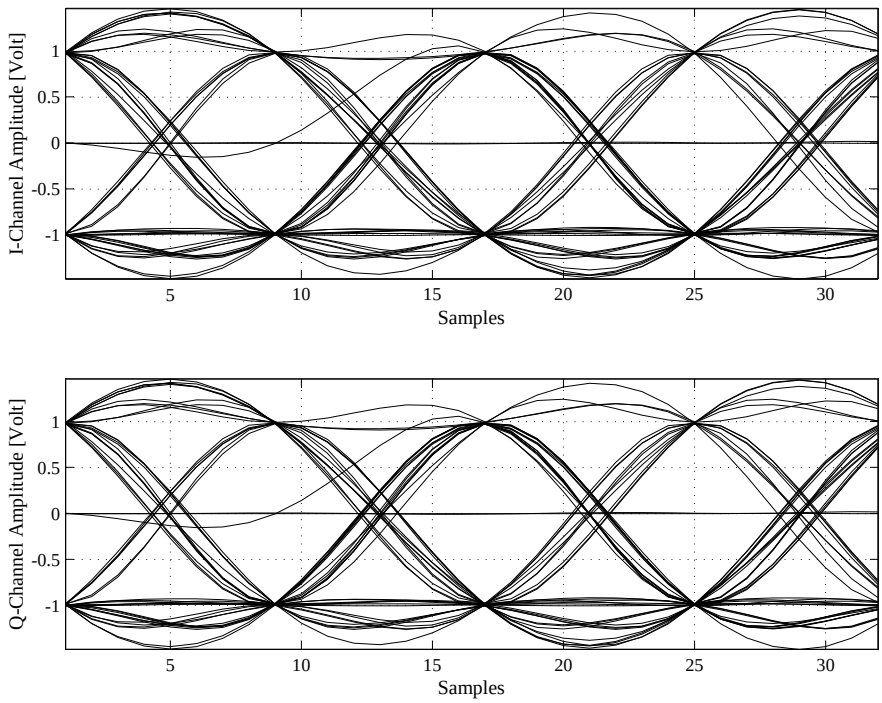

Figure 6.7: Measured Eye Diagrams of the Narrowband Complex QPSK Receiver's I-Channel and Q-Channel Matched Filter Outputs

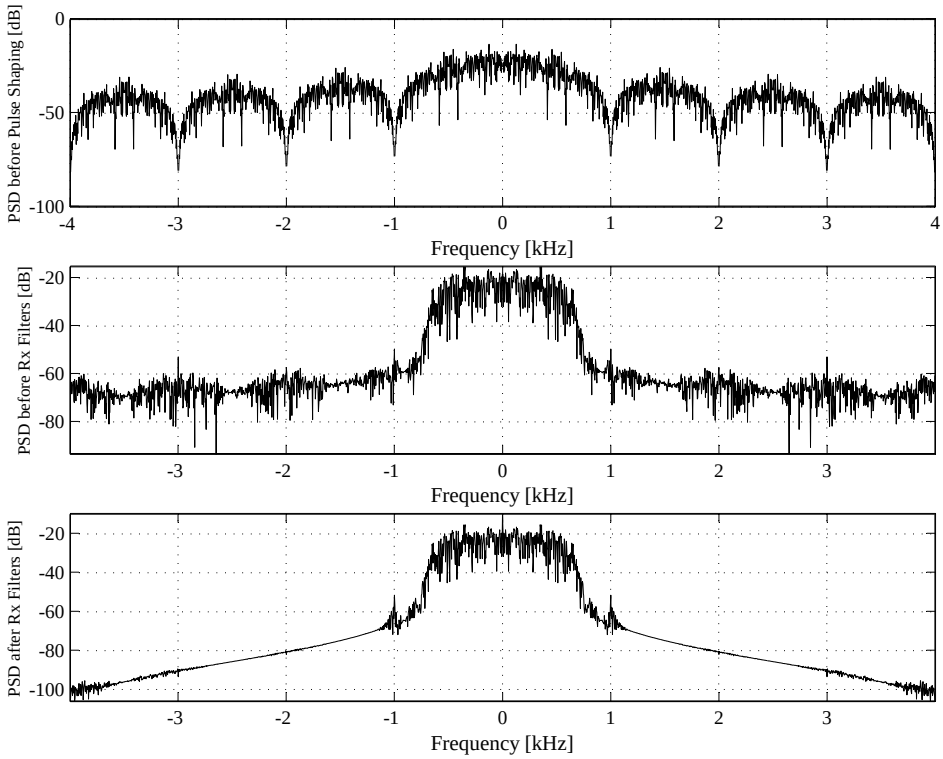

Figure 6.8: Measured PSDs of the Narrowband Complex QPSK Communication System

6.3.4 DISCUSSION OF THE SIMULATION RESULTS

From the eye diagram, time signal and PSD simulation results presented in the preceding subsections, the following observations can be made:

- The square-root Nyquist pulse shaping employed in the narrowband complex QPSK transmitter, effectively reduces the required transmission bandwidth by 25%.
- Applying square-root Nyquist matched filtering in the narrowband complex QPSK receiver, results in open eye diagrams under perfect channel conditions, i.e. no ISI is present in the demodulated signals.
- Initial limiting of the AWGN entering the narrowband complex QPSK receiver is successfully accomplished by the 6^{th} order elliptic lowpass receive filters, present on the I-channel and Q-channel branches (see *Fig.* 5.2). By splitting the Nyquist filtering function between the transmitter and receiver, additional AWGN suppression is achieved.
- The average fading amplitude calculation method proposed in *Section* 5.2.3 proved to be successful. Thus, perfect fading amplitude CSI information can be extracted from the complex flat fading channel simulator for use in the VA (see *Section* 4.4.2.2).

6.4 EVALUATION OF THE RAKE RECEIVER-BASED COMPLEX DS/SSMA QPSK COMMUNICATION SYSTEM

In the following subsections the general operation of the complex RAKE receiver-based DS/SSMA QPSK communication system, described in *Section* 5.3, is evaluated. Recall from *Section* 5.4.3 that

this communication system forms the basis of the simulation platform employed during the BER performance evaluation tests performed in multipath fading channel conditions. The results presented in the following subsections were obtained in noiseless channel conditions, with a single wideband transmitter (see *Fig.* 5.3.1), configured according to *Table* 5.4, and RAKE receiver (see *Fig.* 5.3.2), configured according to *Table* 5.7. Furthermore, the results presented here were obtained using length-63 CSSs.

6.4.1 MEASURED TIME SIGNALS

Time signals were measured at critical points in the complex DS/SSMA QPSK communication system, functioning in noiseless multipath fading channel conditions. This was done to ensure the overall error-free operation of the complex RAKE receiver-based DS/SSMA QPSK system's modulator, demodulator and average fading amplitude estimator (see *Section* 5.3.3). ABC sequences (see *Section* D.3.2.2) and ZC CSSs (see *Section* D.3.1.1) were adequate selections to prove the operation of these building blocks for filtered and unfiltered CSS families, respectively. The complex multipath fading channel simulator (see *Fig.* 2.8 in *Section* 2.6.3.2) employed, were configured according to user-1's channel parameters in *Table* 5.5. *Fig.* 6.9 depicts the measured time signals obtained for the complex

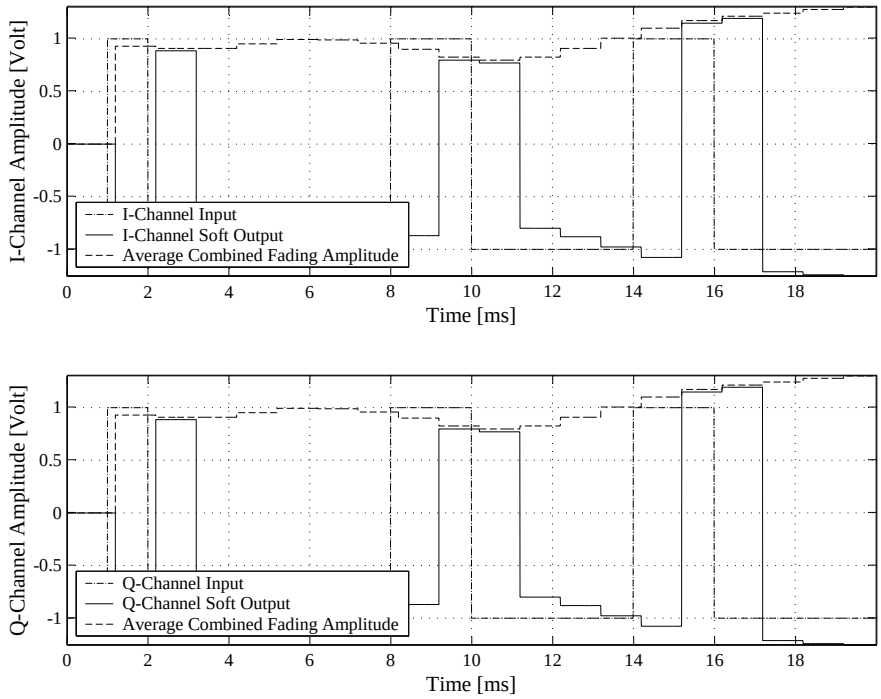

Figure 6.9: Measured I-Channel and Q-Channel Time Signals for a Wideband Complex DS/SSMA QPSK Communication System Employing ABC Sequences (with Rectangular Pulse Shaping) in Noiseless Multipath Fading Channel Conditions

DS/SSMA QPSK communication system using ABC sequences, without any additional chip-level pulse shaping, other than the default rectangular pulse shaping. Similar results are shown in *Fig.* 6.10 for a system employing ZC CSSs with square-root Nyquist pulse shaping (see *Eq.* (5.48)) in the transmitter and matched filtering in the RAKE receiver.

From *Fig.* 6.9 and *Fig.* 6.10 the following observations can be made: Firstly, the same symbols are transmitted on the I-channel and Q-channel, since the system is configured for balanced operation. Secondly, note the minor time delays between the transmitted symbols and demodulated symbols.

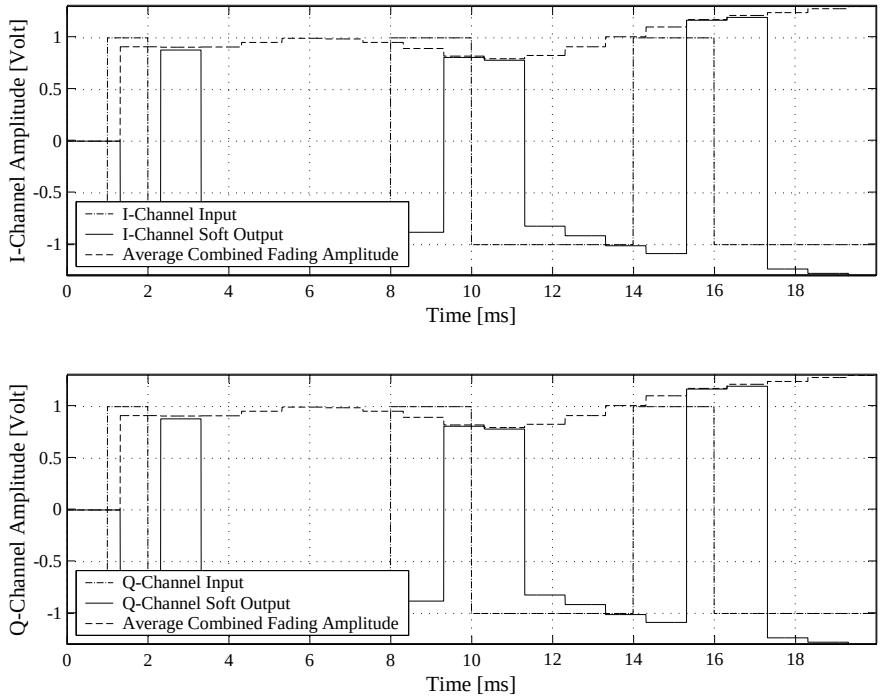

Figure 6.10: Measured I-Channel and Q-Channel Time Signals for a Wideband Complex DS/SSMA QPSK Communication System Employing ZC CSSs (with Square-Root Nyquist Pulse Shaping) in Noiseless Multipath Fading Channel Conditions

This delay is approximately 216 μs ($\tau_{max} = 200\mu$s maximum excess delay (see *Eq.* (2.13)), plus 16 μs rectangular pulse shaping and matched filtering delay) for the system employing ABC sequences and 320 μs ($\tau_{max} = 200\mu$s maximum excess delay, plus 120 μs square-root Nyquist pulse shaping and matched filtering delay) for the system employing ZC CSSs.

6.4.2 MEASURED EYE DIAGRAMS

Shown in *Fig.* 6.11 are the measured eye diagrams of the I-channel and Q-channel pulse shaping filter outputs of a complex DS/SSMA QPSK transmitter, employing QPH CSSs with chip-level square-root Nyquist pulse shaping. The motivation behind using QPH CSSs during the validation of the operation of the wideband complex transmitter's square-root Nyquist pulse shaping filters, are two-fold: Firstly, recall from *Table* 5.4 that no additional pulse shaping is employed for the ABC sequences and DSB CE-LI-RU filtered GCL CSSs (see *Section* D.3.2.1). Secondly, QPH CSSs are chosen over ZC CSSs, due to the fact that these CSSs' chips take on only bipolar amplitude levels on the I-channel and Q-channel branches prior to square-root Nyquist pulse shaping. Conversely, ZC CSSs exhibit a multitude of chip amplitudes (see *Section* D.3.1 in *Appendix D*), resulting in intricate eye diagrams.

As was to be expected, the eyes in *Fig.* 6.11 are not completely open. However, applying square-root Nyquist matched filtering on the I-channel and Q-channel branches in the complex DS/SSMA QPSK RAKE receiver, not only limits the AWGN and MUI entering the receiver, but also thoroughly opens the eyes. *Fig.* 6.12 shows such I-channel and Q-channel matched filter output eye diagrams for a complex RAKE receiver-based DS/SSMA QPSK system employing QPH CSSs (see *Section* D.3.1.2). Note that these eye diagram results were obtained in perfect noiseless channel conditions with no multipath fading effects.

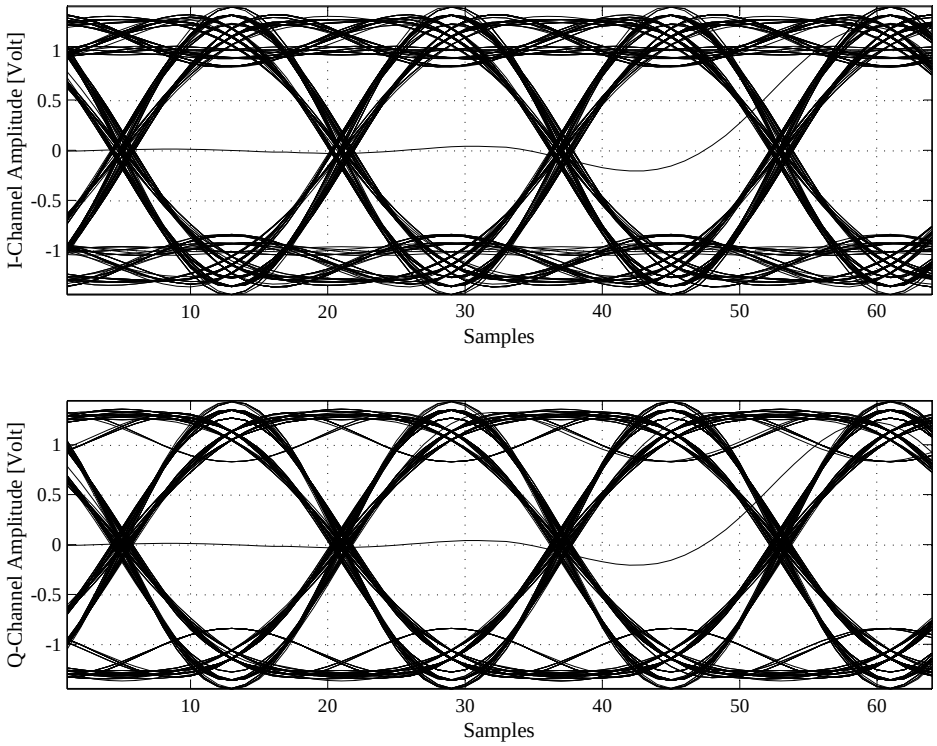

Figure 6.11: Measured Eye Diagrams of the QPH CSS-Based Wideband Complex DS/SSMA QPSK Transmitter's I-Channel and Q-Channel Pulse Shaping Filter Outputs

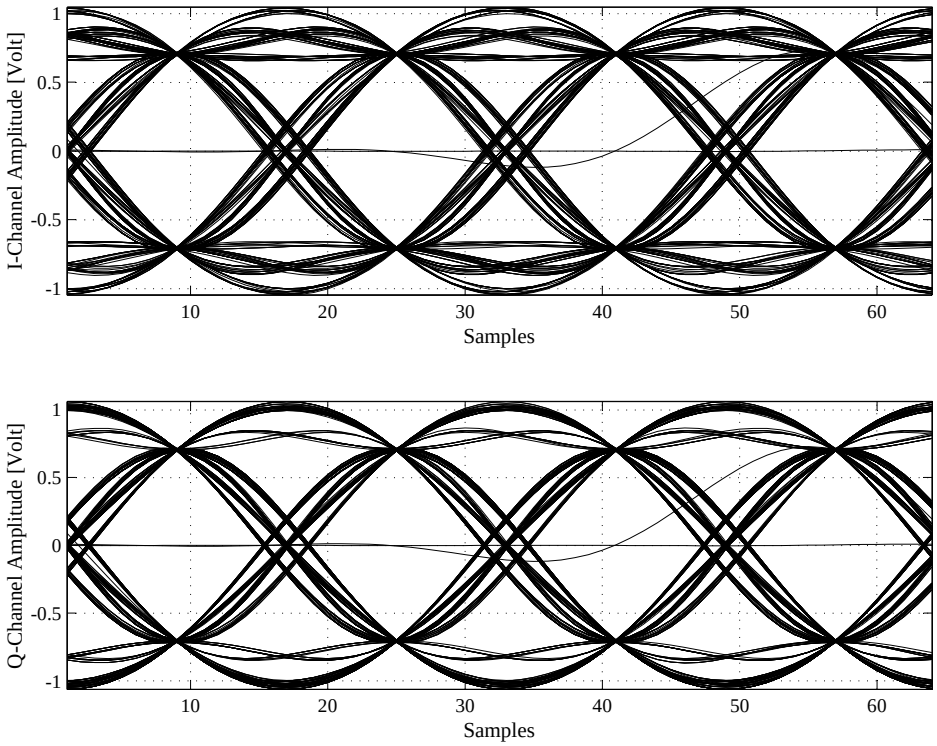

Figure 6.12: Measured Eye Diagrams of the QPH CSS-Based Wideband Complex DS/SSMA QPSK RAKE Receiver's I-Channel and Q-Channel Matched Filter Outputs

6.4.3 MEASURED POWER SPECTRAL DENSITIES

A multitude of PSDs were calculated for RAKE receiver-based complex DS/SSMA QPSK communication systems, employing the filtered and unfiltered CSS families presented in *Appendix D*. The PSDs were computed for transmitter output signals (before and after pulse shaping), as well as elliptic receive filter output signals. Perfect noiseless channel conditions, with no multipath fading effects, were used to obtain the PSD results presented here for DS/SSMA systems using length $M_{seq} = 63$ CSSs.

Fig. 6.13 shows the PSD results obtained for a system employing unfiltered ZC CSSs. Note that the first zero in the spectrum occurs at 63000 kHz, as was to be expected. After square-root Nyquist filtering, the transmission bandwidth required is reduced to approximately $B_{sig} = 47250$ kHz, as was predicted by *Eq.* (5.50). Lastly, the PSD of the output of the 6^{th} order elliptic receive filter (bottom PSD in *Fig.* 6.13) clearly shows a considerable suppression of out-of-band signal components.

Results similar to that of *Fig.* 6.13 are shown in *Fig.* 6.14 for a system employing QPH CSSs. Once again, square-root Nyquist pulse shaping has limited the required transmission bandwidth to approximately $B_{sig} = 47250$ kHz. Furthermore, 6^{th} order elliptic receive filtering suppressed unwanted signal components entering the RAKE receiver outside this band.

The measured PSDs of the first filtered CSS family considered, showed in *Fig.* 6.15, are those of DSB CE-LI-RU filtered GCL sequences. Recall that no additional pulse shaping is employed for these sequences, since built-in filtering occurs during their generation (see *Section* D.3.2.1). Furthermore, from *Fig.* 6.15 it is clear that, when this filtered CSS family is employed in a complex DS/SSMA QPSK system (configured for balanced operation), transmitter output PSD characteristics consistent with Nyquist's minimum (roll-off factor $\varsigma = 0$) bandwidth criteria, as was claimed in *Section* D.3.2.1, are obtained. Thus, the required transmission bandwidth is approximately $B_{sig} = 31500$ Hz, as was predicted by *Eq.* (5.51). According to the bottom figure in *Fig.* 6.15, the elliptic receive filters once again limited the out-of-band noise entering the RAKE receiver.

Finally, the PSDs of a complex DS/SSMA QPSK system, employing ABC sequences in a balanced configuration, fall under the spotlight in *Fig.* 6.16. Note that the application of this CSS family in such a transmitter configuration, results in SSB transmitter output PSDs. For the wideband system presented in this study, upper sideband SSB transmitter output signals are generated. Furthermore, the upper sideband appears in correspondence with Nyquist's minimum (roll-off factor $\varsigma = 0$) bandwidth criteria. Thus, as predicted by *Eq.* (5.52), the required transmission bandwidth is approximately $B_{sig} = 15750$ Hz. Wideband noise (AWGN or MUI) entering the RAKE receiver will be sufficiently bandlimited by the elliptic receive filters, as can be seen from the bottom PSD in *Fig.* 6.16.

6.4.4 DISCUSSION OF THE SIMULATION RESULTS

Some insights into the operation of the complex RAKE receiver-based DS/SSMA QPSK communication system presented in this study, gained from the eye diagram, time signal and PSD simulation results discussed in the preceding subsections, are as follows:

- The transmission bandwidth of complex DS/SSMA QPSK transmitters, employing unfiltered ZC and QPH CSSs, were reduced by 25% by employing square-root Nyquist pulse shaping. Furthermore, the square-root Nyquist matched filtering, applied in the complex DS/SSMA RAKE receivers for these CSS families, delivered open eye diagrams under perfect channel conditions.

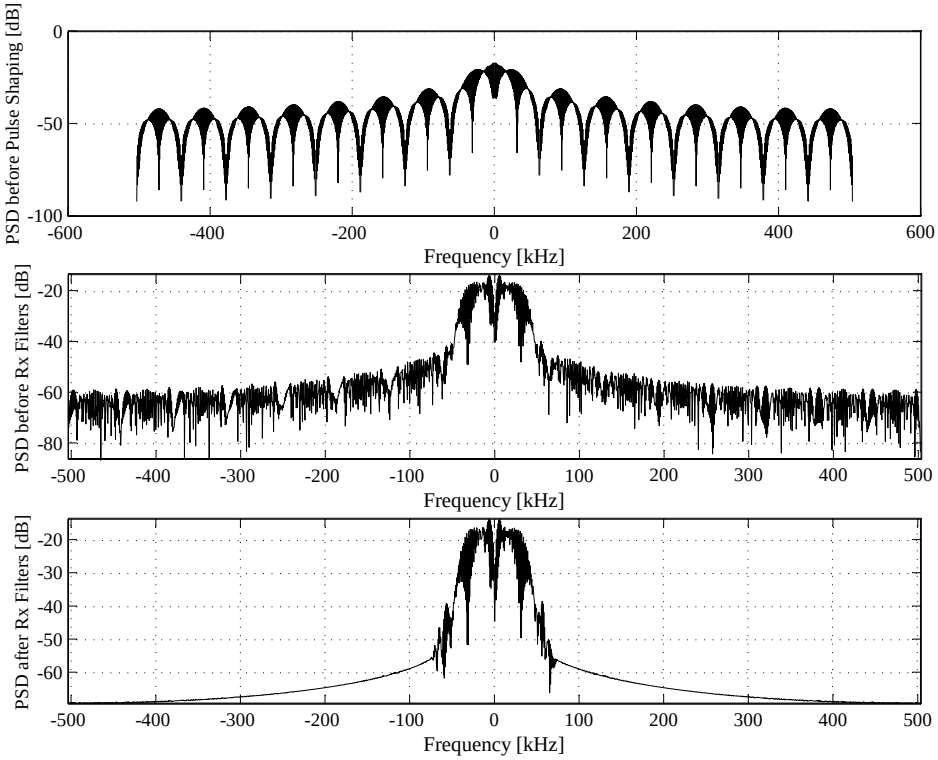

Figure 6.13: Measured PSDs of a Wideband Complex DS/SSMA QPSK Communication System Employing Length-63 ZC CSSs

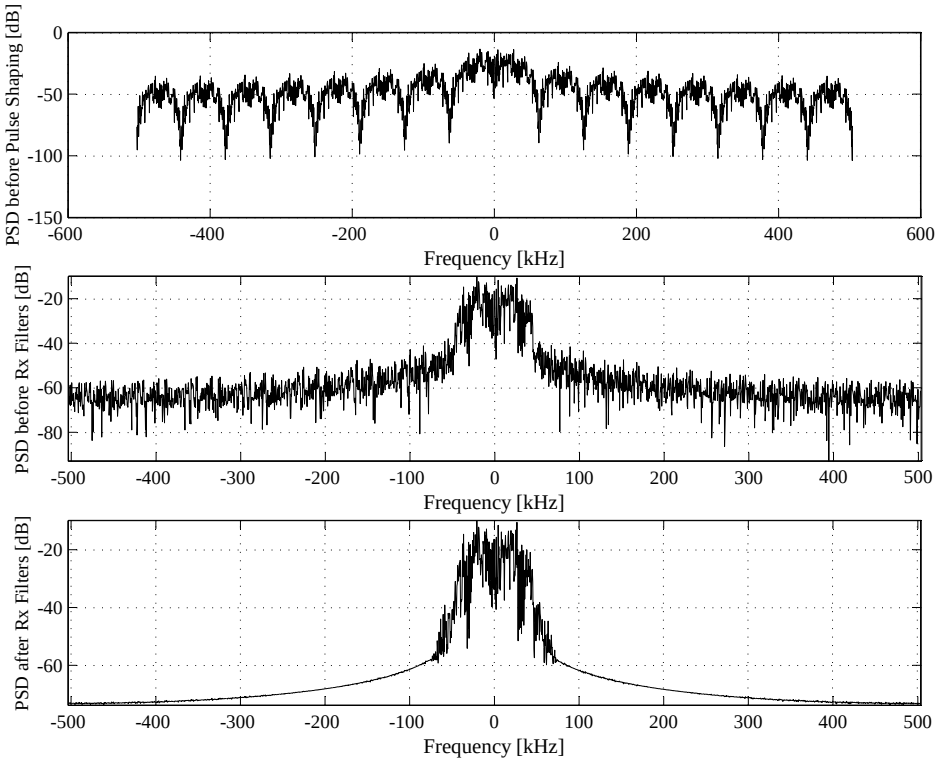

Figure 6.14: Measured PSDs of a Wideband Complex DS/SSMA QPSK Communication System Employing Length-63 QPH CSSs

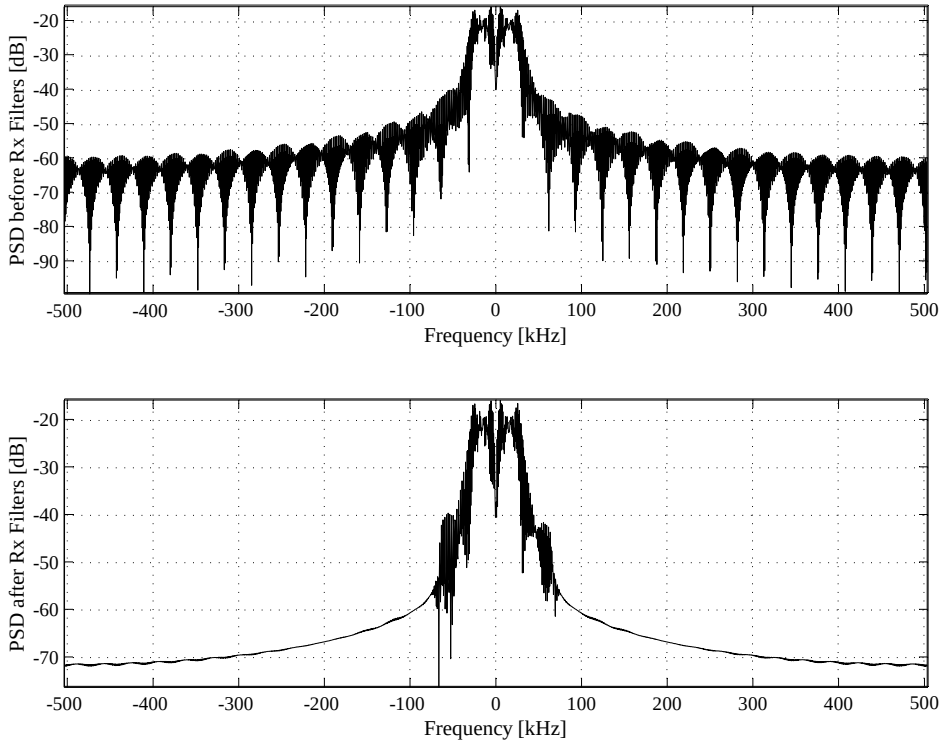

Figure 6.15: Measured PSDs of a Wideband Complex DS/SSMA QPSK Communication System Employing Length-63 DSB CE-LI-RU filtered GCL CSSs

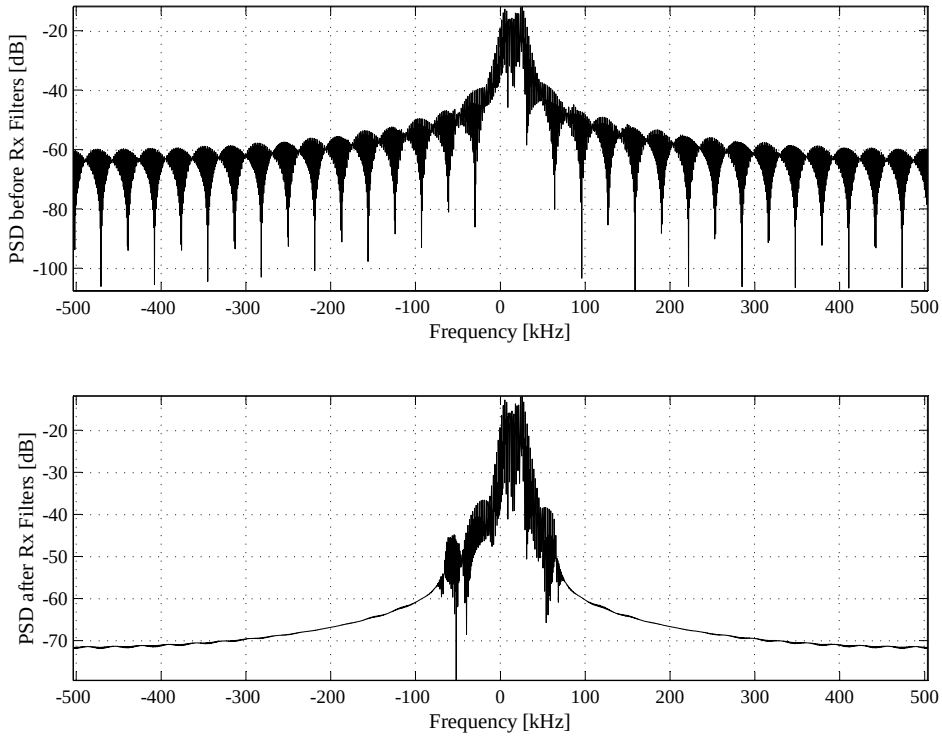

Figure 6.16: Measured PSDs of a Wideband Complex DS/SSMA QPSK Communication System Employing Length-63 ABC Sequences

- By employing filtered CSSs, even greater improvements were made on the required transmission bandwidth: DSB CE-LI-RU filtered GCL sequences require 66.67% of the transmission bandwidth that the unfiltered CSSs (with chip-level square-root Nyquist pulse shaping) require. Moreover, by generating SSB wideband transmitter output signals, ABC sequences further reduce this bandwidth requirement to only 33.33%.

- Primary limiting of AWGN and MUI entering the wideband complex DS/SSMA QPSK RAKE receiver is effectively accomplished by the 6^{th} order elliptic lowpass filters, present on both the I-channel and Q-channel branches (see *Fig.* 5.4). Further noise and interference suppression is performed by the matched filtering, which attempts to maximise the SNR.

- From *Fig.* 6.9 and *Fig.* 6.10 it is clear that the average fading amplitude calculation scheme for complex DS/SSMA QPSK RAKE receivers, proposed in *Section* 5.3.3, is successful for systems employing filtered or unfiltered CSSs. Thus, perfect fading amplitude CSI information can be extracted, from a complex multipath fading channel simulator, for use in the VA (see *Section* 4.4.2.2).

- The PSDs of the QPH CSSs, shown in *Fig.* 6.13, exhibit classic *sinc*-like profiles, since these sequences are generated using multiple, unique binary sequences (see *Section* D.3.1.2). However, the GCL CSSs [9] considered, i.e. ZC, ABC and DSB CE-LI-RU filtered GCL CSSs, appear to possess relatively flat PSDs in their respective transmission bandwidths. This can be attributed to their chirp-like natures (see *Section* D.3).

- Recall from *Table* 5.4 that the symbol rate of the complex DS/SSMA QPSK transmitters, employing length $M_{seq} = 63$ CSSs, are 1000 Hz prior to spreading. Hence, using *Eq.* (D.4) and *Eq.* (D.5) from *Section* D.2.4, it follows that $SF = 63$ and $PG = 17.99$ dB for all of the CSS families considered. Thus, in the presence of narrowband interferers or jamming signals, length-63 CSSs will be able to improve the SNR (or signal-to-inference ratio, to be precise) of the wideband communication system by at least 17.99 dB. Since ABC sequences only occupy half of the transmission bandwidth required by the other CSSs considered, it can be argued that DS/SSMA communication systems employing these sequences will only be affected by jamming signals, attacking half of the effective transmission bandwidth required by the non-SSB CSSs. Hence, it can be postulated that ABC sequences will exhibit superior narrowband interference suppression, when compared to the other CSSs families. In this study, however, SS was investigated purely as a MA mechanism, and not as a narrowband interference suppression approach. As such, in this study the *Processing Gain* (PG) is not of such great importance, but rather the periodic auto-correlation (see *Section* D.2.2) and cross-correlation (see *Section* D.2.3) characteristics of the CSSs employed, since these characteristics govern the BER performance of a DS/SSMA system due to the presence of MUI.

- An inspection of the PSDs presented in *Fig.* 6.13 to *Fig.* 6.16 reveals that, when compared to DS/SSMA systems using binary spreading sequences or unfiltered CSSs, wideband systems employing either square-root Nyquist chip-level pulse shaping or the filtered CSS families described in *Appendix D*, require less transmission bandwidth. This is most apparent for the ABC and DSB CE-LI-RU filtered GCL CSSs. Thus, for a fixed data rate, using square-root Nyquist pulse shaping, or CE-LI-RU filtering, in conjunction with CSSs, it is possible to employ longer sequences without conceding PG or exceeding the transmission bandwidth requirements of an equivalent DS/SSMA system using, for example, unfiltered binary Gold spreading sequences. This sequence length increase (and resultant user capacity increase) can be modelled as an equivalent *Spreading Sequence Length Diversity* (SSLD), a novel concept which is introduced in *Section* D.2.6. Using the calculated bandwidth results, given by *Eq.* (5.50) to *Eq.* (5.52), for an unspreaded bit rate of 1000 b/s and CSS length of $M_{seq} = 63$, the *Bandwidth Expansion Factor*s (BEF) (see *Section* D.2.5) and SSLDs given in *Table* 6.1 were calculated for wideband complex DS/SSMA systems employing the CSS families presented in *Appendix D*. Also given in this table, are the BEFs and SSLDs for

DS/SSMA systems employing unfiltered binary Gold sequences, unfiltered ZC CSSs and unfiltered QPH CSSs. According to *Table* 6.1, in order to occupy a 126 kHz transmission bandwidth, it is

Table 6.1: Comparison of the BEFs and SSLDs for Different Filtered and Unfiltered Spreading Sequence Families with $f_{bit} = 1000$ b/s, $M_{seq} = 63$ chips and $f_{chip} = 63000$ Hz.

Spreading Sequence Family	**BEF**	**SSLD**
Unfiltered Binary Gold Sequences	63	1
Unfiltered ZC CSSs	63	1
Unfiltered QPH CSSs	63	1
Square-Root Nyquist (Roll-off Factor $\varsigma = 0.5$) Filtered ZC CSSs	47.25	1.333
Square-Root Nyquist (Roll-off Factor $\varsigma = 0.5$) Filtered QPH CSSs	47.25	1.333
DSB CE-LI-RU filtered GCL CSSs	31.5	2
ABC Sequences	15.75	4

possible to use ABC sequences with four times the length (for example length $M_{seq} = 251$) of unfiltered binary Gold sequences, thereby producing a 6 dB improvement in PG, better periodic correlation characteristics (i.e. lowered RAKE self-noise and MUI levels), but most importantly, a higher CDMA user capacity. To illustrate this statement, consider an arbitrary size-$M_{fam}^{filtered}$ family of filtered length-$M_{seq}^{filtered}$ GCL-like CSSs (such as ABC or DSB CE-LI-RU filtered GCL CSSs). If $M_{seq}^{filtered}$ is a prime number, $M_{fam}^{filtered}$ is calculated as follows (derived from *Eq.* (D.9)):

$$\begin{aligned} M_{fam}^{filtered} &= M_{seq}^{filtered} - 1 \\ &\approx SSLD.M_{seq}^{unfiltered} - 1 \\ &\approx SSLD.\left(M_{fam}^{unfiltered} + 1\right) - 1 \end{aligned} \tag{6.1}$$

In this equation $M_{seq}^{unfiltered}$ and $M_{fam}^{unfiltered}$ respectively denote the CSS length (also a prime number) and family size of an unfiltered CSS family, requiring the same transmission bandwidth as the filtered CSS family. For example, a DS/SSMA system using unfiltered length $M_{seq} = 61$ ZC CSSs will require approximately the same transmission bandwidth as a system using length $M_{seq} = 241$ ABC sequences. However, the ZC sequence-based system supports only 60 users, whereas the ABC sequence-based system supports approximately $243 = 4.(60 + 1) - 1$ users (to be precise, it supports up to 240 users). Although the remainder of this study presents BER performances for coded wideband RAKE receiver-based complex DS/SSMA systems using only length $M_{seq} = 63$ CSSs, the influence of sequence length on MUI in uncoded wideband complex DS/SSMA systems, employing ABC sequences, is briefly investigated in *Section* 6.5.1.3.3.

6.5 BIT-ERROR-RATE PERFORMANCE EVALUATION RESULTS

The following subsections present the BER performances results obtained for several different coding schemes under AWGN, flat fading and multipath fading channel conditions. These coding schemes include uncoded systems, NSC codes (see *Section* 3.2.1.3.1), RSC codes (see *Section* 3.2.1.3.2), binary cyclic block codes (VA decoded using original and reduced trellis structures (see *Section* 4.3.2)), binary Hamming block codes (see *Section* 3.2.2.3.1) (with classic ML and VA decoding), binary BCH block codes (see *Section* 3.2.2.3.2) with VA decoding, as well as non-binary RS block codes (see *Section* 3.2.2.3.3) with *Berlekamp-Massey* (see *Appendix B*) and VA decoding. The influence of

puncturing (see *Section* 3.2.4) and interleaving (see *Section* 3.2.3) are also investigated for several of these coding schemes.

Simple narrowband complex QPSK (see *Section* 5.2) transmitters (configured according to *Table* 5.1) and receivers (configured according to *Table* 5.2) were employed in the AWGN and flat fading BER performance evaluation platforms, shown in *Fig.* 5.5 (see *Section* 5.4.1) and *Fig.* 5.8 (see *Section* 5.4.2), respectively. *Table* 5.3 summarises the different channel configurations considered during the flat fading channel BER performance tests.

Multipath fading BER performance test results were obtained using the simulation platform portrayed in *Fig.* 5.9 (see *Section* 5.4.3). *Table* 5.4 and *Table* 5.7 detail the respective complex DS/SSMA QPSK transmitter (see *Section* 5.3.1) and RAKE receiver (see *Section* 5.3.2) configurations employed by each of the users in the CDMA system. Up to 10 users were supported in these performance evaluation tests in order to investigate the effects of MUI. *Table* 5.5 and *Table* 5.6 contain the individual complex multipath fading channel simulator (see *Section* 2.6.3.2) configurations, associated with each of the 10 possible CDMA users. Results presented here not only contrast the BER performances obtained using different CSS families, but also the influence of CSS length and sequence selection approach for ABC sequence-based CDMA system.

6.5.1 UNCODED COMMUNICATION SYSTEMS

In the following two subsections simulated and theoretical BER performance results are presented for uncoded narrowband complex QPSK communication systems (see *Section* 5.2), functioning in AWGN (see *Section* 2.2) and flat fading (see *Section* 2.5.1.1) channel conditions. Thereafter, simulated BER performance results are presented for uncoded wideband complex DS/SSMA QPSK systems (see *Section* 5.3), employing the filtered and unfiltered CSSs of *Appendix D*, in multi-user frequency selective fading (see *Section* 2.5.1.1) channel conditions. The results given here will be used as baseline references for the simulated BER performance results of the coded systems, presented in the remainder of this chapter.

6.5.1.1 AWGN CHANNEL RESULTS

Fig. 6.17 shows the simulated BER performance of an uncoded complex QPSK communication system (see *Section* 5.2) in an AWGN environment (see *Section* 2.2). The theoretical curve, defined by *Eq.* (5.20), is also present on this figure.

6.5.1.2 FLAT FADING CHANNEL RESULTS

The simulated BER performance results for uncoded complex QPSK systems (see *Section* 5.2), operating in flat fading channel conditions with maximum Doppler spreads (see *Section* 2.4.3.3) of $B_{D,i} = 33$ Hz and $B_{D,i} = 100$ Hz, are shown in *Fig.* 6.18 and *Fig.* 6.19, respectively. The simulated results shown here include BER curves for Rician factors (see *Section* 2.5.2.2) of $K_i = -100$ dB (i.e. fading amplitudes with near-Rayleigh PDFs), $K_i = 0$ dB and $K_i = 9$ dB. Also depicted on these figures are the uncoded system's AWGN BER performance curve, as well as the theoretical BER performance curve for slow Rayleigh flat fading channel conditions, given by *Eq.* (5.24).

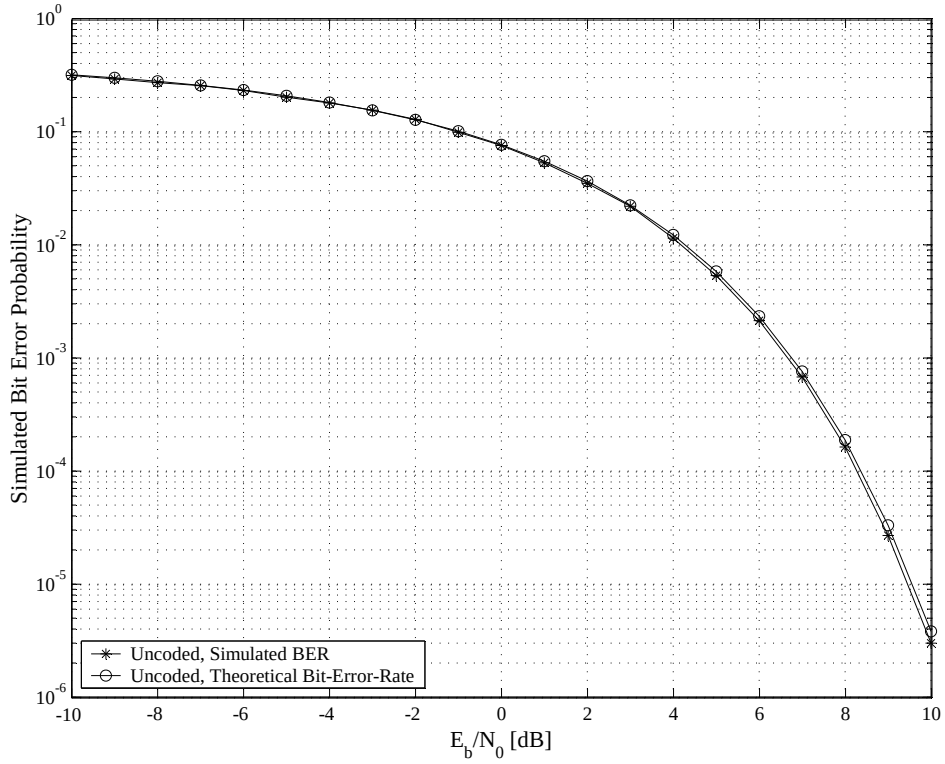

Figure 6.17: BER Performances of an Uncoded Narrowband Complex QPSK Communication System in AWGN Channel Conditions

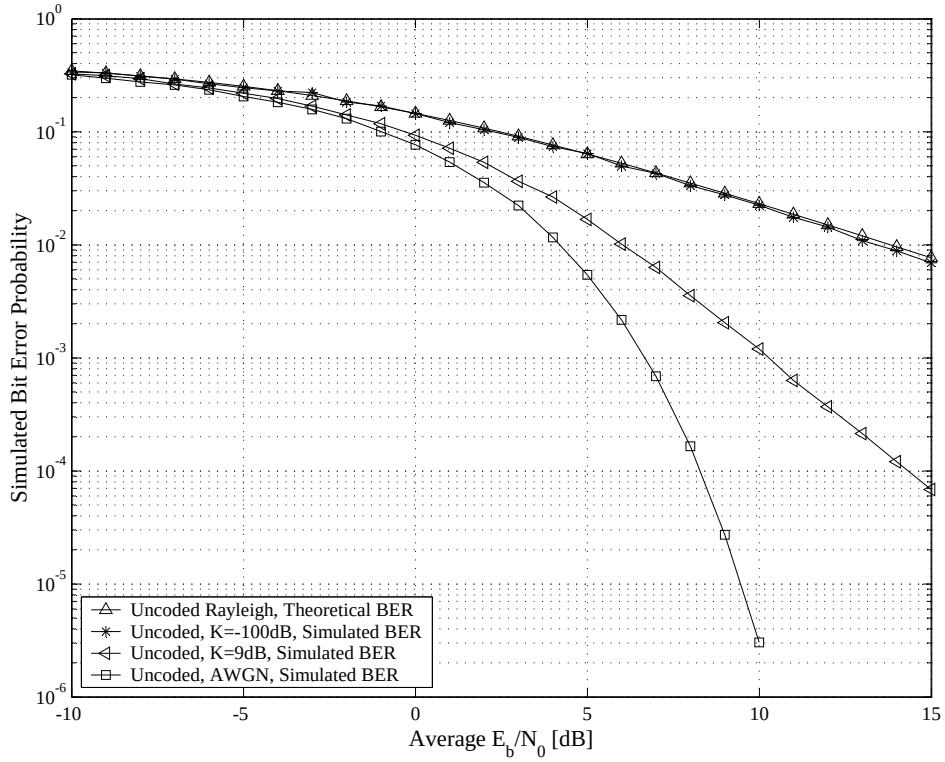

Figure 6.18: BER Performances of an Uncoded Narrowband Complex QPSK Communication System in Flat Fading Channel Conditions, $B_{D,i} = 33$ Hz

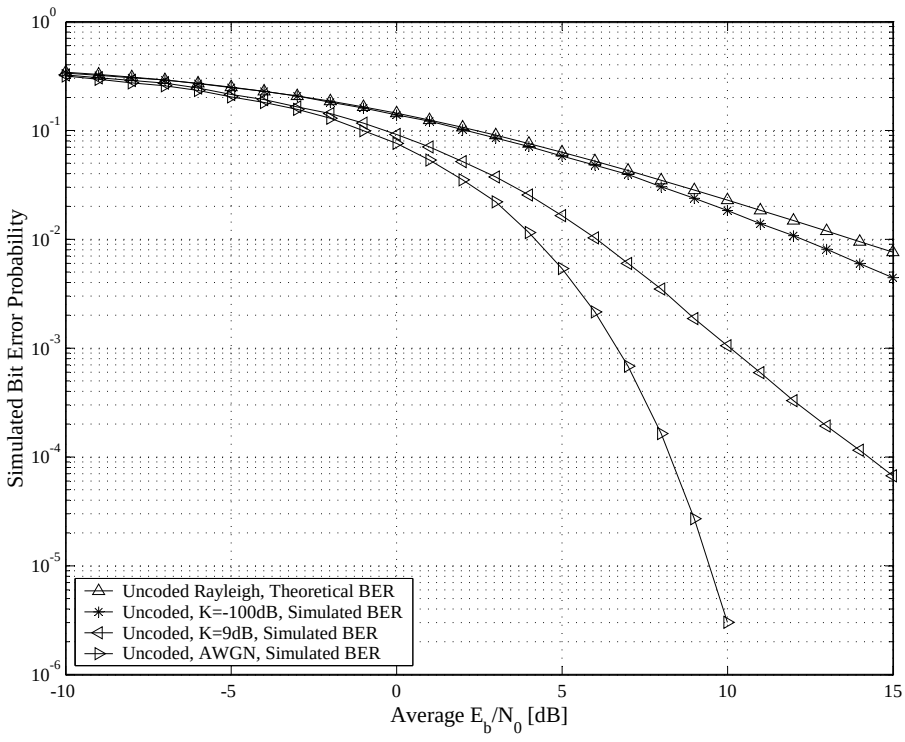

Figure 6.19: BER Performances of an Uncoded Narrowband Complex QPSK Communication System in Flat Fading Channel Conditions, $B_{D,i} = 100$ Hz

6.5.1.3 MULTIPATH FADING CHANNEL RESULTS

6.5.1.3.1 BER Performance Results for the Different CSS Families

The simulated BER performance curves for uncoded RAKE receiver-based complex DS/SSMA QPSK communication systems, employing length $M_{seq} = 63$ ABC (see *Section* D.3.2.2), DSB CE-LI-RU filtered GCL (see *Section* D.3.2.1), ZC (see *Section* D.3.1.1) and QPH (see *Section* D.3.1.2) CSSs in multipath fading channel conditions, are shown in *Fig.* 6.20, *Fig.* 6.21, *Fig.* 6.22 and *Fig.* 6.23, respectively. Note that sequences were optimally selected (see *Section* 6.5.1.3.2) for the ABC sequences scenario, whereas arbitrarily selected sequences were used during the experiments with DSB CE-LI-RU filtered GCL, ZC and QPH CSSs. The reasoning behind this sequence selection approach is motivated in *Section* 6.5.1.3.2.

In *Fig.* 6.20 to *Fig.* 6.23 simulated BER performance curves are shown for complex DS/SSMA QPSK communication systems employing two different types of receiver structures: Firstly, the BER performance curves for systems employing classic non-RAKE receiver structure (i.e. single tap RAKE receivers) are shown. Secondly, simulated BER performance results for systems using the complex DS/SSMA QPSK RAKE receiver structure of *Fig.* 5.4, are depicted. In the case of the RAKE receiver-based simulations, user-1's receiver was configured according to *Table* 5.7, with the RAKE receiver's tap delays and weights configured for perfect MRC (see *Section* 5.3.2) by matching them to user-1's unique multipath fading channel parameters. Due to their obvious superior performances, only RAKE receiver structures were used to obtain the multipath fading channel simulation results presented in the remainder of this chapter. For reference purposes, the BER performance of an uncoded DS/SSMA QPSK communication system (without a RAKE receiver), operating in a single path, non-fading AWGN channel, is also present on these figures.

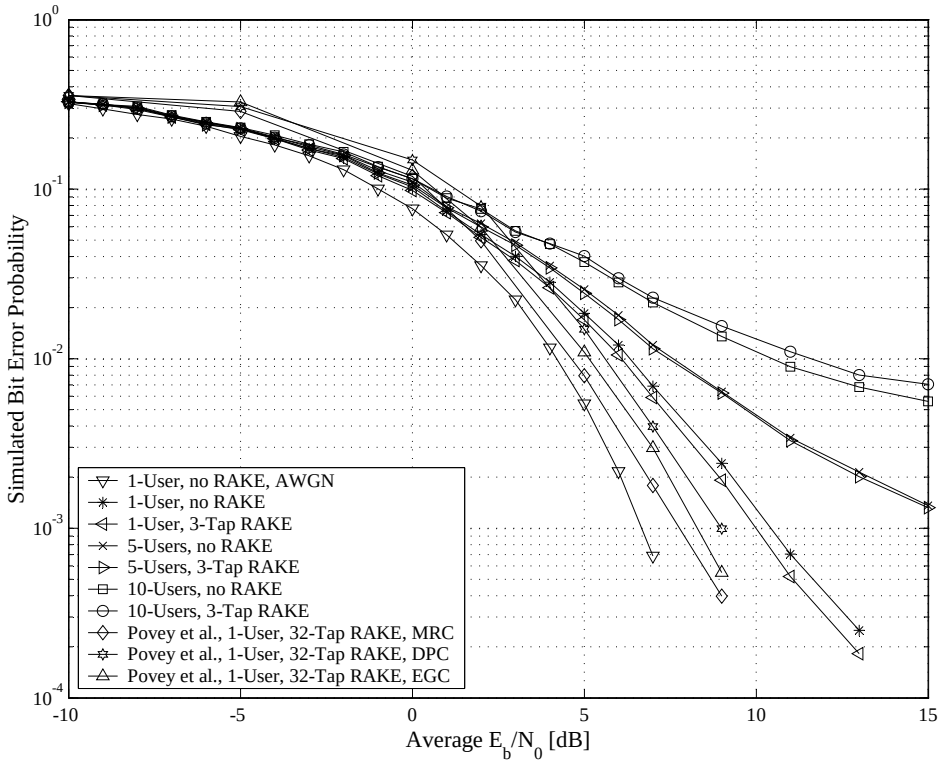

Figure 6.20: BER Performances of Uncoded Wideband Complex QPSK Communication Systems Employing ABC Sequences in Multi-User Multipath Fading Channel Conditions, $M_{seq} = 63$

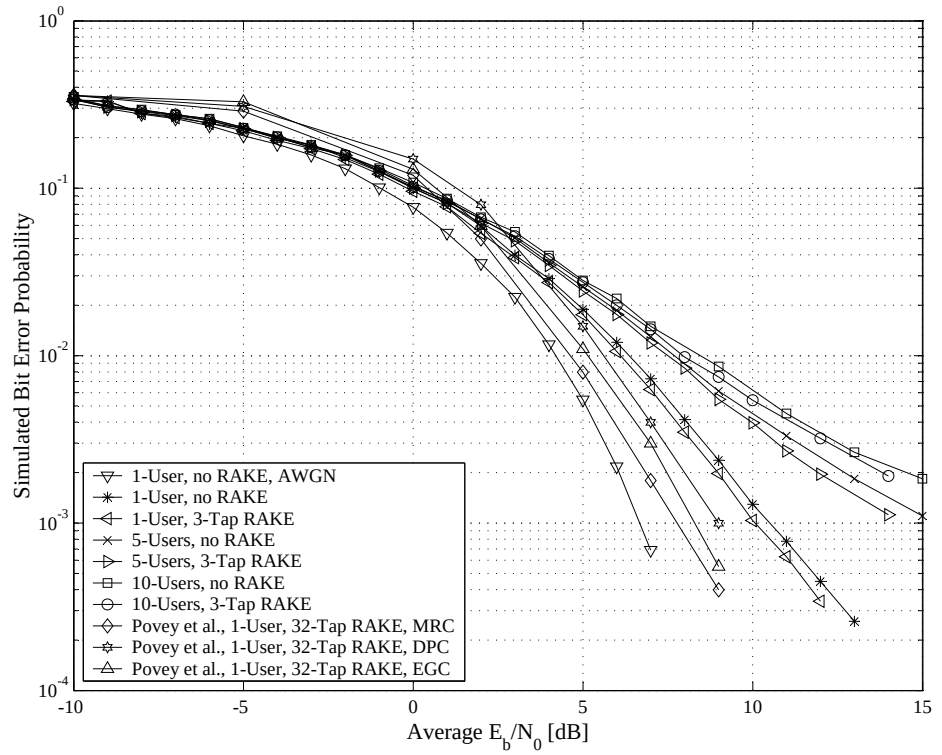

Figure 6.21: BER Performances of Uncoded Wideband Complex QPSK Communication Systems Employing DSB CE-LI-RU Filtered GCL CSSs in Multi-User Multipath Fading Channel Conditions, $M_{seq} = 63$

The simulated BER performance results, presented by *Povey et al.* in [158] for a DS/SSMA system a employing 32-tap RAKE receiver structure, are also included in *Fig.* 6.20, *Fig.* 6.21, *Fig.* 6.22 and *Fig.* 6.23. In [158], *Povey et al.* considered a DS/SSMA *Differential Phase Shift Keying* (DPSK) system, configured for a bit rate of 4.8 kb/s and a PN spreading sequence of length $M_{seq} = 1024$ chips. The multipath fading channel model *Povey et al.* employed during their Monte Carlo simulations, consisted of $L = 32$ resolvable paths, each path configured to generate a Rayleigh fading distribution (see *Section* 2.5.2.1) and maximum Doppler spread of $B_{D,i} = 100$ Hz (see *Section* 2.4.3.3). Furthermore, this multipath fading channel implements an exponential decay power delay profile (see *Section* 2.6.3.3) and a maximum excess delay of $\tau_{max} = 6.5$ μs (see *Section* 2.4.3.1), with the 32 paths evenly spread over this time frame. In their study, *Povey et al.* considered MRC, DPC and EGC RAKE combining techniques.

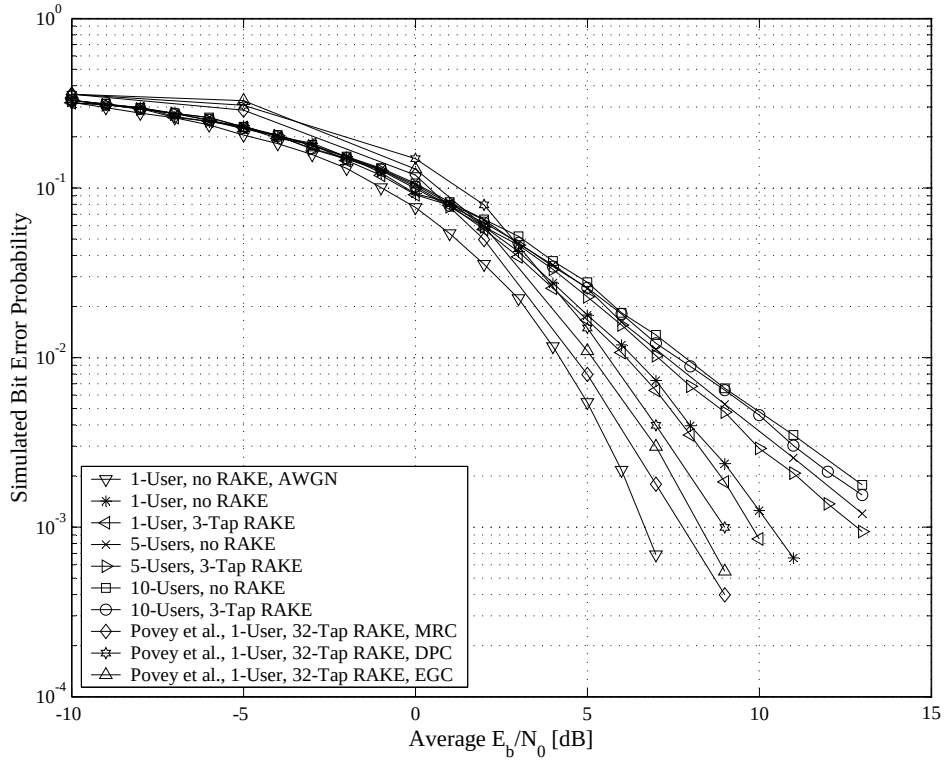

Figure 6.22: BER Performances of Uncoded Wideband Complex QPSK Communication Systems Employing ZC CSSs in Multi-User Multipath Fading Channel Conditions, $M_{seq} = 63$

6.5.1.3.2 The Influence of CSS Selection - An ABC Sequences Case Study

Not only is it intuitively understandable, but also a known fact that the spreading sequence length M_{seq} is the predominant factor dictating the sequence family size M_{fam}. For example, for the GCL sequences [9] considered in this study (ABC, DSB CE-LI-RU filtered GCL and ZC CSSs), the family size can be determined using *Eq.* (D.9). From this equation it is apparent that the largest sequence families are obtained using prime sequence lengths. This notwithstanding, generation of GCL CSSs [9] require the selection of sequence numbers that are relatively prime to M_{seq}. As such, in order to obtain a valid length-63 ABC sequence, the sequence number a must be selected such that $a \in SN_v$,

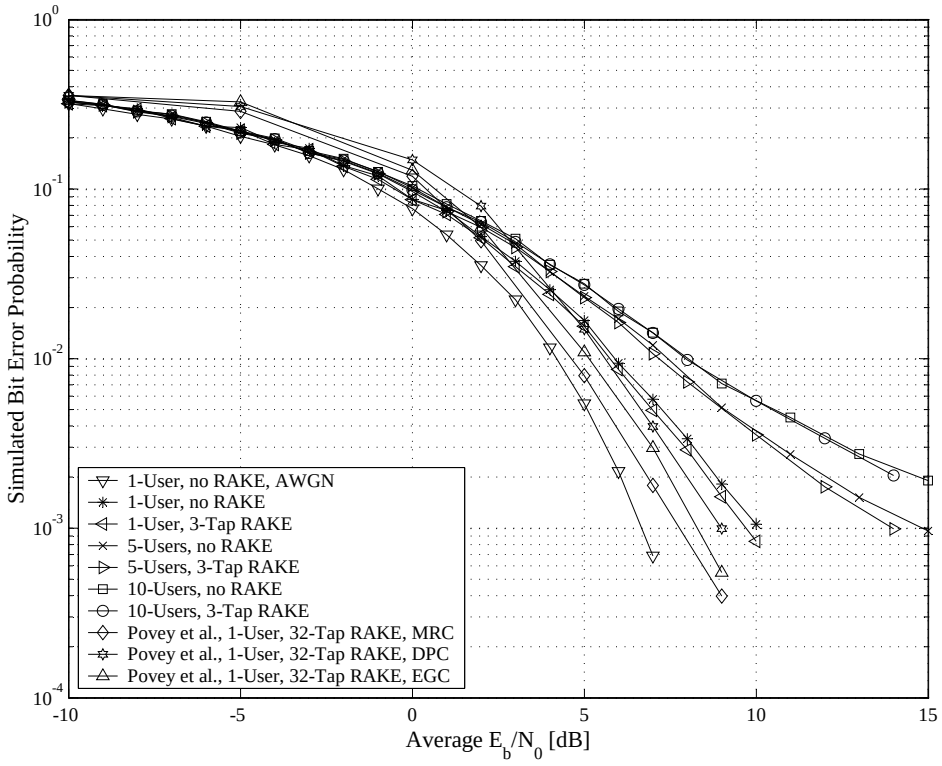

Figure 6.23: BER Performances of Uncoded Wideband Complex QPSK Communication Systems Employing QPH CSSs in Multi-User Multipath Fading Channel Conditions, $M_{seq} = 63$

with SN_v the valid sequence number set, given by:

$$\begin{aligned} SN_v &= \left\{ SN_v^1, SN_v^2, ..., SN_v^{M_{fam}} \right\} \\ &= \{1, 2, 4, 5, 8, 10, 11, 13, 16, 17, 19, 20, 22, 23, 25, 26, 29, 31, 32, \\ &\quad 34, 37, 38, 40, 41, 43, 44, 46, 47, 50, 52, 53, 55, 58, 59, 61, 62\} \end{aligned} \tag{6.2}$$

Although all of these sequence numbers represent unique CSSs that can be assigned to M_{user} unique CDMA users, care must be taken during this assignment process in order to maximising the BER performance of the DS/SSMA system with regards to MUI, especially when $M_{fam} > M_{user}$. Optimal sequence selection for a M_{user}-user CDMA system involves finding the M_{user} CSSs which exhibit the best periodic auto-correlation and cross-correlation properties (see *Section* D.2) for all possible pair-wise comparisons of sequences in the family. This exhaustive search selection process can be extremely tedious to perform manually, as well as fairly complex to automate, especially for long CSSs that exhibit intricate periodic correlation functions [48]. Hence, spreading sequence designers are always interested in finding simple rule-of-thumb sequence selection algorithms for popular spreading sequence families. One such a rule-of-thumb selection method for GCL CSSs has been proposed by *Staphorst* and *Linde* in [162]. The proposed optimal GCL CSS selection method generates the subset of optimal valid sequence numbers $SN_o \subseteq SN_v$, with $SN_o = \left\{ SN_o^1, ..., SN_o^{M_{optimal}} \right\}$. This is accomplished by firstly setting $SN_o^1 = 1$, followed by exhaustively extracting all $SN_o^i \in SB_v$, with $i = 2, ..., M_{optimal}$, for which $SN_o^i \bmod \left(SN_v^j \right) \neq 0$, with $j = 2, ..., M_{fam}$ and $j \neq i$. Thus, according to the proposed selection algorithm, the optimal values of the sequence number a must not only be limited to integer values relatively prime to M_{seq}, but also all possible pair-wise combinations of the elements in SN_o, except for pairings with $SN_o^1 = 1$, must be relatively prime. Executing this

selection procedure for the valid sequence number set given by *Eq.* (6.2) for length $M_{seq} = 63$ ABC sequences, the following optimal valid sequence number subset is obtained:

$$SN_o = \{1, 2, 5, 11, 13, 17, 19, 23, 29, 31\} \tag{6.3}$$

Fig. 6.24 presents the simulated multi-user multipath fading BER performance curves obtained for uncoded complex DS/SSMA QPSK systems, employing length-63 ABC sequences arbitrarily selected from *Eq.* (6.2)'s valid sequence number set and sequentially selected from *Eq.* (6.3)'s optimal sequence number set. Both non-RAKE and RAKE complex receiver structures are considered.

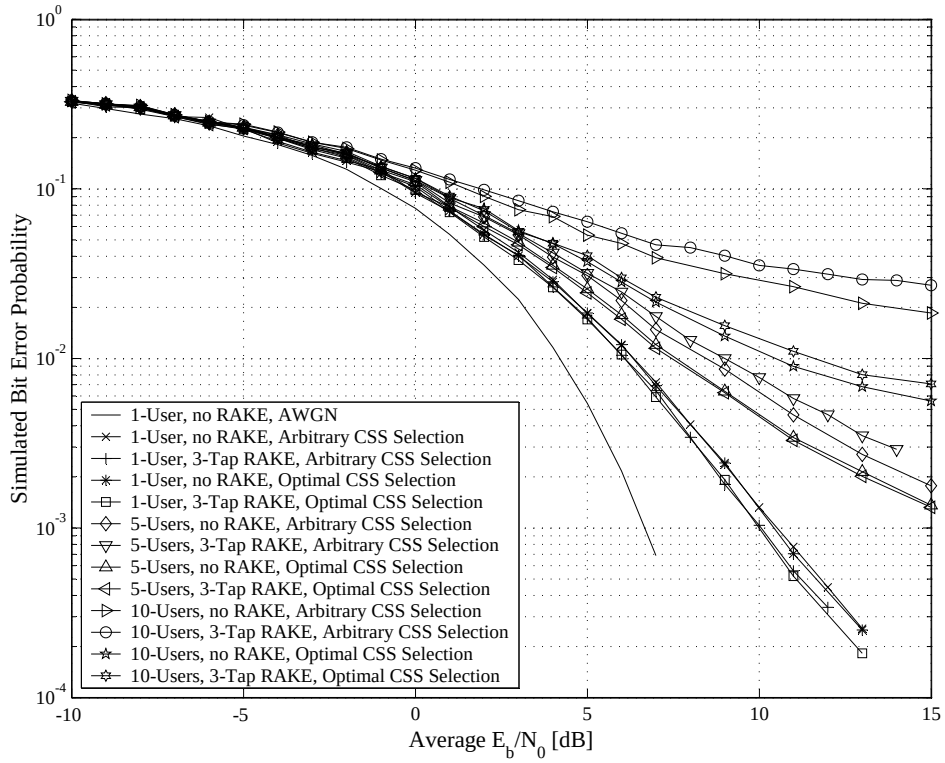

Figure 6.24: BER Performances of Uncoded Wideband Complex QPSK Communication Systems Employing Arbitrarily and Optimally Selected ABC Sequences in Multi-User Multipath Fading Channel Conditions, $M_{seq} = 63$

Similar experiments were performed with complex DS/SSMA systems employing DSB CE-LI-RU filtered GCL and ZC CSSs, but no major BER performance improvements were obtained. Thus, the success of the proposed sequence selection technique is limited to ABC sequences. As such, the multi-user multipath fading results presented in the remainder of this chapter were obtained with optimally selected ABC sequences and arbitrarily selected DSB CE-LI-RU filtered GCL, ZC and QPH CSSs.

6.5.1.3.3 The Influence of CSS Length - An ABC Sequences Case Study

According to the discussion in *Section* 6.4.4 on the comparison of the spectral characteristics of the different CSS families considered in this study, it is possible to increase the length of filtered CSSs by a factor of SSLD in order to produce a BEF equivalent to that obtained when direct spreading is performed with unfiltered CSSs or binary sequences. Longer sequence lengths provide larger se-

quence family sizes, which in turn allows for increased user capacity in the DS/SSMA system without increasing transmission bandwidth or relinquishing PG. Moreover, at a fixed user load, longer CSSs produce better BER performances than shorter CSSs, due to their improved periodic correlation characteristics [48]. *Fig.* 6.25 depicts the multi-user multipath fading channel BER performances obtained using length 61, 64, 63, and 127 ABC sequences in a complex RAKE receiver-based DS/SSMA system. Length-127 ABC sequences are of particular interest, since these sequences produce a BEF nearly identical to that of length-63 DSB CE-LI-RU filtered GCL CSSs, which is used extensively during the remainder of this chapter's multi-user multipath fading channel simulations. Simulated curves are included on *Fig.* 6.25 for length-61 and length-64 ABC sequences in order to investigate the validity of widespread beliefs that prime length and even length ABC sequences produce superior and inferior MUI BER performances, respectively. Note that, for all of the sequence lengths considered, the ABC sequences assigned to CDMA users were optimally selected from the respective sequence families, as described in *Section* 6.5.1.3.2.

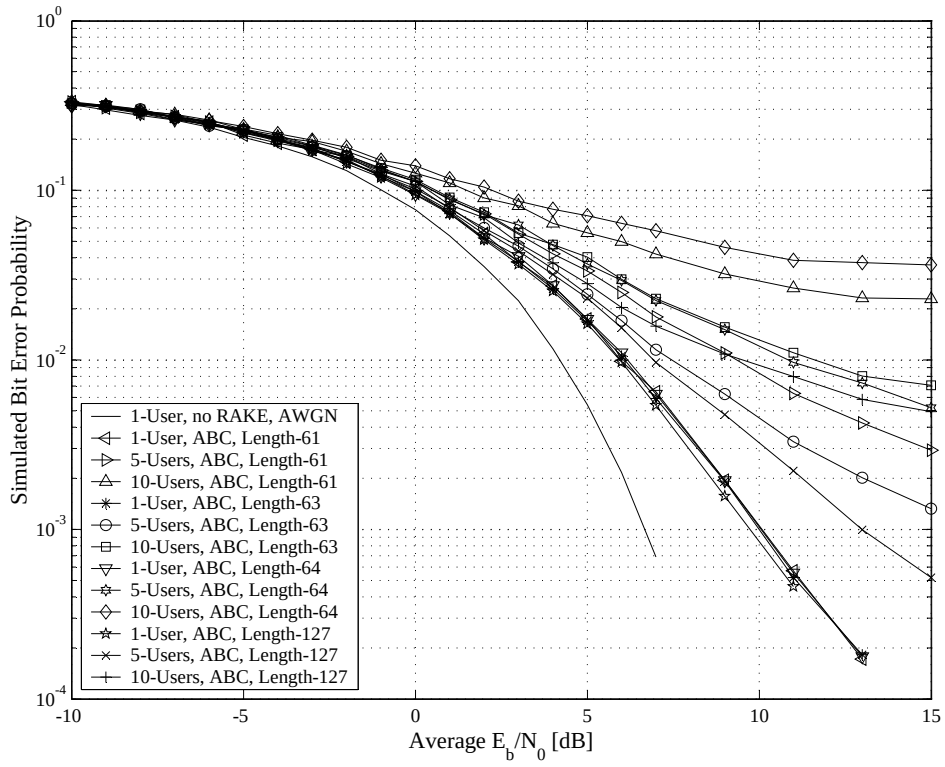

Figure 6.25: BER Performances of Uncoded Wideband Complex QPSK Communication Systems Employing ABC Sequences of Different Lengths in Multi-User Multipath Fading Channel Conditions

6.5.1.4 DISCUSSION OF THE SIMULATION RESULTS

The following important observations can be made from the uncoded narrowband and wideband communication systems' AWGN, flat fading and multipath fading channel BER performance results, presented in the preceding three subsections:

1. Conclusions and observations from the AWGN channel results:

   - The simulated and theoretical BER performance curves for narrowband complex QPSK communication systems, operating in AWGN channel conditions, shown in *Fig.* 6.17, are almost

identical, as was to be expected. The slight deviation between these two curves can be attributed to the AWGN-limiting operation of the elliptic receive filters (see *Section* 5.4.1).

2. Conclusions and observations from the flat fading channel results:

   - The BER performance curve shown in *Fig.* 6.18 for flat fading channel conditions with a Rician factor of $K_i = -100$ dB (i.e. Rayleigh fading amplitude PDF) and a maximum Doppler spread of $B_{D,i} = 33$ Hz, closely resembles the theoretical curve, defined by *Eq.* (5.24). However, the same can not be said for the $B_{D,i} = 100$ Hz maximum Doppler spread scenario (shown in *Fig.* 6.19), especially at high $\overline{E}_b/N_0$ values. The difference in the degree of similarity between the theoretical and simulated curves for different maximum Doppler spread scenarios can easily be explained: Recall from *Section* 5.2.4.2 that a slow flat fading channel, where the fading amplitude stays essentially constant during each symbol interval, was assumed in the derivation of *Eq.* (5.24). As such, for the symbol rate of 1000 Hz (see *Table* 5.1), a maximum Doppler spread of $B_{D,i} = 33$ Hz results in a slow flat fading channel scenario, which is similar to the theoretical channel conditions assumed in *Section* 5.2.4.2.

3. Conclusions and observations from the multi-user multipath fading channel results:

   (a) Comparison of complex DS/SSMA systems employing length-63 CSSs from the different families considered in this study:

   - From the multipath fading channel results shown in *Fig.* 6.20 to *Fig.* 6.23, it is clear that, for a single user scenario, the 3-tap RAKE receivers perform better than the non-RAKE receivers for all families of CSSs considered in this study. This is also true for the 5-user and 10-user CDMA systems employing DSB CE-LI-RU filtered GCL, ZC and QPH CSSs. In the case of ABC sequences, the RAKE receiver structure produces results that are inferior to regular single branch DSSS/MA QPSK receivers. This can be attributed to the weak periodic auto-correlation and cross-correlation properties [48] (see *Section* D.2.3) of ABC sequences, which result in the generation of excessive self-noise and MUI on each of the respective taps of the complex DS/SSMA QPSK RAKE receiver (see *Fig.* 5.4). DSB CE-LI-RU filtered GCL CSSs also suffer from poor periodic correlation characteristics [48], which are arguably the major contributing factors for the RAKE receiver's less than impressive BER performance results (if weighed against the BER performances of the non-RAKE receiver), when compared to that of the ZC and QPH CSS-based systems.
   - The DSB CE-LI-RU filtered GCL and ABC sequences tend to exhibit inferior periodic cross-correlation properties [48]. As a result, these CSSs generate more MUI than the ZC and QPH CSSs, which yields poor BER performances at high user loads. For example, from *Fig.* 6.21, a 10-user complex RAKE receiver-based DS/SSMA QPSK system, employing DSB CE-LI-RU filtered GCL CSSs, operating at $\overline{E}_b/N_0 = 13$ dB, has a BER of $P_b(e) \approx 1/430$, whereas system employing ABC sequences performs even worse with an error floor of $P_b(e) \approx 1/140$. In contrast, of all the CSS families considered, a 10-user CDMA system employing ZC CSSs delivers the best performance at $\overline{E}_b/N_0 = 13$ dB, with a BER of $P_b(e) \approx 1/650$.
   - In general, the use of RAKE receivers did not results in large BER performance improvements over that of the non-RAKE receivers. This can be attribute to the fact that the first propagation path in each CDMA user's exponential decay power delay profile (see *Section* 2.6.3.3) carries the majority of the transmitted output power. From *Table* 5.5 it follows that, if user-1 transmits at 1 W output power, 0.9684 W, 0.0306 W and 0.00096841 W of the transmitted power will be carried by paths 1, 2 and 3, respectively. As such, a non-RAKE receiver effectively processes 0.9684 W of the total

received power. Thus, by using RAKE receiver structures, a tentative improvement of at least $10.\log_{10}\left(\frac{1}{0.9684}\right) = 0.1394$ dB in average E_b/N_0 was to be expected. The fact that gains higher than this are achieved, especially at low user loads, is the nett result of the diversity obtained through the RAKE receiver's MRC operation.

- From *Fig.* 6.20, *Fig.* 6.21, *Fig.* 6.22 and *Fig.* 6.23 it is abundantly clear that, irrespective of the CSS family employed, the 32-tap RAKE receiver system, presented by *Povey et al.* in [158], outperforms the 3-tap RAKE receiver system presented in this study, even though the multipath fading channel environment they considered was far more severe ($L = 32$ independent paths with no LOS signal component present on any of the paths). However, their RAKE receiver linearly processes 32 distinct copies of the transmitted signal, thereby achieving extremely high diversity gains. According to the CLT [47], by combining such a high number of statistically independent Rayleigh paths, more ideal, Gaussian-like channel conditions are produced. Furthermore, the length $M_{seq} = 1024$ PN sequence considered in their study has near-perfect periodic auto-correlation properties (see *Section* D.2.2). Hence, no detrimental self-noise is generated inside the RAKE receiver structure. However, the same can not be said of RAKE receiver structures employing the CSSs presented in *Appendix D*.
- The BER performance results obtained by *Povey et al.* [158], presented in *Fig.* 6.20, *Fig.* 6.21, *Fig.* 6.22 and *Fig.* 6.23, indicate that MRC is a more powerful RAKE combining technique than EGC or DPC [158]. As such, it justifies this study's use of MRC in the RAKE receiver structures of the wideband complex DS/SSMA QPSK systems used throughout the multi-user multipath fading channel simulations.

(b) Investigation into the influence of the sequence selection approach on the BER performance of a ABC sequence-based DS/SSMA system:

- *Fig.* 6.24 is evidence that a complex DS/SSMA system employing length-63 ABC sequences, chosen according to *Staphorst* and *Linde*'s proposed optimal GCL sequence selection method [162] (detailed in *Section* 6.5.1.3.2), has a BER performance superior to that of a system employing arbitrarily selected sequences. This is especially true for high user loads. For example, when employed in a 10-user RAKE receiver-based complex DS/SSMA system at a BER of $P_b(e) = 3/100$, optimally selected ABC sequences show a gain of 6 dB over arbitrarily selected ABC sequences. These remarkable gains, however, are only obtainable for ABC sequences, since using the proposed optimal sequence selection method in conjunction with DSB CE-LI-RU filtered GCL and ZC CSSs, deliver mediocre BER performance improvements.
- By allowing only the CSSs with the best periodic cross-correlation characteristics (see *Section* D.2.3) to be assigned to CDMA users, the proposed optimal sequence selection method of [162] (see *Section* 6.5.1.3.2) not only improves the overall BER performance of a complex DS/SSMA system employing ABC sequences, but also improves the BER performances of RAKE receivers relatively to non-RAKE receivers for non-unity user loads. From *Fig.* 6.20 and *Fig.* 6.24 it is apparent that MRC RAKE reception is outperformed by non-RAKE reception for 5-user and 10-user complex DS/SSMA systems employing arbitrarily selected ABC sequences. Optimally selecting CSSs, however, improves the 5-user RAKE receiver-based system to a comparable level as the non-RAKE receiver-based system. Unfortunately, at high user loads, such as the 10-user scenario, the optimal sequence selection method of *Section* 6.5.1.3.2 is incapable of avoiding the poor periodic cross-correlation characteristics of ABC sequences [48]. Hence, for this user load the self-noise generated by the RAKE receiver structure still outweighs the diversity gains it achieves through MRC.

(c) Investigation into the influence of sequence length on the BER performance of ABC sequence-based DS/SSMA systems:

- As was to be expected, the complex RAKE receiver-based DS/SSMA system employing length-127 ABC sequences outperforms all of the other complex DS/SSMA systems employing shorter ABC sequences. This can be attributed to the improvement of the CSSs' periodic correlation characteristics as the sequence length increases [48]. Unfortunately, for a 10-user CDMA environment, the BER performance of the RAKE receiver-based complex DS/SSMA system employing length-127 ABC sequences is only marginally better than that of a system using length-63 DSB CE-LI-RU filtered GCL CSSs (see *Fig.* 6.21). Note that both these systems have similar BEFs. However, by arbitrarily selecting CSSs, the length-127 ABC sequence-based system supports a maximum of 126 CDMA users, whereas the length-63 DSB CE-LI-RU filtered GCL CSS-based system supports only 36 users (see *Eq.* (6.2)). Hence, it can be concluded that, using ABC sequences instead of binary or unfiltered CSSs, increases the PG and user capacity (directly related to the SSLD, introduced in *Section* D.2.6) of DS/SSMA systems, without unduly increasing their BEFs. The increased user capacity does, however, come at the expense of inferior BER performances, making this CSS family a poor choice for CDMA purposes.
- Comparing *Fig.* 6.21's BER performance results for the RAKE receiver-based complex DS/SSMA systems employing length-61 and length-63 ABC sequences (these systems have comparable PGs and BEFs), it is apparent that the popular belief [48] that GCL CSSs with prime numbered sequence lengths exhibit superior periodic cross-correlation properties (see *Section* D.2.3), resulting in lower MUI levels, is fallacious. However, using prime numbered sequence lengths do increase the user capacity of the system dramatically, as shown by *Eq.* (D.9) in *Section* D.3.1.1.
- From *Fig.* 6.21 it is clear that the RAKE receiver-based complex DS/SSMA system employing length-64 ABC sequences exhibits the weakest BER performance results, due to the high levels of MUI present in the CDMA system. Hence, even numbered sequence lengths must be avoided for GCL CSSs, not only because of the limited family sizes that can be generated (see *Eq.* (D.9)), but also because of these sequences' poor periodic cross-correlation characteristics (see *Section* D.2.3).

6.5.2 BINARY CONVOLUTIONAL CODED COMMUNICATION SYSTEMS

The following subsections present simulated BER performance results for classic binary 4-state, rate $R_c = 1/2$ NSC (see *Section* 3.2.1.3.1) and 8-state, rate $R_c = 2/3$ RSC (see *Section* 3.2.1.3.2) coded narrowband complex QPSK systems (see *Section* 5.2) in AWGN and flat fading channel conditions, as well as wideband complex DS/SSMA QPSK communication systems (see *Section* 5.3) in multi-user multipath fading channel conditions. Note that length $M_{seq} = 63$ CSSs were employed in the RAKE receiver-based complex DS/SSMA communication systems during the multi-user multipath fading channel simulations. The ABC sequences used were selected for optimum periodic cross-correlation (see *Section* 6.5.1.3.2), whereas the CSSs used from the other families were arbitrarily selected. The BER performance results discussed here serve as baseline references during the examination of the simulation results for the VA decoded linear block codes, presented later in this chapter.

6.5.2.1 4-STATE, RATE $R_C = 1/2$ NSC CODED COMMUNICATION SYSTEMS

In the following subsections the BER performance results of the 4-state, rate $R_c = 1/2$ NSC code, defined by the following generator matrix (see *Section* 3.2.1.1):

$$G_{CC}(D) = \left[\begin{array}{cc} 1 + D^2 & 1 + D + D^2 \end{array} \right] \tag{6.4}$$

are presented and examined. From [47] the minimum free distance (see *Section* 3.2.1.2) of this binary NSC code is $d_{free} = 5$. Furthermore, according to *Section* 3.2.1.2, this NSC code has a minimal encoder structure with a constraint length of $v = 2$. As such, a simple sliding window VA decoder (see *Section* 3.3.1) with a window size [47] of $\omega = 5.v = 10$ trellis sections (see *Section* 3.3.1.1) was employed as ML decoder. Both hard and soft decision (see *Section* 4.4.2.2) decoding approaches were considered. In the case of soft decision decoding, the effects of using perfect fading amplitude CSI (see *Section* 3.3.5) in the VA metric calculations on the BER performance results, were also investigated.

6.5.2.1.1 AWGN Channel Results

Fig. 6.26 shows several simulated BER performance curves for 4-state, rate $R_c = 1/2$ NSC coded (see *Section* 3.2.1.3.1) narrowband complex QPSK communication systems (see *Section* 5.2), operating in AWGN channel conditions (see *Section* 2.2). Hard and soft decision (without using fading amplitude CSI in the VA branch metric calculations) decoding BER performance results are present on *Fig.* 6.26. Also depicted on this figure is the BER performance curve of an uncoded narrowband QPSK system in AWGN, theoretically defined by *Eq.* (5.20).

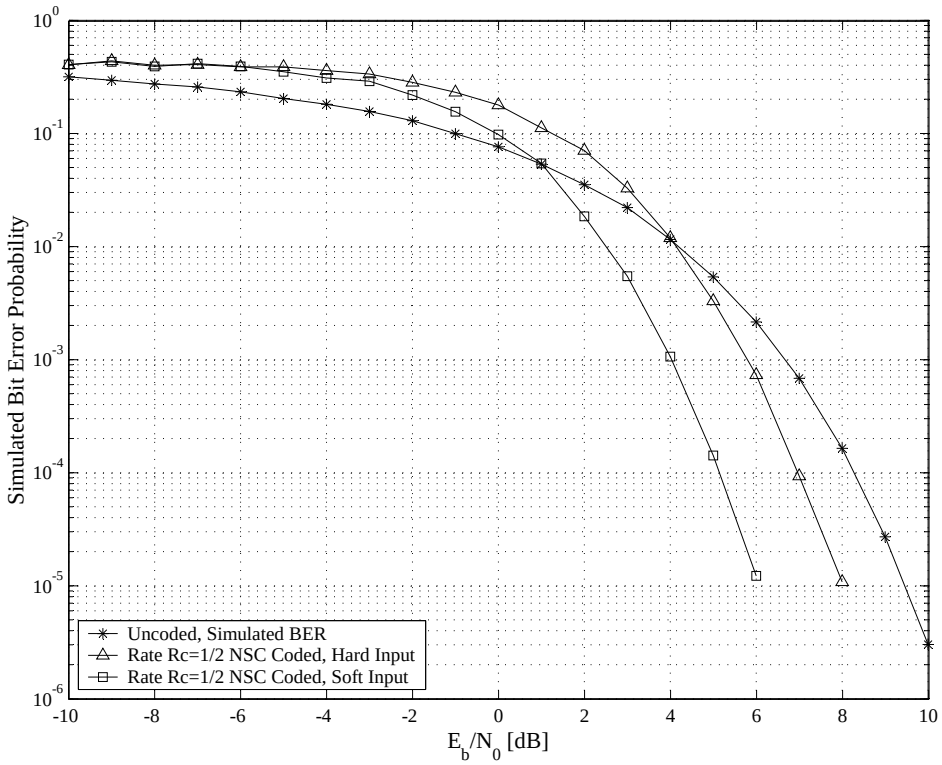

Figure 6.26: BER Performances of 4-State, Rate $R_c = 1/2$ NSC Coded Narrowband Complex QPSK Communication Systems in AWGN Channel Conditions

6.5.2.1.2 Flat Fading Channel Results

Simulated flat fading channel (see *Section* 2.5.1.1) BER performance results of 4-state, rate $R_c = 1/2$ NSC (see *Section* 3.2.1.3.1) coded narrowband complex QPSK communication systems (see *Section* 5.2) for maximum Doppler spreads (see *Section* 2.4.3.3) of $B_{D,i} = 33$ Hz and $B_{D,i} = 100$ Hz, are shown in *Fig.* 6.27 and *Fig.* 6.28, respectively. These figures depict simulated BER performance

results for Rician factors (see *Section* 2.5.2.2) of $K_i = -100$ dB, $K_i = 0$ dB and $K_i = 9$ dB. Furthermore, two soft decision decoding approaches were investigated, namely soft decision decoding without any fading amplitude CSI and soft decision decoding with perfect fading amplitude CSI (see *Section* 3.3.5 and *Section* 5.2.3). Also depicted on these figures are simulated BER performance curves for uncoded QPSK systems in AWGN, as well as *Eq.* (5.24)'s theoretical BER performance curve for uncoded narrowband QPSK systems in slow Rayleigh flat fading channel conditions.

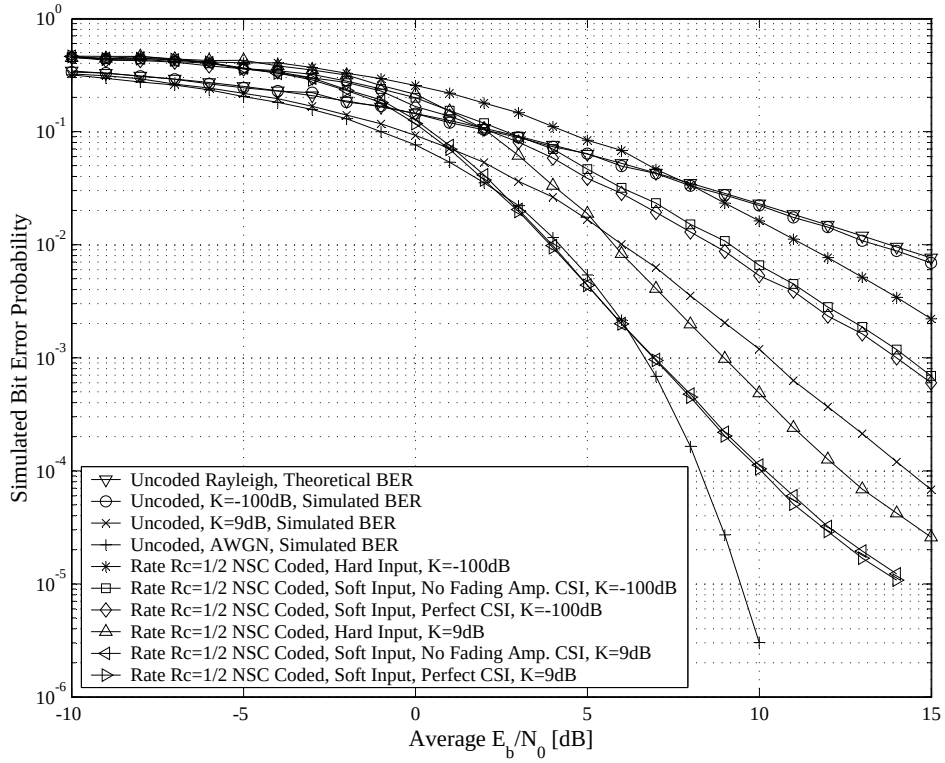

Figure 6.27: BER Performances of 4-State, Rate $R_c = 1/2$ NSC Coded Narrowband Complex QPSK Communication Systems in Flat Fading Channel Conditions, $B_{D,i} = 33$ Hz

6.5.2.1.3 Multipath Fading Channel Results

Fig. 6.29, *Fig.* 6.30, *Fig.* 6.31 and *Fig.* 6.32 present the simulated multi-user multipath fading channel BER performance results obtained for 4-state, rate $R_c = 1/2$ NSC coded RAKE receiver-based wideband complex DS/SSMA QPSK systems (see *Section* 5.3), employing length $M_{seq} = 63$ ABC (see *Section* D.3.2.2), DSB CE-LI-RU filtered GCL (see *Section* D.3.2.1), ZC (see *Section* D.3.1.1) and QPH (see *Section* D.3.1.2) CSSs, respectively. Results are shown for sliding window VA decoding using hard decisions, soft decisions without any fading amplitude CSI and soft decisions with perfect fading amplitude CSI (see *Section* 3.3.5 and *Section* 5.3.3). For comparative purposes, the simulated BER performances for the uncoded RAKE receiver-based wideband complex DS/SSMA QPSK systems, presented in *Section* 6.5.1.3.1, are also present on these figures. Also shown is the BER performance of an uncoded DS/SSMA QPSK communication system (without a RAKE receiver), operating in a non-fading AWGN environment.

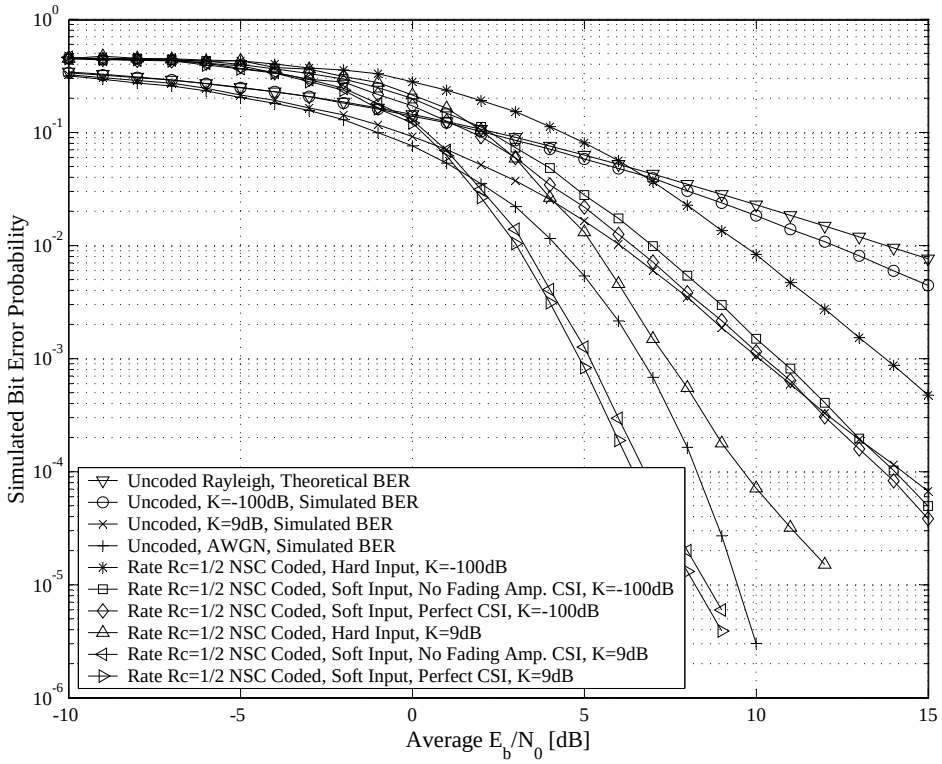

Figure 6.28: BER Performances of 4-State, Rate $R_c = 1/2$ NSC Coded Narrowband Complex QPSK Communication Systems in Flat Fading Channel Conditions, $B_{D,i} = 100$ Hz

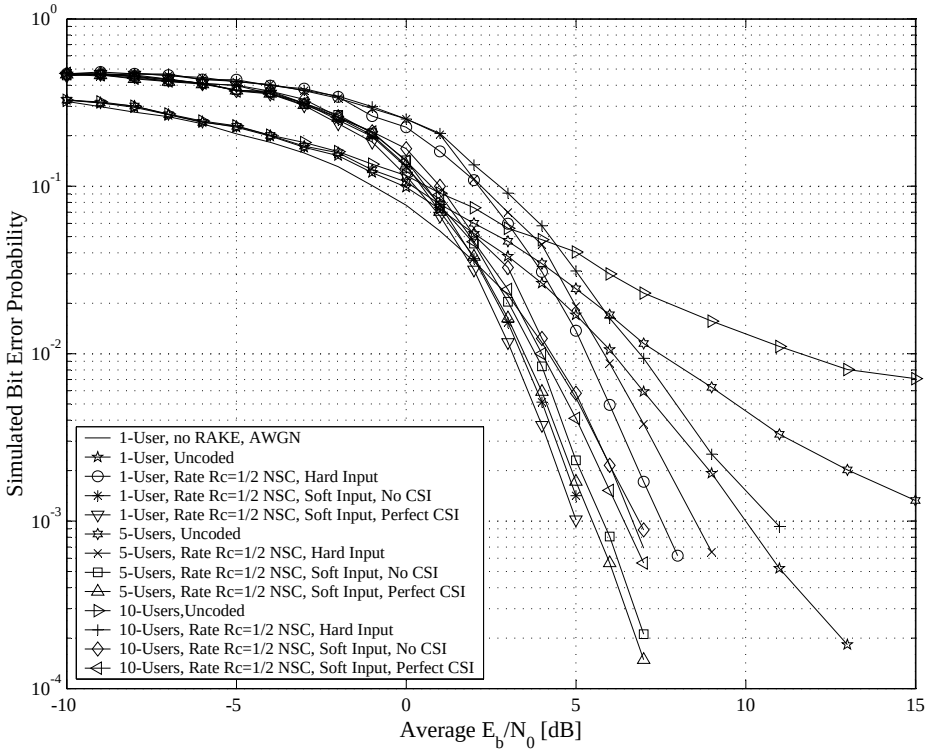

Figure 6.29: BER Performances of 4-State, Rate $R_c = 1/2$ NSC Coded Wideband Complex QPSK Communication Systems Employing ABC Sequences in Multi-User Multipath Fading Channel Conditions, $M_{seq} = 63$

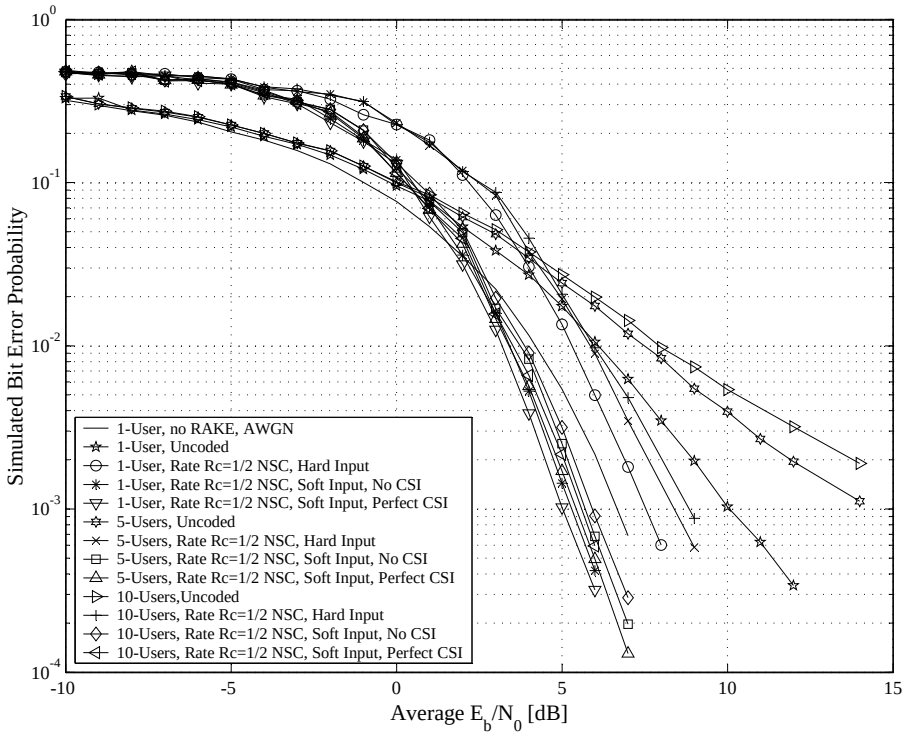

Figure 6.30: BER Performances of 4-State, Rate $R_c = 1/2$ NSC Coded Wideband Complex QPSK Communication Systems Employing DSB CE-LI-RU Filtered GCL CSSs in Multi-User Multipath Fading Channel Conditions, $M_{seq} = 63$

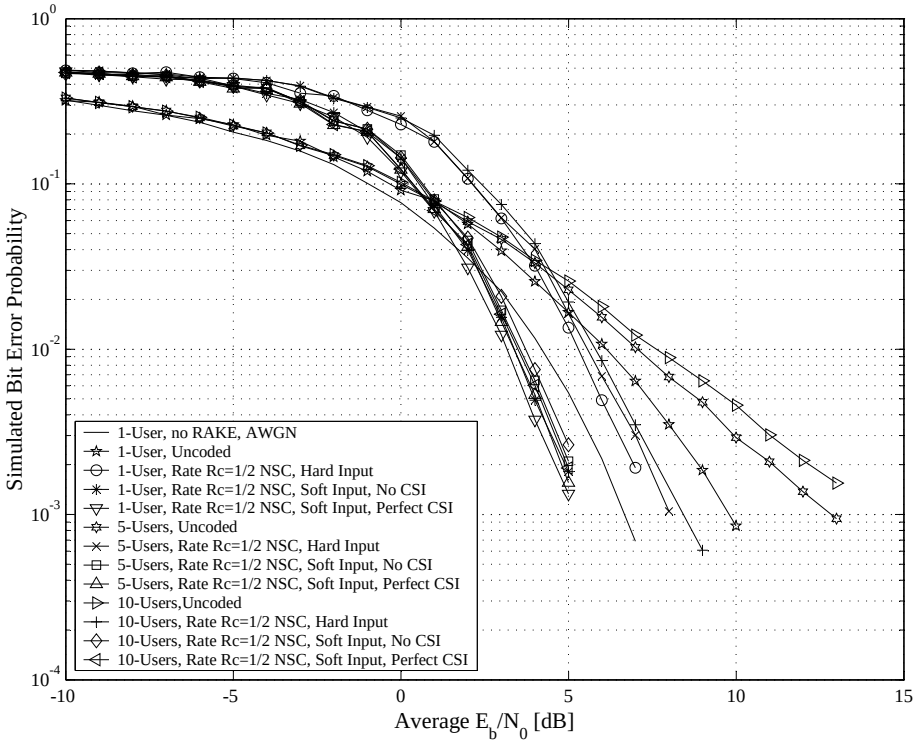

Figure 6.31: BER Performances of 4-State, Rate $R_c = 1/2$ NSC Coded Wideband Complex QPSK Communication Systems Employing ZC CSSs in Multi-User Multipath Fading Channel Conditions, $M_{seq} = 63$

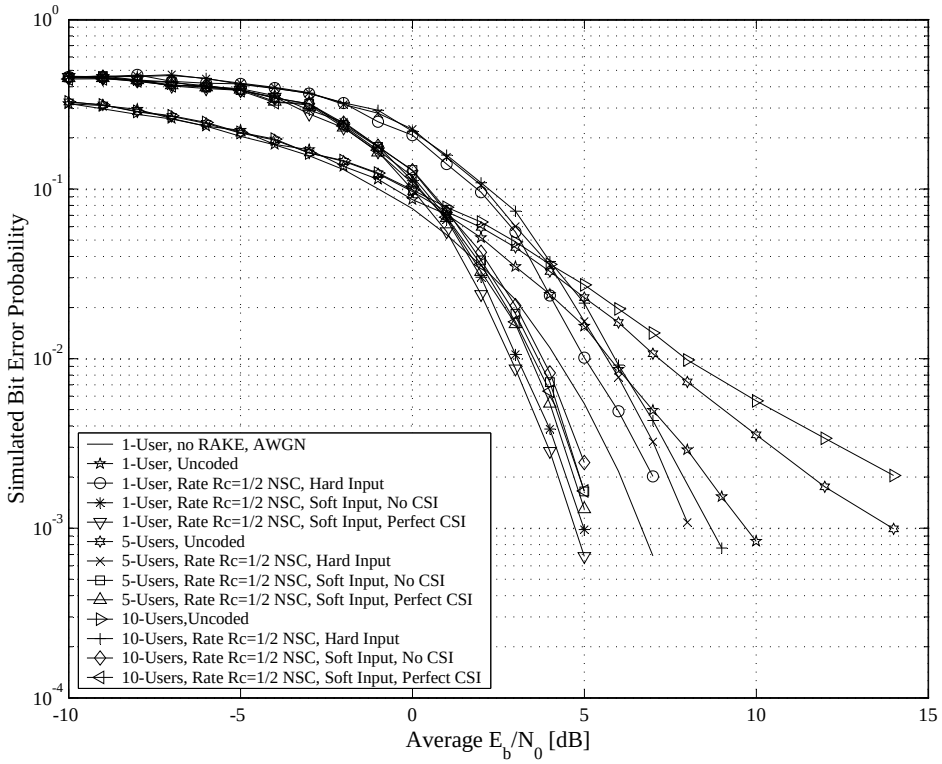

Figure 6.32: BER Performances of 4-State, Rate $R_c = 1/2$ NSC Coded Wideband Complex QPSK Communication Systems Employing QPH CSSs in Multi-User Multipath Fading Channel Conditions, $M_{seq} = 63$

6.5.2.1.4 Discussion of the Simulation Results

From the simulated AWGN, flat fading and multi-user multipath fading channel BER performance results for the 4-state, rate $R_c = 1/2$ NSC coded narrowband and wideband communication systems, presented in the preceding subsections, the following conclusions can be drawn:

1. Conclusions and observations from the AWGN channel results:

   - From the simulated AWGN channel BER performances for 4-state, rate $R_c = 1/2$ NSC coded narrowband complex QPSK communication systems, shown in *Fig.* 6.26, it is clear that the system employing soft decision VA decoding of the convolutional code exhibits a measured asymptotic gain of approximately 3.6 dB over the uncoded system. This measured coding gain corresponds with *Eq.* (3.8)'s calculated maximum asymptotic gain of $CG_{CC}^{soft} = 3.98$ dB.
   - Comparing *Fig.* 6.26's soft decision VA decoding BER performance results with that of the hard decision decoding approach, a 2 dB asymptotic gain is evident, as was to be expected [47] (see *Section* 3.2.1.2).
   - At low E_b/N_0 values, hard and soft decision VA decoding of the rate $R_c = 1/2$ NSC code in AWGN channel conditions result in poorer BER performances than the uncoded system. To be precise, soft decision VA decoding starts to show gains for $E_b/N_0 > 1$ dB, whereas hard decision VA decoding is only useful for $E_b/N_0 > 4.2$ dB. The E_b/N_0 points at which coded systems start to show gains over the uncoded system are commonly referred to as the *BER cross-over points* [47].

2. Conclusions and observations from the flat fading channel results:

   - On closer investigation of the flat fading channel simulation results (presented in *Fig.* 6.27 and *Fig.* 6.28), it is evident that the BER performances of hard and soft decision VA decoded rate $R_c = 1/2$ NSC codes improve as the Rician factor K_i (see *Section* 2.5.2.2) increases. Since binary NSC codes were initially intended for FEC purposes in AWGN channel conditions, this BER performance improvement can be attributed to the increase in the channel's LOS component, resulting in the fading amplitude PDF changing from a Rayleigh-like distribution to a Gaussian-like distribution (see *Section* 2.5.2.2).
   - A comparison of *Fig.* 6.27 and *Fig.* 6.28 shows that the hard and soft decision VA decoded rate $R_c = 1/2$ NSC codes' BER performances deteriorate as the maximum Doppler spread frequency decreases. At fixed symbol rate of 1000 symbols/s (see *Section* 5.4.2), a maximum Doppler spread of $B_{D,i} = 33$ Hz will result in more information bits being corrupted during a slow deep fade, than during a faster $B_{D,i} = 100$ Hz deep fade. Thus, for a maximum Doppler spread of $B_{D,i} = 100$ Hz, bit error occurrences incurred by the channel will appear less bursty in nature. Since binary NSC codes are not intended to combat bursty errors, they are better suited for fast flat fading channels than for slow flat fading channels.
   - From *Fig.* 6.27 and *Fig.* 6.28 it is apparent that hard decision VA decoding lags soft decision decoding (without any fading amplitude CSI) by approximately 2 dB. Soft decision VA decoding, with fading amplitude CSI, in turn performs better that soft decision decoding without fading amplitude CSI. However, this performance improvement is minuscule. For the $B_{D,i} = 33$ Hz scenario, an improvement of approximately 0.15 dB was obtained for all Rician factors, whereas an average improvement of 0.25 dB can be observed for $B_{D,i} = 100$ Hz.
   - The simple binary rate $R_c = 1/2$ NSC code shows impressive coding gains over uncoded systems. For example, for $B_{D,i} = 100$ Hz and $K_i = 9$ dB, soft decision VA decoding (without fading amplitude CSI) shows a gain of 5 dB at a BER of $P_b(e) = 10^{-3}$. Furthermore, comparing the results of *Fig.* 6.27 and *Fig.* 6.28 for a fixed K_i, it is clear that the rate $R_c = 1/2$ NSC code exhibits larger coding gains for $B_{D,i} = 100$ Hz than for $B_{D,i} = 33$ Hz.

3. Conclusions and observations from the multi-user multipath fading channel results:

   - From the multi-user multipath fading channel results shown in *Fig.* 6.29, *Fig.* 6.30, *Fig.* 6.31 and *Fig.* 6.32, it is apparent that the increased MUI, created by additional CDMA users sharing the mobile communication environment, has a definite negative impact on the BER performance of the rate $R_c = 1/2$ NSC code. However, even for ABC sequences, no error floors are apparent at high $\overline{E}_b/N_0$. Thus, for the unfiltered and filtered CSS families considered, this binary NSC code effectively combats MUI through code diversity. In fact, for the 1-user and 5-user scenarios, better BER performances were obtained through soft decision VA decoding than that achievable by a single user uncoded system, operating purely in AWGN.
   - From a comparison of the results given in *Fig.* 6.29, *Fig.* 6.30, *Fig.* 6.31 and *Fig.* 6.32 it is evident that rate $R_c = 1/2$ NSC coded complex DS/SSMA systems employing the unfiltered CSS families perform superior to those using the pre-filtered CSS families. Specifically, pre-filtered ABC sequences exhibited the weakest BER performances, whereas QPH CSSs showed the best performances, marginally outperforming ZC CSSs. For example, for a 10-user CDMA environment, ZC CSSs performed no worse than 0.25 dB below QPH CSSs for hard decision VA decoding.
   - For 1-user and 5-user CDMA environments, it is barely possible to distinguish between the BER performance results of the rate $R_c = 1/2$ NSC coded complex DS/SSMA systems

employing the unfiltered ZC and QPH CSS families, both for the hard and soft decision VA decoding scenarios. These exceptional BER performances, even at high user loads, can be attributed to the unfiltered CSS families' superior periodic cross-correlation properties, as was also observed for the uncoded systems in *Section* 6.5.1.3.1. For a 10-user system, however, there is a marked decrease in BER performance, even for the unfiltered CSS families.

- A comparison of hard decision and soft decision VA decoding of the rate $R_c = 1/2$ NSC code in multi-user multipath fading channel conditions, indicates that, at low user loads, hard decision decoding asymptotically lags soft decision decoding (without fading amplitude CSI) by the characteristic 2 dB margin, irrespective of the CSS family used by the wideband complex DS/SSMA communication systems. This observation also remains true at high user loads, except for ABC sequences, where the asymptotic gain of soft decision (without fading amplitude CSI) over hard decision VA decoding expands to approximately 2.5 dB. Furthermore, inclusion of perfect fading amplitude CSI during soft decision decoding results in a further 0.25 dB improvement, regardless of the user load or the CSS family employed in the CDMA system.

6.5.2.2 8-STATE, RATE $R_C = 2/3$ RSC CODED COMMUNICATION SYSTEMS

The binary IIR RSC code (see *Section* 3.2.1.3.2) considered here is depicted in *Fig.* A.2 of *Appendix A* and is defined by the generator matrix given in *Eq.* (3.11). According to *Table* A.5, the minimum free distance (see *Section* 3.2.1.2) of this code is $d_{free} = 4$. Furthermore, the RSC code considered here has a constraint length (see *Section* 3.2.1.2) of $v = 3$. As such, a simple sliding window VA, with a window size of $\omega = 5.v = 15$ trellis sections, was employed as ML decoder. Both hard and soft decision decoding (with and without perfect fading amplitude CSI (see *Section* 3.3.5)) approaches are considered. Due to time constraints, this code's BER performances were determined, through extensive simulations, for only AWGN and flat fading channel conditions.

6.5.2.2.1 AWGN Channel Results

Several simulated BER performance curves for 8-state, rate $R_c = 2/3$ RSC coded (see *Section* 3.2.1.3.2) narrowband complex QPSK communication systems (see *Section* 5.2), functioning in AWGN channel conditions (see *Section* 2.2), are shown in *Fig.* 6.33. Note from this figure that VA decoding using both hard and soft decision metric calculations were considered. Obviously, in the case of soft decision decoding no fading amplitude CSI was used. The BER performance curve of an uncoded narrowband QPSK system in AWGN channel conditions, theoretically defined by *Eq.* (5.20), is also depicted in this figure.

6.5.2.2.2 Flat Fading Channel Results

Fig. 6.34 and *Fig.* 6.35 show simulated flat fading channel (see *Section* 2.5.1.1) BER performance results of 8-state, rate $R_c = 2/3$ RSC (see *Section* 3.2.1.3.2) coded narrowband complex QPSK communication systems (see *Section* 5.2) for maximum Doppler spreads (see *Section* 2.4.3.3) of $B_{D,i} = 33$ Hz and $B_{D,i} = 100$ Hz, respectively. Simulated BER performance results for Rician factors (see *Section* 2.5.2.2) of $K_i = -100$ dB, $K_i = 0$ dB and $K_i = 9$ dB are present on these figures. Hard and soft decision VA decoding of the 8-state, rate $R_c = 2/3$ RSC codes were considered. Note that two soft decision decoding approaches were investigated, namely soft decision decoding without any fading amplitude CSI and soft decision decoding with perfect fading amplitude CSI (see *Section* 3.3.5 and *Section* 5.2.3). These figures also include simulated BER performance curves for uncoded QPSK systems in AWGN, as well as theoretical BER performance curves for uncoded QPSK systems in slow Rayleigh flat fading channel conditions, defined by *Eq.* (5.24).

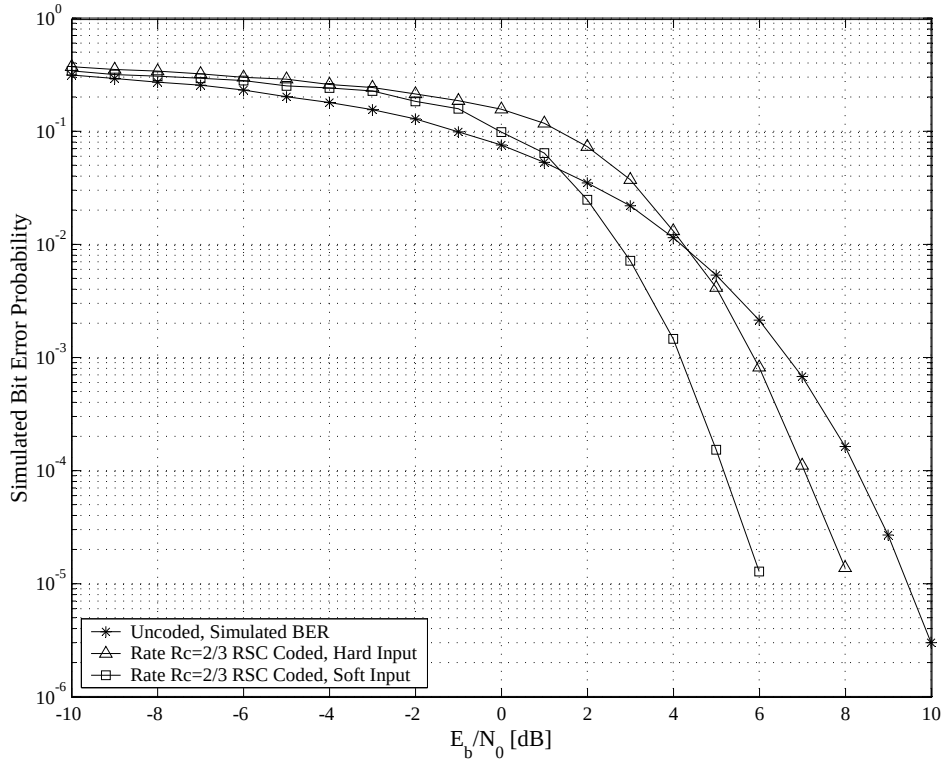

Figure 6.33: BER Performances of 8-State, Rate $R_c = 2/3$ RSC Coded Narrowband Complex QPSK Communication Systems in AWGN Channel Conditions

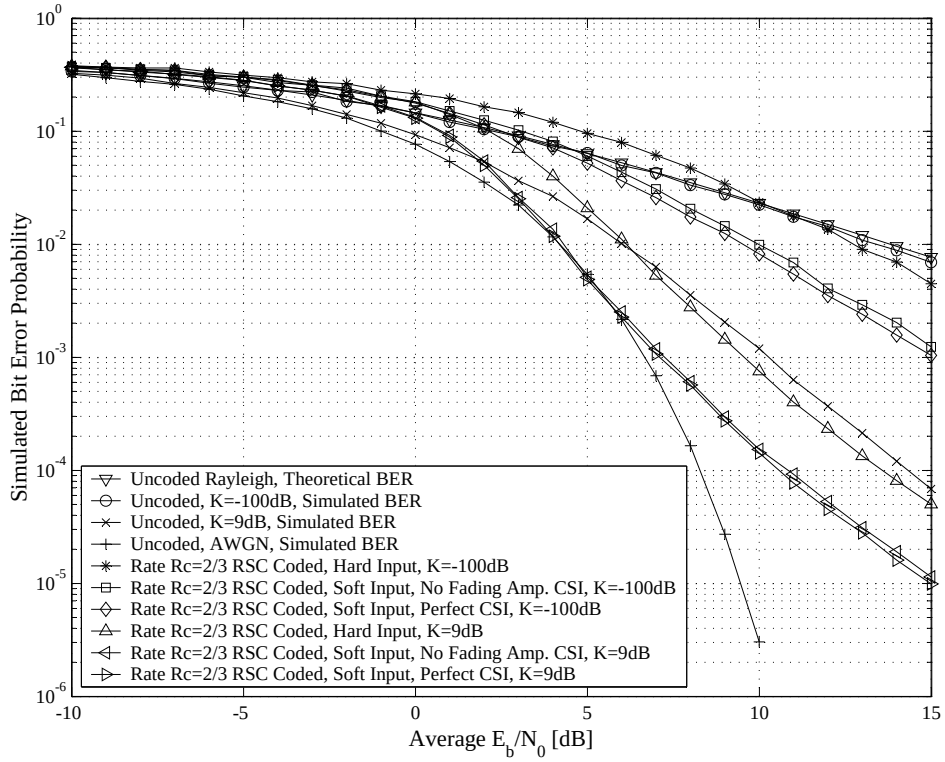

Figure 6.34: BER Performances of 8-State, Rate $R_c = 2/3$ RSC Coded Narrowband Complex QPSK Communication Systems in Flat Fading Channel Conditions, $B_{D,i} = 33$ Hz

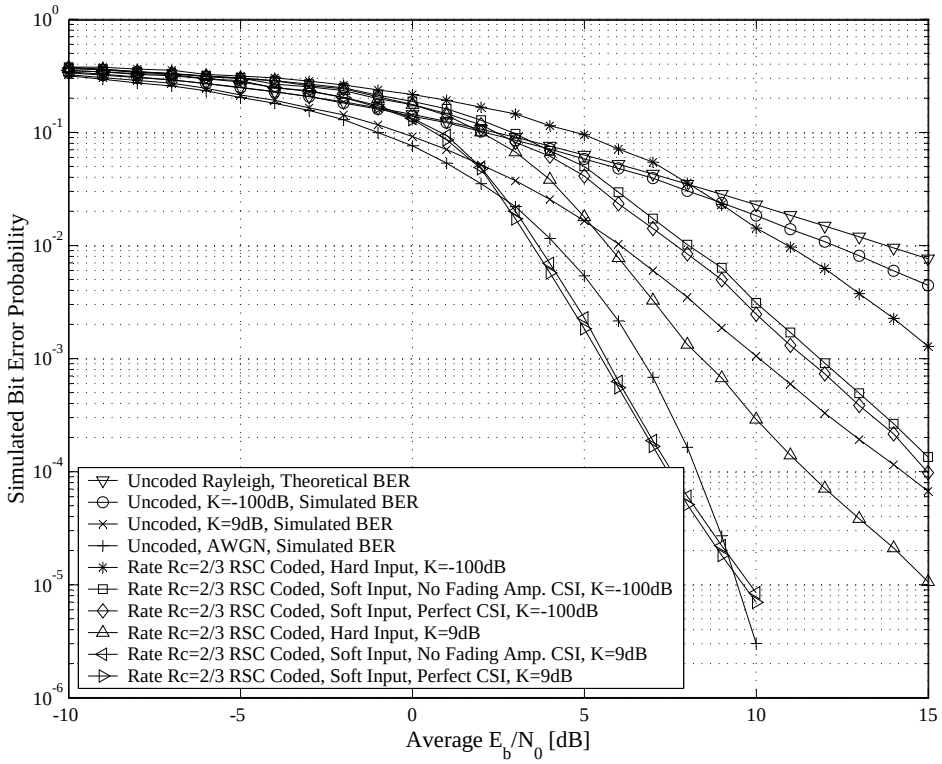

Figure 6.35: BER Performances of 8-State, Rate $R_c = 2/3$ RSC Coded Narrowband Complex QPSK Communication Systems in Flat Fading Channel Conditions, $B_{D,i} = 100$ Hz

6.5.2.2.3 Discussion of the Simulation Results

Listed below are several conclusions, drawn from the simulated AWGN and flat fading channel BER performance results for the 8-state, rate $R_c = 2/3$ RSC coded narrowband complex QPSK communication systems, presented in the preceding subsections:

1. Conclusions and observations from the AWGN channel results:

   - With a measured AWGN channel asymptotic coding gain of 3.8 dB over an uncoded narrowband complex QPSK communication system, *Fig.* 6.33 corroborates *Eq.* (3.8)'s theoretical maximum coding gain of $CG_{CC}^{soft} = 4.23$ dB for the soft decision VA decoded 8-state, rate $R_c = 2/3$ RSC code. Note that this code's coding gain is not only superior to that of the 4-state, rate $R_c = 1/2$ NSC code, considered in *Section* 6.5.2.1, but it also requires a lower bandwidth sacrifice. However, decoding complexity for the RSC code exceeds that of the NSC code, since the RSC code's VA functions on a 8-state trellis (see *Section* 3.3.1.1), whereas the NSC code's VA employs a 4-state trellis.
   - A comparison of *Fig.* 6.33's hard and soft decision VA decoding results in AWGN, reveals an expected asymptotic coding gain of 2.1 dB for soft decision decoding over the hard decision decoding.
   - The cross-over points for hard and soft decision VA decoding in AWGN channel conditions are 1.7 dB and 4.3 dB, respectively. Although the RSC code considered here is more powerful than *Section* 6.5.2.1's NSC code in terms of coding gain, its error correcting capabilities only become useable at higher E_b/N_0 values. This undesirable characteristic, inherent in all RSC codes, is the major reason why NSC codes have attracted more attention since the inception

of convolutional coding in the 1960's. However, the introduction of TCs has sparked a new and vigourous interest in RSC codes, due to their inherent recursive structures [88].

2. Conclusions and observations from the flat fading channel results:

   - *Fig.* 6.34 and *Fig.* 6.35 confirm that an increase in the flat fading channel's Rician factor K_i (see *Section* 2.5.2.2), results in improved BER performances for both hard and soft decision VA decoded rate $R_c = 2/3$ RSC codes.
   - From the flat fading channel simulation results (presented in *Fig.* 6.34 and *Fig.* 6.35), it is clear that the binary RSC code investigated here is better suited for non-bursty type errors, since its BER performances for $B_{D,i} = 100$ Hz exceed that of $B_{D,i} = 33$ Hz.
   - As was the case with the AWGN channel conditions, hard decision VA decoding of the rate $R_c = 2/3$ RSC code in a flat fading environment produced BER performance results inferior to that obtained through soft decision decoding. Specifically, soft decision VA decoding (without fading amplitude CSI), shows a familiar 2 dB asymptotic gain over hard decision decoding for all K_i and $B_{D,i} = 100$ Hz. However, for $B_{D,i} = 33$ Hz, this soft decision over hard decision gain is less, measuring approximately 1.7 dB for both $K_i = -100$ dB and $K_i = 9$ dB.
   - The inclusion of perfect fading amplitude CSI during soft decision VA decoding produced gains of 0.2 dB and 0.1 dB over standard soft decision decoding (i.e. without fading amplitude CSI) in flat fading channel conditions with $B_{D,i} = 100$ Hz and $B_{D,i} = 33$ Hz, respectively.
   - The coding gains observed for the rate $R_c = 2/3$ RSC in flat fading conditions are far less impressive than those obtained for the rate $R_c = 1/2$ NSC code, considered in *Section* 6.5.2.1. This can be largely attributed to the fact that the d_{free} of the RSC code is smaller than that of the NSC code. It is also interesting to note that, just as was the case with the binary NSC code of *Section* 6.5.2.1, better BER performances are obtained at higher maximum Doppler spreads.

6.5.3 COMMUNICATION SYSTEMS EMPLOYING VITERBI DECODED LINEAR BLOCK CODES

The following subsections present simulated BER performances of Viterbi decoded binary Hamming $(7, 4, 3)$ and non-binary RS $(7, 5, 3)$ coded communication systems under varying channel conditions. These codes were tested in AWGN and flat fading channel conditions, using narrowband complex QPSK communication systems (presented in *Section* 5.2), as well as multi-user multipath fading channel conditions, using wideband complex DS/SSMA communication systems (presented in *Section* 5.3). The RAKE receiver-based complex DS/SSMA communication systems employed length $M_{seq} = 63$ CSSs. For all of the CSS families considered, except ABC sequences, CSSs were arbitrarily selected from their respective sequence families. With the ABC sequences, CSSs were optimally selected, as discussed in *Section* 6.5.1.3.2.

6.5.3.1 BINARY HAMMING $(7, 4, 3)$ CODED COMMUNICATION SYSTEMS

Simulated AWGN, flat fading and multi-user multipath fading BER performance results for the classic binary Hamming $(7, 4, 3)$ code (see *Section* 3.2.2.3.1), described by the generator matrix defined in *Eq.* (4.4), are presented and examined in this subsection. Note that the binary Hamming code considered here is systematic and, like all other Hamming codes, has a minimum Hamming distance (see *Section* 3.2.2.2) of $d_{min} = 3$ bits. Furthermore, its BCJR trellis (see *Section* 4.2), which is not shown here due to its fairly complex structure, has a depth of 8 layers of nodes, each layer consisting of 8 nodes with 2 branches emanating from each active node. Both classic ML (brute force code book

searches) and VA (see *Section* 4.4) decoding approaches were considered using hard and soft (with and without perfect fading amplitude CSI) decision (see *Section* 4.4.2) strategies.

6.5.3.1.1 AWGN Channel Results

In *Fig.* 6.36 simulated AWGN channel (see *Section* 2.2) BER performances are shown for binary Hamming $(7, 4, 3)$ coded (see *Section* 3.2.2.3.1) narrowband complex QPSK communication systems (see *Section* 5.2). Both hard decision and soft decision (without using any fading amplitude CSI) classic ML [47] and VA decoding (see *Section* 4.4) results are present on this figure. Furthermore, the BER performance curve of an uncoded narrowband QPSK system in AWGN channel conditions, theoretically defined by *Eq.* (5.20), is also given in this figure as baseline reference.

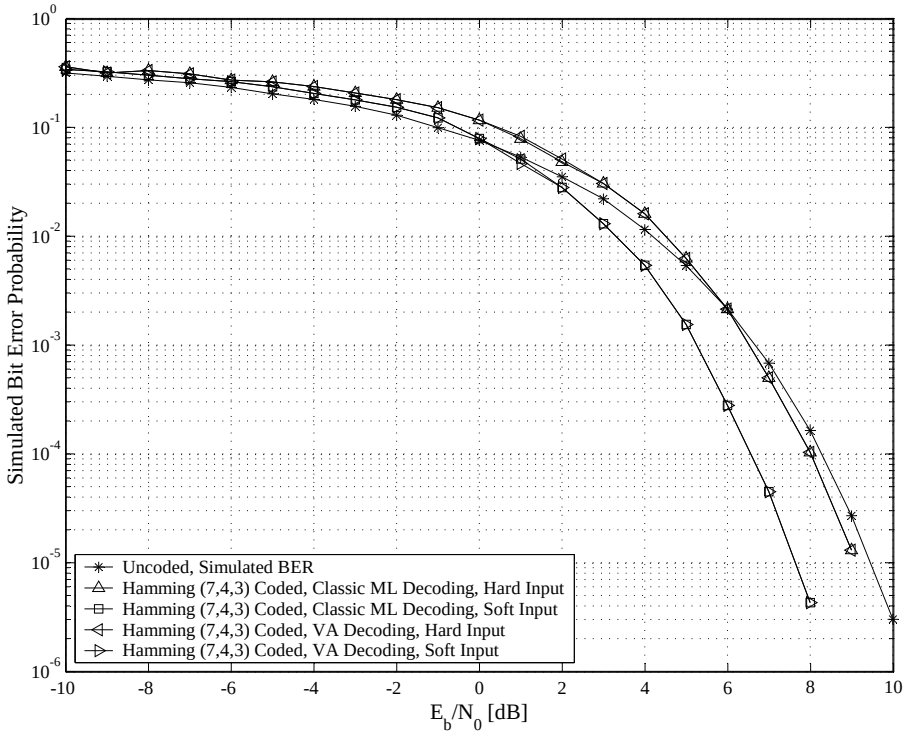

Figure 6.36: BER Performances of Binary Hamming $(7, 4, 3)$ Coded Narrowband Complex QPSK Communication Systems in AWGN Channel Conditions

6.5.3.1.2 Flat Fading Channel Results

Simulated BER performance results are shown in *Fig.* 6.37 and *Fig.* 6.38 for classic ML decoded binary Hamming $(7, 4, 3)$ coded narrowband complex QPSK communication systems (see *Section* 5.2) in flat fading channel conditions (see *Section* 2.5.1.1) with maximum Doppler spreads (see *Section* 2.4.3.3) of $B_{D,i} = 33$ Hz and $B_{D,i} = 100$ Hz, respectively. Similar results are shown respectively in *Fig.* 6.39 and *Fig.* 6.40 for VA decoding. Hard and soft (with and without perfect fading amplitude CSI) decision decoding were considered for both the classic ML and the VA decoding approaches. Furthermore, for both $B_{D,i} = 33$ Hz and $B_{D,i} = 100$ Hz, results include simulated BER curves for Rician factors (see *Section* 2.5.2.2) of $K_i = -100$ dB, $K_i = 0$ dB and $K_i = 9$ dB. The theoretical BER performance curves for uncoded QPSK systems in slow Rayleigh flat fading channel conditions, defined by *Eq.* (5.24), as well as simulated BER performance curves for uncoded QPSK systems in AWGN channel conditions are present on all four figures.

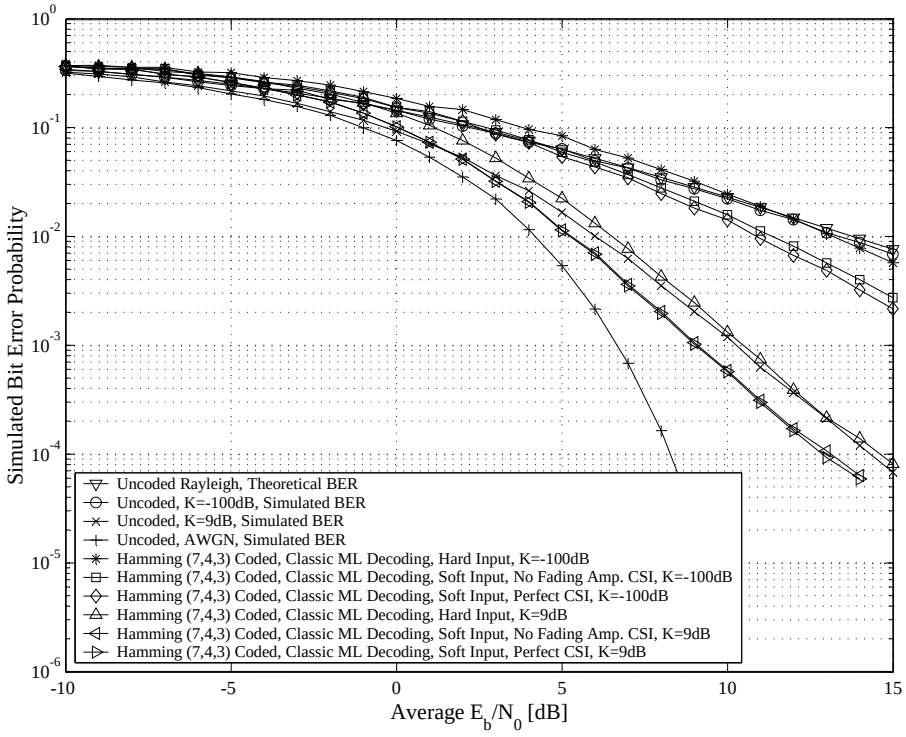

Figure 6.37: BER Performances of Binary Hamming $(7, 4, 3)$ Block Coded Narrowband Complex QPSK Communication Systems in Flat Fading Channel Conditions, $B_{D,i} = 33$ Hz, Classic ML Decoding

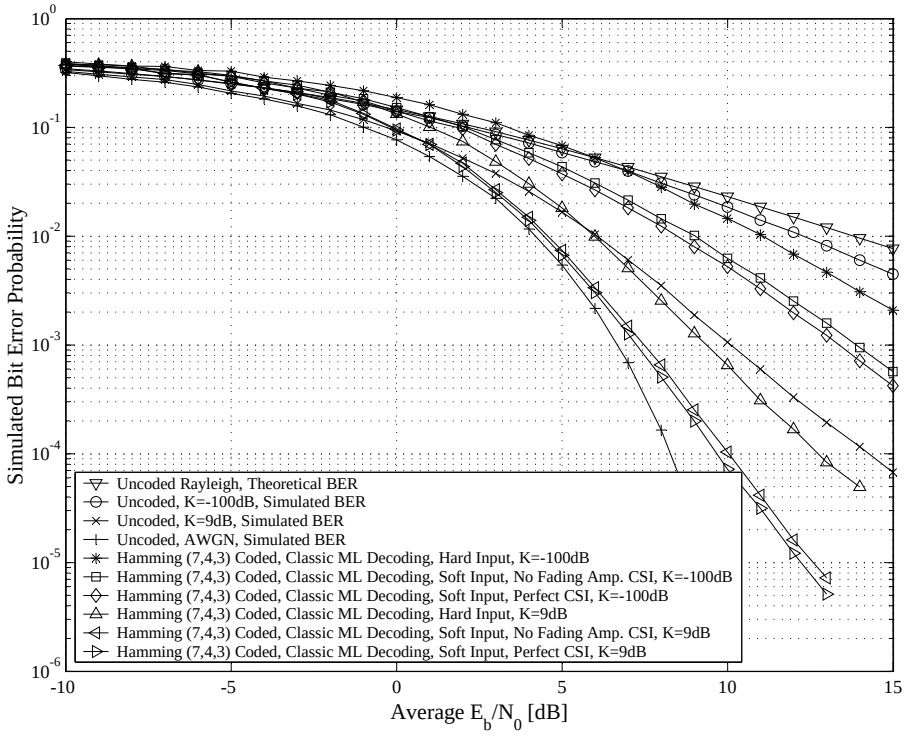

Figure 6.38: BER Performances of Binary Hamming $(7, 4, 3)$ Block Coded Narrowband Complex QPSK Communication Systems in Flat Fading Channel Conditions, $B_{D,i} = 100$ Hz, Classic ML Decoding

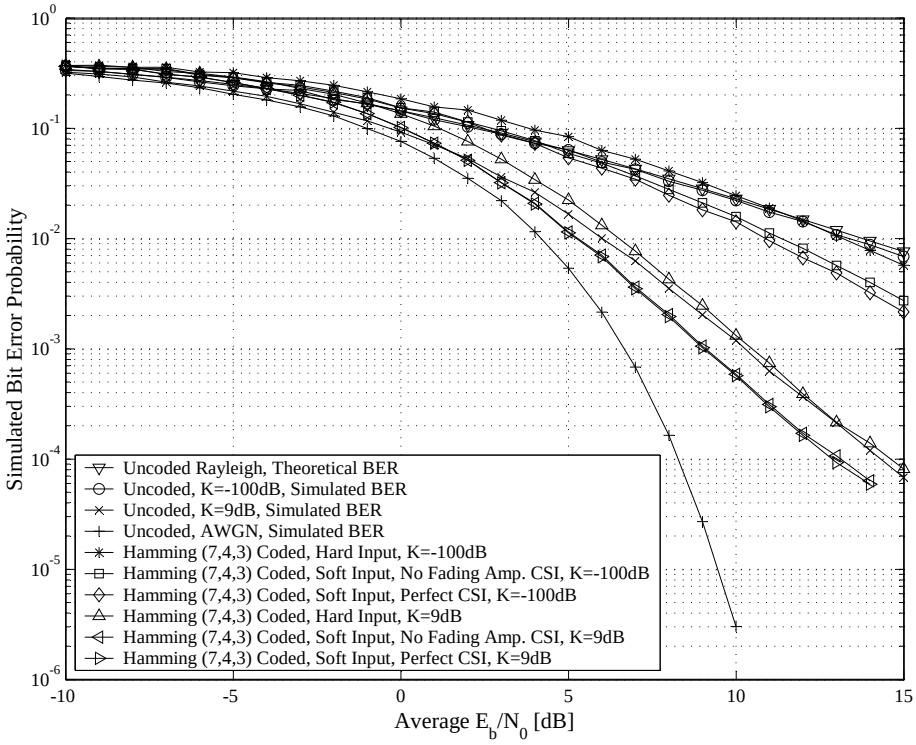

Figure 6.39: BER Performances of Binary Hamming $(7, 4, 3)$ Block Coded Narrowband Complex QPSK Communication Systems in Flat Fading Channel Conditions, $B_{D,i} = 33$ Hz, VA Decoding

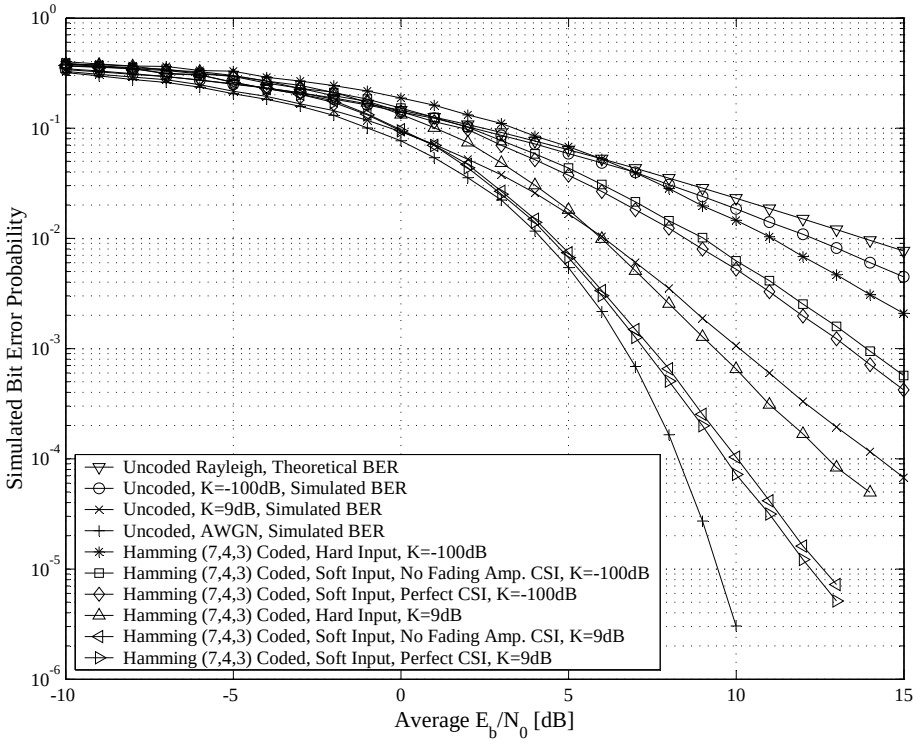

Figure 6.40: BER Performances of Binary Hamming $(7, 4, 3)$ Block Coded Narrowband Complex QPSK Communication Systems in Flat Fading Channel Conditions, $B_{D,i} = 100$ Hz, VA Decoding

6.5.3.1.3 Multipath Fading Channel Results

Simulated multi-user multipath fading channel BER performance results for binary Hamming $(7, 4, 3)$ coded RAKE receiver-based wideband complex DS/SSMA QPSK systems (see *Section* 5.3) with VA decoding, employing length $M_{seq} = 63$ ABC (see *Section* D.3.2.2), DSB CE-LI-RU filtered GCL (see *Section* D.3.2.1), ZC (see *Section* D.3.1.1) and QPH (see *Section* D.3.1.2) CSSs, are shown in *Fig.* 6.41, *Fig.* 6.42, *Fig.* 6.43 and *Fig.* 6.44, respectively. Hard and soft decision (with and without fading amplitude CSI (see *Section* 3.3.5 and *Section* 5.3.3)) VA decoding (see *Section* 4.4) were considered during these simulations. Also depicted on these figures are the simulated BER performances for uncoded RAKE receiver-based wideband complex DS/SSMA QPSK systems (presented in *Section* 6.5.1.3.1), as well as the BER performance of an uncoded system, without a RAKE receiver, operating in a purely AWGN environment.

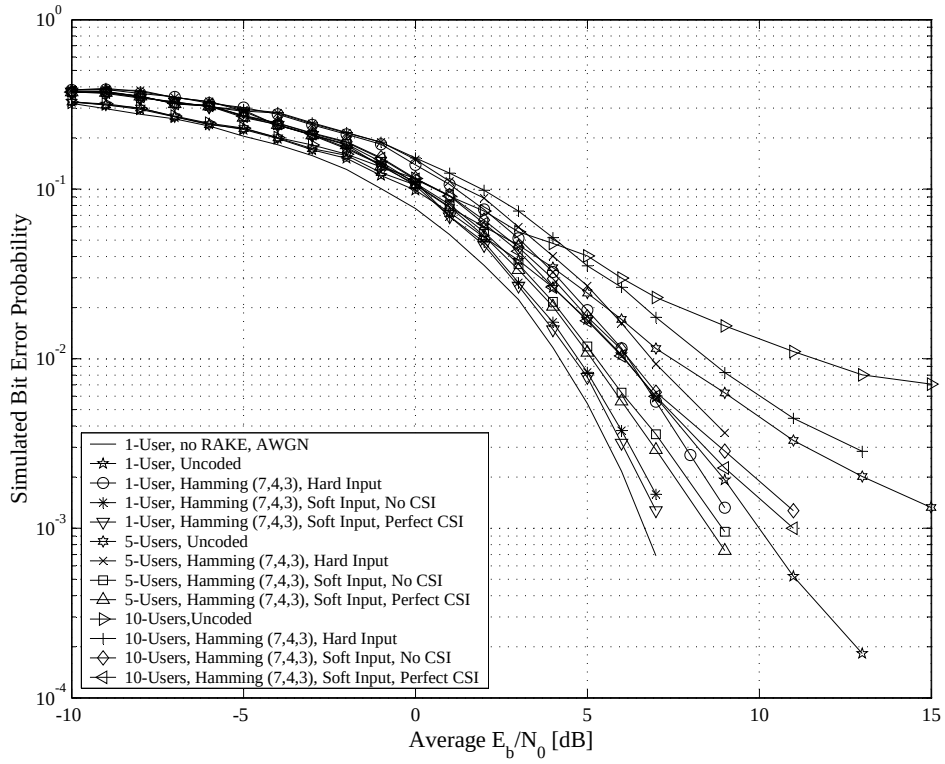

Figure 6.41: BER Performances of Binary Hamming $(7, 4, 3)$ Coded Wideband Complex QPSK Communication Systems Employing ABC Sequences in Multi-User Multipath Fading Channel Conditions, $M_{seq} = 63$

6.5.3.1.4 Discussion of the Simulation Results

The preceding subsections' simulated AWGN, flat fading and multi-user multipath fading channel BER performance results for VA decoded binary Hamming $(7, 4, 3)$ codes, running on narrowband complex QPSK communication systems and RAKE receiver-based wideband complex DS/SSMA QPSK systems, were thoroughly examined. The list below summarises the conclusions drawn from these results:

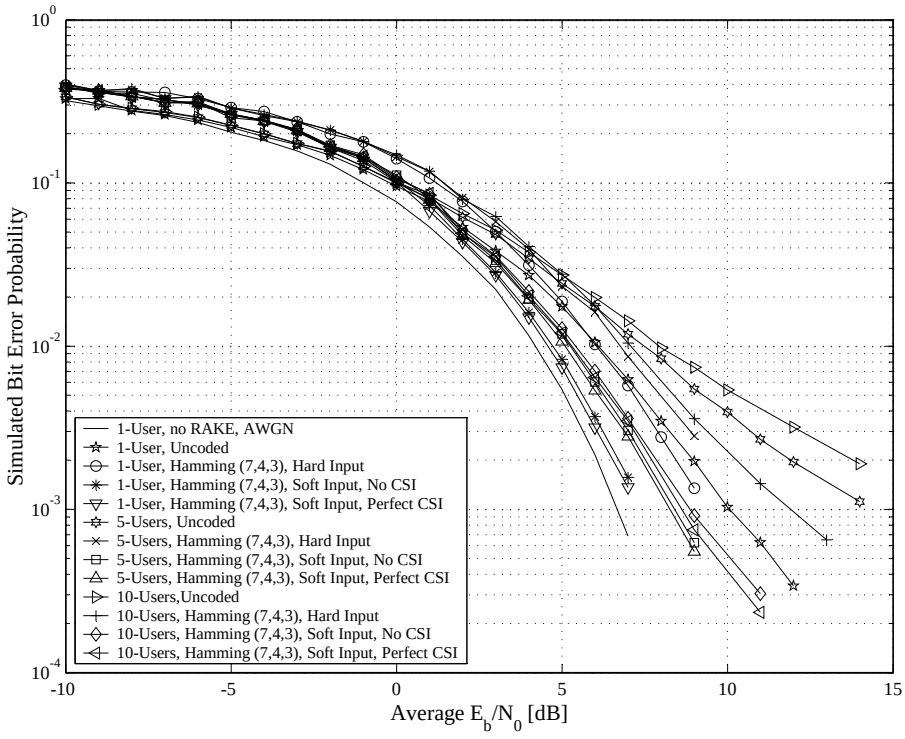

Figure 6.42: BER Performances of Binary Hamming $(7, 4, 3)$ Coded Wideband Complex QPSK Communication Systems Employing DSB CE-LI-RU Filtered GCL CSSs in Multi-User Multipath Fading Channel Conditions, $M_{seq} = 63$

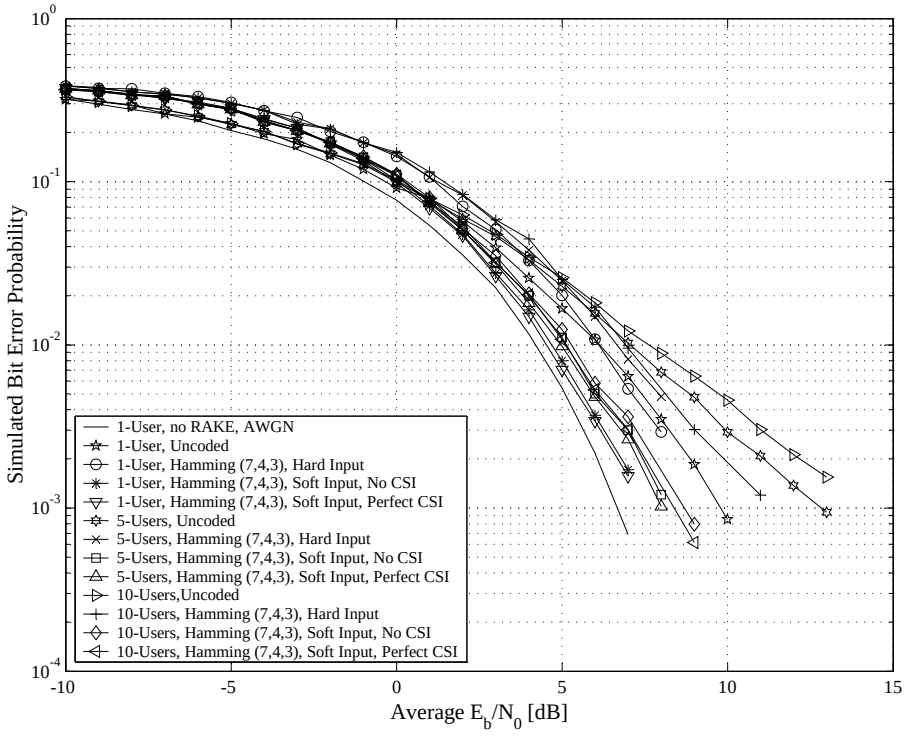

Figure 6.43: BER Performances of Binary Hamming $(7, 4, 3)$ Coded Wideband Complex QPSK Communication Systems Employing ZC CSSs in Multi-User Multipath Fading Channel Conditions, $M_{seq} = 63$

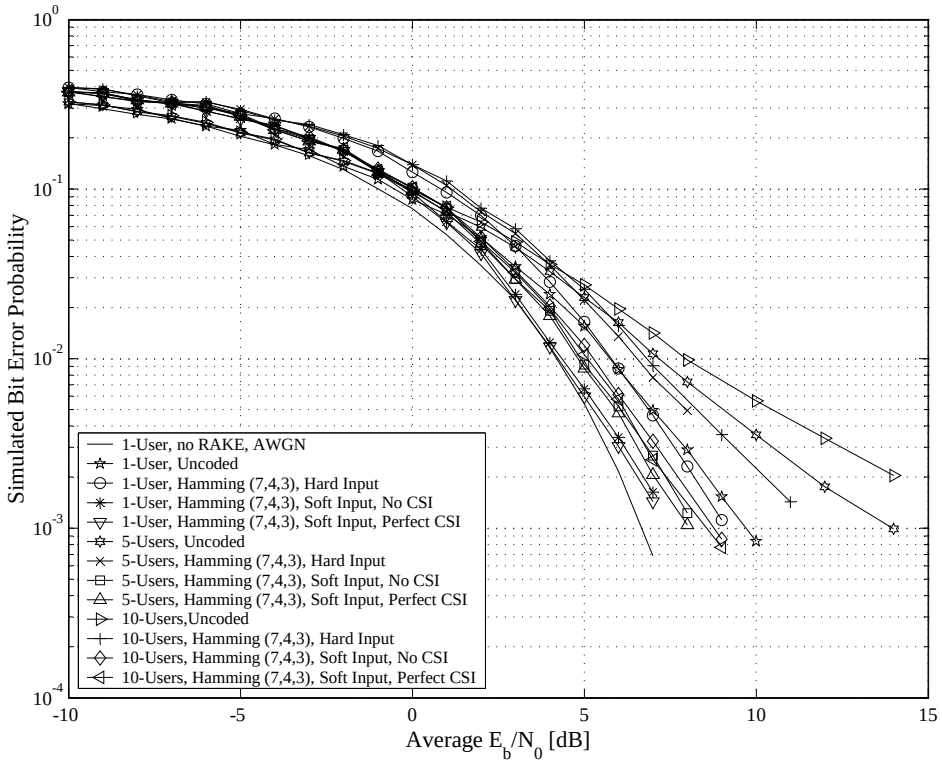

Figure 6.44: BER Performances of Binary Hamming $(7, 4, 3)$ Coded Wideband Complex QPSK Communication Systems Employing QPH CSSs in Multi-User Multipath Fading Channel Conditions, $M_{seq} = 63$

1. Conclusions and observations from the AWGN channel results:

   - According to *Eq.* (3.25), a soft decision ML decoded binary Hamming $(7, 4, 3)$ code, implemented on narrowband complex QPSK communication system in an AWGN environment, delivers a theoretical maximum asymptotic coding gain of $CG_{BC}^{soft} = 2.11$ dB at $E_b/N_0 = 15$ dB. *Fig.* 6.36 shows this theoretical coding gain to be adequately accurate for both classic ML and VA decoding with soft decisions, since a measured asymptotic coding gain of 1.9 dB can be observed for both decoding strategies.
   - From *Fig.* 6.36 it is apparent that hard and soft decision VA decoding of binary Hamming $(7, 4, 3)$ codes, employed on narrowband complex QPSK systems in AWGN channel conditions, deliver BER performances virtually identical to classic hard and soft decision ML decoding (brute force code book searches [47]).
   - Soft decision ML decoding's distinctive 2 dB gain over hard decision ML decoding in AWGN [47] is unmistakeably noticeable from *Fig.* 6.36. Furthermore, note that the system complexity associated with a hard decision ML decoded binary Hamming $(7, 4, 3)$ code barely justifies the resultant improvement in BER performance. However, for soft decision ML decoding a cross-over point (see *Section* 6.5.2.1.4) of approximately 0.5 dB can be observed. As such, it can be argued that the use of simple binary Hamming $(7, 4, 3)$ codes (with soft decision VA decoding) in high SNR applications warrants the increased system complexity.

2. Conclusions and observations from the flat fading channel results:

- Comparisons of *Fig.* 6.37 with *Fig.* 6.39, and *Fig.* 6.38 with *Fig.* 6.40 verify that, for both hard and soft decision metric calculations, classic ML decoding and VA trellis decoding of the binary Hamming $(7, 4, 3)$ code achieve equivalent BER performances in varying flat fading channel conditions.
- From the myriad of flat fading simulation results presented in *Section* 6.5.3.1.2, it is abundantly clear that the BER performance of VA and classic ML decoded binary Hamming $(7, 4, 3)$ codes, employed in narrowband QPSK systems, improve as the channel's LOS signal component increases with respect to the NLOS signal component. On average, however, the increased BER performance obtained by increasing K_i, is most evident at $B_{D,i} = 100$ Hz. This was to be expected, since the binary Hamming $(7, 4, 3)$ code is not designed to mitigate the detrimental effects of error bursts, which manifested itself with increased durations as the fading rate becomes slower.
- A comparison of hard decision decoding with soft decision decoding (without fading amplitude CSI) in a flat fading environment reveals soft decision decoding's renowned 2 dB gain over hard decision decoding. Inclusion of perfect fading amplitude CSI during soft decision decoding resulted in a marginal improvement in the measured performances. This improvement, which is most noticeable at $K_i = -100$ dB, was approximately 0.25 dB for $B_{D,i} = 100$ Hz, whereas as an average gain of 0.4 dB is discernible for $B_{D,i} = 33$ Hz.

3. Conclusions and observations from the multi-user multipath fading channel results:

- Substantiating the AWGN and flat fading channel observations, the results presented in *Fig.* 6.41, *Fig.* 6.42, *Fig.* 6.43 and *Fig.* 6.44 for VA decoded binary Hamming $(7, 4, 3)$ block codes in multi-user multipath fading channel conditions indicate that this linear block code is not particularly effective for FEC purposes. For the single user scenario, hard decision VA decoded Hamming $(7, 4, 3)$ codes, implemented on RAKE receiver-based wideband complex DS/SSMA QPSK communication systems, only starts to show gains for $\overline{E}_b/N_0 > 6$ dB, irrespective of the CSS family employed. Strangely enough, as the user load increases, hard decision VA decoding makes headway over uncoded systems at lower average E_b/N_0 values. The conclusion that can be formulated from this is that the binary Hamming $(7, 4, 3)$ code does have some potency against the effects of MUI, even though it was not designed for that purpose. When soft decision VA decoding (without fading amplitude CSI) is employed in a single user CDMA system, asymptotic gains of up to 2.5 dB and 2.2 dB are achieved by the filtered and unfiltered CSS families, respectively. This correlates well with the expected AWGN coding gain of $CG_{BC}^{soft} = 2.11$ dB, predicted by *Eq.* (3.25).
- As was to be expected, the pre-filtered CSSs were once again outperformed by the unfiltered CSS families. According to *Fig.* 6.41, *Fig.* 6.42, *Fig.* 6.43 and *Fig.* 6.44, VA decoded binary Hamming $(7, 4, 3)$ linear block codes, running on RAKE receiver-based complex DS/SSMA QPSK systems employing ABC sequences deliver the poorest BER performance results, whereas QPH CSSs has the best BER performance results at high user loads, closely followed by ZC CSSs. In fact, the performance difference between ZC and QPH CSSs never exceeds 0.25 dB. In third place is DSB CE-LI-RU filtered GCL CSSs, which outperform ABC sequences for all decoder approaches and user load scenarios. Also worth mentioning is that this filtered CSS family performs comparable with the unfiltered families considered, even for a 10-user load.
- Once again the unfiltered CSS families' superior periodic cross-correlation properties are evident. For both hard and soft decision VA decoding, the 1-user and 5-user BER performance results for binary Hamming $(7, 4, 3)$ coded complex DS/SSMA systems employing the unfiltered ZC and QPH CSS families are nearly the same. However, for a 10-user CDMA system, there is a marked decrease in BER performance, even for the unfiltered CSS families.

- At low user loads soft decision (without fading amplitude CSI) VA decoding of the binary Hamming $(7, 4, 3)$ linear block code in multi-user multipath fading channel conditions performs approximately 2 dB better than hard decision VA decoding, regardless of the CSS family used. At higher user loads, this asymptotic gain decreases. For example, at a BER of $P_b(e) = 2/100$ for a 10-user QPH CSS-based CDMA system, soft decision decoding (without fading amplitude CSI) exhibits a gain of only 1.8 dB over hard decision decoding. This performance decrease at high user loads is most severe for the filtered CSS families. Furthermore, an additional average improvement of 0.2 dB is attained by including perfect fading amplitude CSI during soft decision VA decoding, irrespective of the user load or the CSS family employed in the CDMA system.

6.5.3.2 NON-BINARY REED-SOLOMON $(7, 5, 3)$ CODED COMMUNICATION SYSTEMS

Gauging the BER performances of Viterbi decoded non-binary RS block codes (see *Section* 3.2.2.3.3) in AWGN, flat fading and multi-user multipath fading channel conditions is the focus of the following subsections. Due to the complexity of the BCJR trellis structures (see *Section* 4.3) of non-binary linear block codes, the applicability of the block-wise VA as efficient ML trellis decoder was evaluated only on the simple RS $(7, 5, 3)$ code, operating in $GF\left(2^3\right)$, defined by the generator polynomial of *Eq.* (3.35). Since this RS code is cyclic (see *Section* 3.2.2.2), its non-systematic generator matrix can be constructed using the procedure outlined in *Section* 3.2.2.2. This non-systematic generator matrix can be reworked into a systematic form (see *Section* 3.2.2.2) by performing a number of row and column permutations (using, for example, Gaussian elimination) in $GF\left(2^3\right)$, resulting in the following systematic generator matrix:

$$G_{BC} = \begin{bmatrix} 1 & 0 & 0 & 0 & 0 & \varphi^4 & \varphi \\ 0 & 1 & 0 & 0 & 0 & \varphi^5 & \varphi \\ 0 & 0 & 1 & 0 & 0 & \varphi^5 & \varphi^3 \\ 0 & 0 & 0 & 1 & 0 & 1 & 1 \\ 0 & 0 & 0 & 0 & 1 & \varphi^4 & \varphi^3 \end{bmatrix} \tag{6.5}$$

where φ is a primitive element of $GF\left(2^3\right)$. This code has a minimum Hamming distance of $d_{min} = 3$ $GF\left(2^3\right)$ symbols and its BCJR trellis (see *Section* 4.2), which is not shown here due to its extremely complex structure, has a depth of 8 layers of nodes, each layer consisting of 64 nodes with 8 branches emanating from each active node.

Also included in the simulation results presented in the following subsections, are the BER performance curves obtained using Berlekamp-Massey syndrome decoding (see *Appendix B*). These results act as baseline references for the hard decision VA decoding (see *Section* 4.4) results. Soft decision VA decoding (see *Section* 4.4.2.2) with no fading amplitude CSI is compared to soft decision VA decoding with perfect fading amplitude CSI (see *Section* 3.3.5).

6.5.3.2.1 AWGN Channel Results

Fig. 6.45 depicts simulated AWGN channel BER performances for narrowband complex QPSK communication systems (see *Section* 5.2) employing non-binary RS $(7, 5, 3)$ codes (see *Section* 3.2.2.3.3), with message and code word symbols from $GF\left(2^3\right)$. Not only are hard decision and soft decision (without using any fading amplitude CSI) VA decoding (see *Section* 4.4) results present on this figure, but also hard decision results obtained through classic Berlekamp-Massey syndrome decoding (see *Appendix B*). As baseline reference, the theoretical BER performance curve of an uncoded narrowband QPSK system in AWGN channel conditions, defined by *Eq.* (5.20), is also present on this figure.

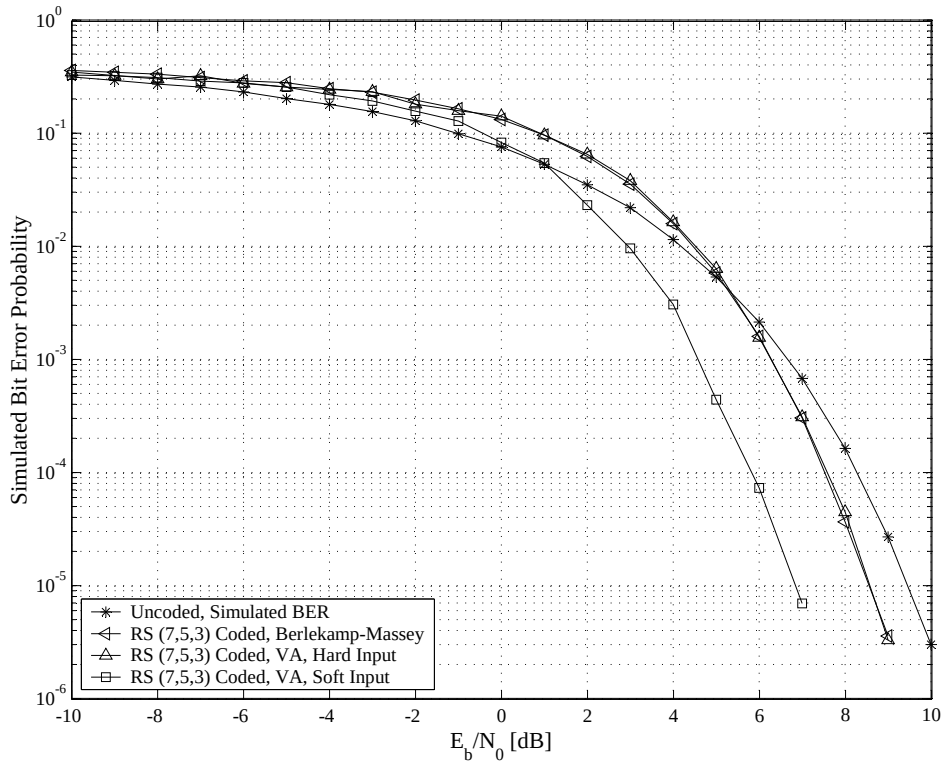

Figure 6.45: BER Performances of Non-Binary RS $(7, 5, 3)$ Coded Narrowband Complex QPSK Communication Systems in AWGN Channel Conditions

6.5.3.2.2 Flat Fading Channel Results

Fig. 6.46 and *Fig.* 6.47 depict BER performance results (obtained through simulations) for non-binary RS $(7, 5, 3)$ (see *Section* 3.2.2.3.3) coded narrowband complex QPSK communication systems (see *Section* 5.2) operating in flat fading channel (see *Section* 2.5.1.1) conditions with maximum Doppler spreads (see *Section* 2.4.3.3) of $B_{D,i} = 33$ Hz and $B_{D,i} = 100$ Hz, respectively. As shown on these figures, Rician factors (see *Section* 2.5.2.2) of $K_i = -100$ dB, $K_i = 0$ dB and $K_i = 9$ dB were considered. Furthermore, note that both hard and soft decision VA decoding (see *Section* 4.4) of the RS $(7, 5, 3)$ codes were evaluated, with fading amplitude CSI (see *Section* 3.3.5 and *Section* 5.2.3) of varying degrees of accuracy being employed during the soft decision decoding simulation experiments. Also included on both figures are the simulated BER performance curves of uncoded QPSK systems in AWGN channel conditions, as well as *Eq.* (5.24)'s theoretical BER performance curve for uncoded QPSK systems in slow Rayleigh flat fading channel conditions.

6.5.3.2.3 Multipath Fading Channel Results

Fig. 6.48, *Fig.* 6.49, *Fig.* 6.50 and *Fig.* 6.51 depict simulated multi-user multipath fading channel BER performance results for non-binary RS $(7, 5, 3)$ coded (see *Section* 3.2.2.3.3) RAKE receiver-based wideband complex DS/SSMA QPSK systems (see *Section* 5.3), which make use of length $M_{seq} = 63$ ABC (see *Section* D.3.2.2), DSB CE-LI-RU filtered GCL (see *Section* D.3.2.1), ZC (see *Section* D.3.1.1) and QPH (see *Section* D.3.1.2) CSSs, respectively. VA decoding (see *Section* 4.4) was employed, with both hard and soft decision (with and without fading amplitude CSI (see

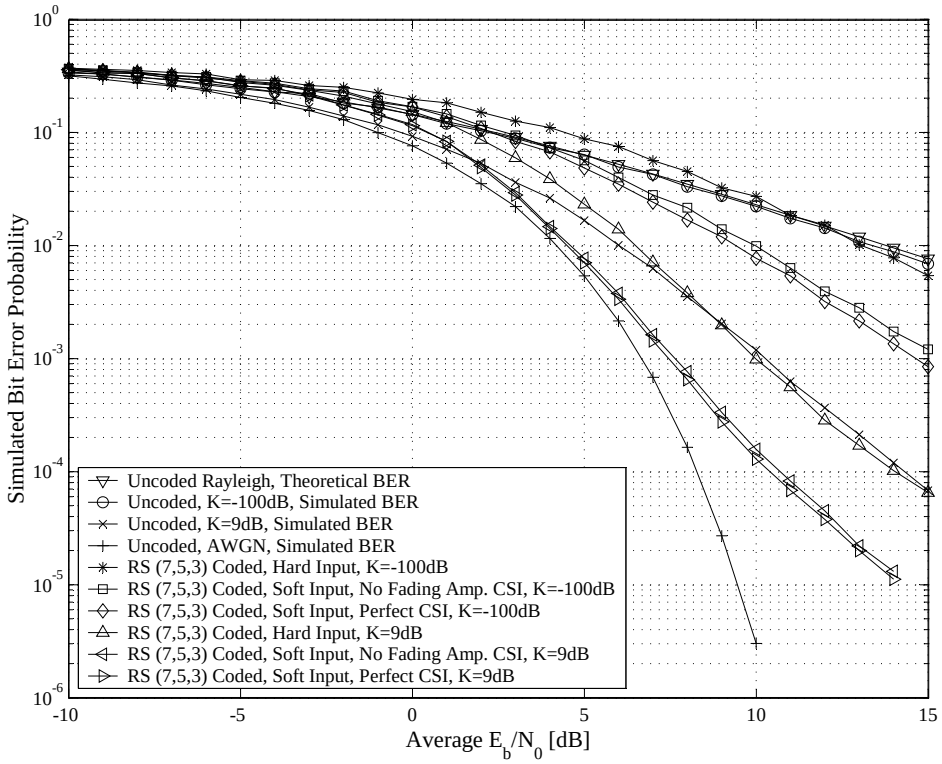

Figure 6.46: BER Performances of Non-binary RS $(7, 5, 3)$ Coded Narrowband Complex QPSK Communication Systems in Flat Fading Channel Conditions, $B_{D,i} = 33$ Hz

Section 3.3.5 and *Section* 5.3.3)) BER performance results shown on these figures for each of the CSS families. Furthermore, *Section* 6.5.1.3.1's uncoded RAKE receiver-based wideband complex DS/SSMA QPSK systems' simulated BER performances, as well as the BER performance of an uncoded system (without a RAKE receiver), operating in a purely AWGN environment, are also shown for baseline reference purposes.

6.5.3.2.4 Discussion of the Simulation Results

Numerous simulated AWGN, flat fading and multi-user multipath fading channel BER performance results are presented in the preceding subsections for non-binary RS $(7, 5, 3)$ coded narrowband complex QPSK communication systems and RAKE receiver-based wideband complex DS/SSMA QPSK systems. Classic Berlekamp-Massey and block-wise VA decoding approaches were considered. From these results the following interesting observations and valuable conclusions can be made:

1. Conclusions and observations from the AWGN channel results:

   - *Fig.* 6.45's simulated AWGN channel BER performance results undeniably affirms the applicability of the hard decision VA as a viable ML decoder replacement for the classic Berlekamp-Massey syndrome decoding algorithm (see *Appendix B*).
   - The simulated AWGN channel soft decision VA decoding results for a non-binary RS $(7, 5, 3)$ coded narrowband complex QPSK system, presented in *Fig.* 6.45, not only exhibit the expected 2 dB improvement over hard decision decoding, but also an asymptotic coding gain of 2.8 dB over an uncoded system. This measurement correlates well with *Eq.* (3.25)'s theoretical maximum coding gain of $CG_{BC}^{soft} = 3.1$ dB at $E_b/N_0 = 15$ dB.

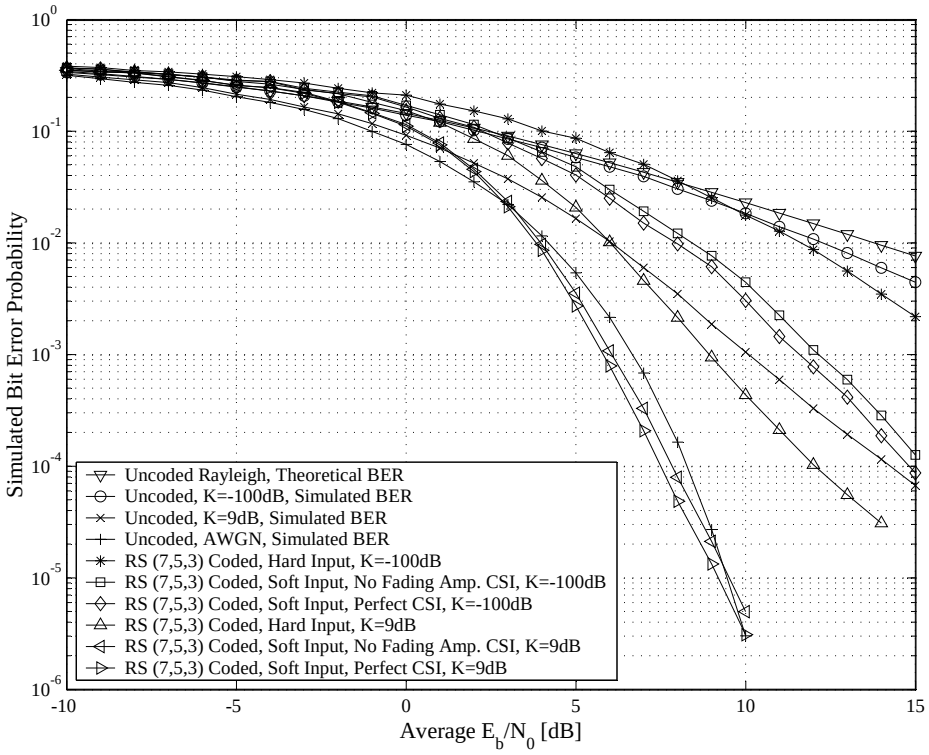

Figure 6.47: BER Performances of Non-binary RS $(7, 5, 3)$ Coded Narrowband Complex QPSK Communication Systems in Flat Fading Channel Conditions, $B_{D,i} = 100$ Hz

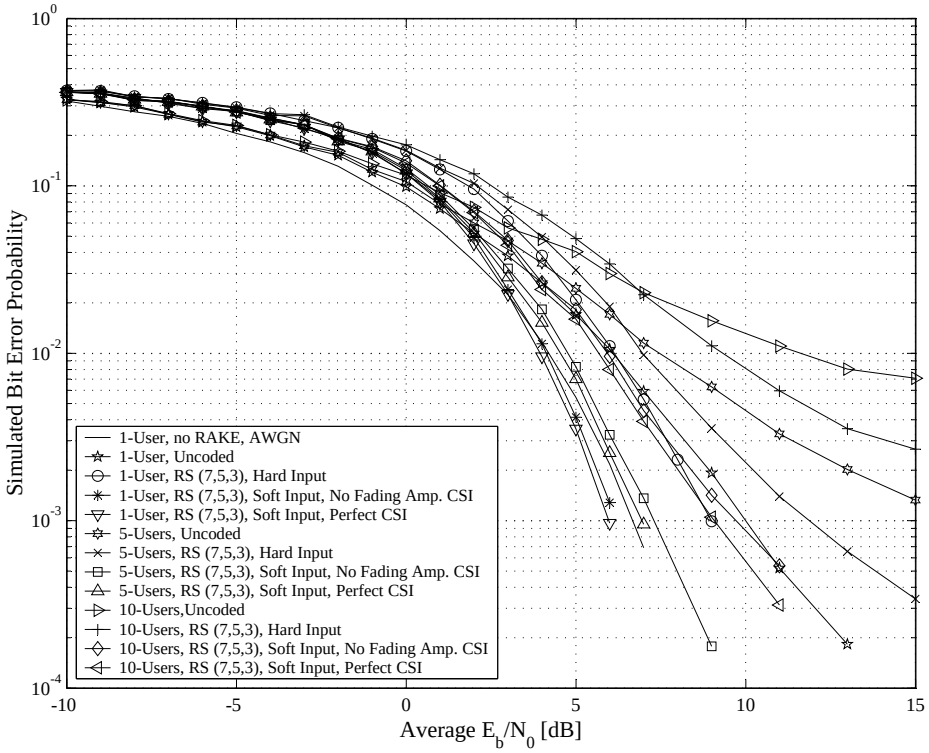

Figure 6.48: BER Performances of Non-Binary RS $(7, 5, 3)$ Coded Wideband Complex QPSK Communication Systems Employing ABC Sequences in Multi-User Multipath Fading Channel Conditions, $M_{seq} = 63$

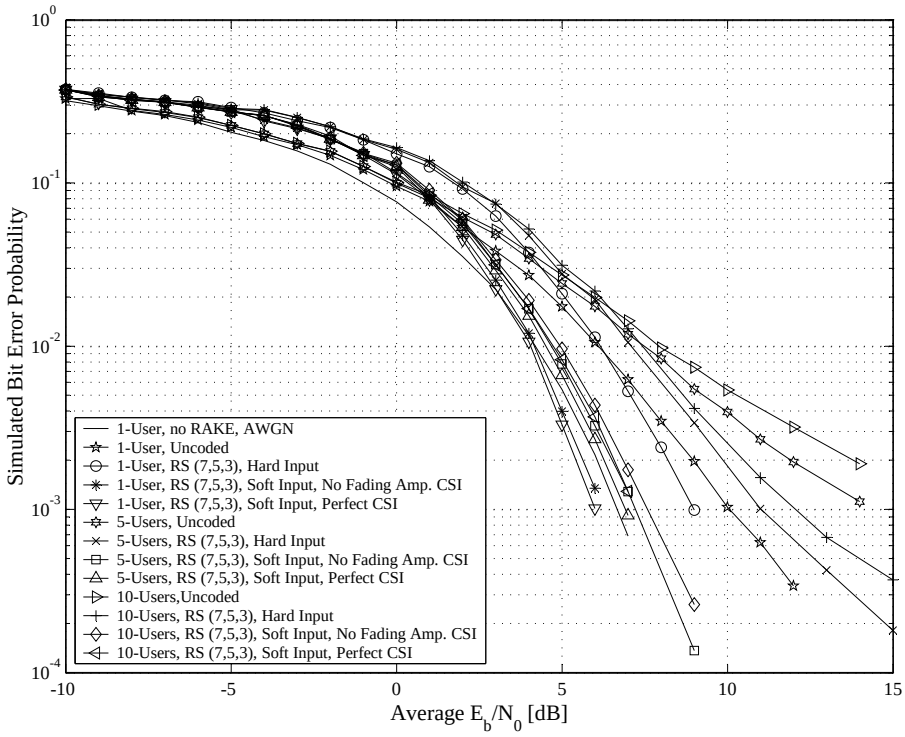

Figure 6.49: BER Performances of Non-Binary RS $(7, 5, 3)$ Coded Wideband Complex QPSK Communication Systems Employing DSB CE-LI-RU Filtered GCL CSSs in Multi-User Multipath Fading Channel Conditions, $M_{seq} = 63$

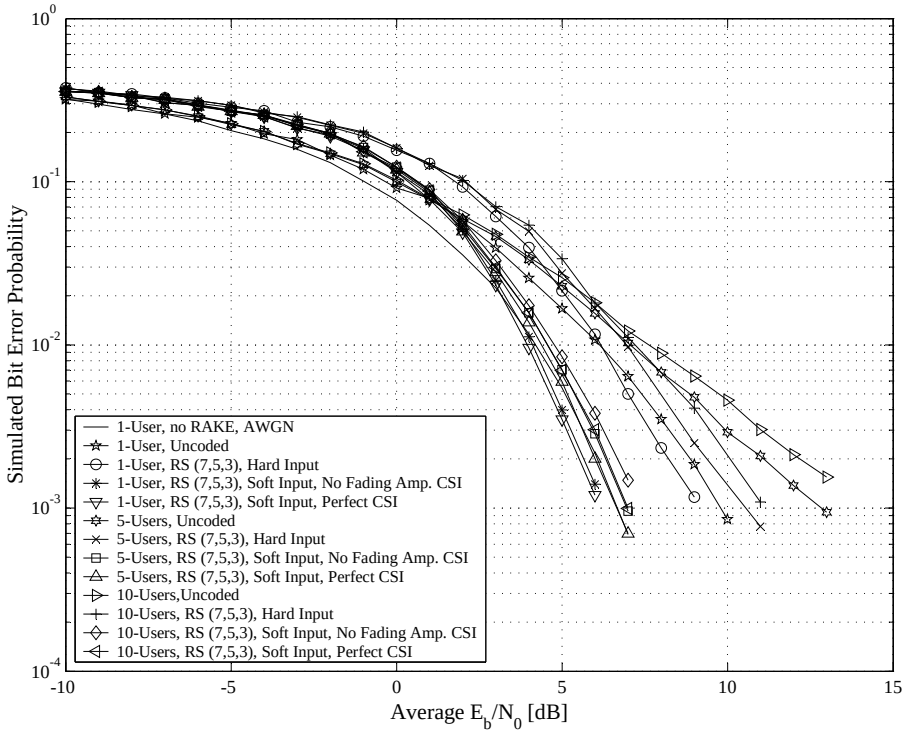

Figure 6.50: BER Performances of Non-Binary RS $(7, 5, 3)$ Coded Wideband Complex QPSK Communication Systems Employing ZC CSSs in Multi-User Multipath Fading Channel Conditions, $M_{seq} = 63$

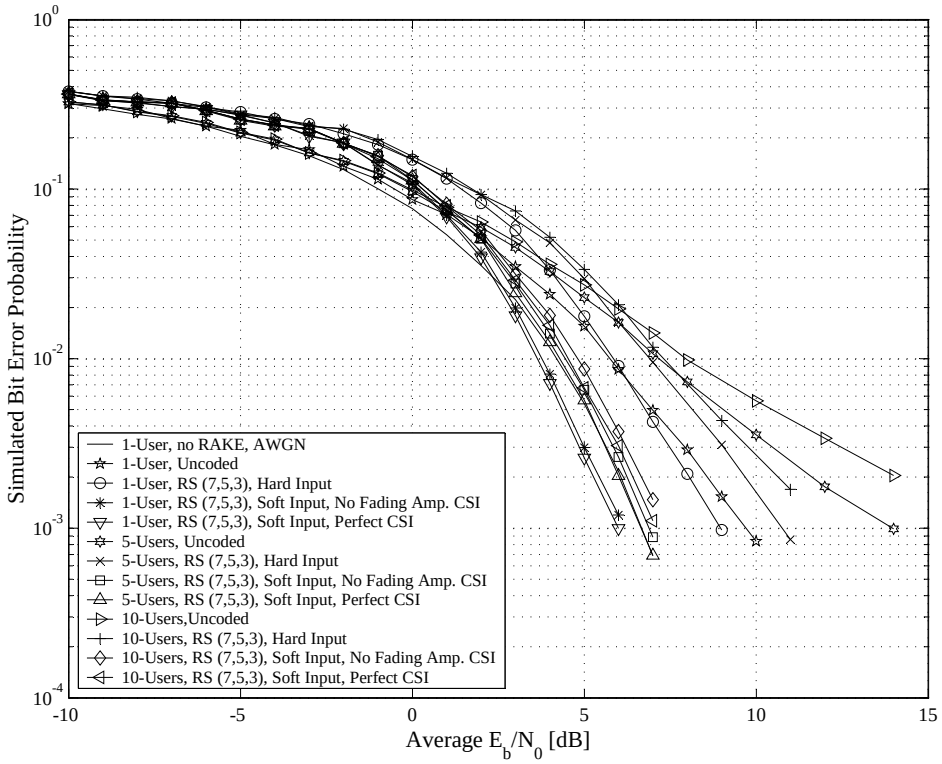

Figure 6.51: BER Performances of Non-Binary RS $(7, 5, 3)$ Coded Wideband Complex QPSK Communication Systems Employing QPH CSSs in Multi-User Multipath Fading Channel Conditions, $M_{seq} = 63$

- The respective cross-over points (see *Section* 6.5.2.1.4) for hard and soft decision VA decoded non-binary RS $(7, 5, 3)$ codes on narrowband complex QPSK systems are 5 dB and 1 dB. Strangely enough, these cross-over points are akin to those of the binary Hamming $(7, 4, 3)$ code (considered in *Section* 6.5.3.1), which is a substantially less powerful linear block code.

2. Conclusions and observations from the flat fading channel results:

   - As indicated by *Fig.* 6.46 and *Fig.* 6.47, VA decoded non-binary RS $(7, 5, 3)$ linear block codes show marked BER performance improvements in flat fading channel conditions as the channels' Rician factors K_i (see *Section* 2.5.2.2) increase. This was to be expected, since an increase in a flat fading channel's Rician factor tends to make it appear more Gaussian-like in nature, which is necessary requirement by all linear block codes, including RS codes, for optimal BER performances.
   - Inspection of *Fig.* 6.46 and *Fig.* 6.47 not only shows that VA decoded non-binary RS codes, implemented on a narrowband complex QPSK communication system, perform better at higher maximum Doppler spreads, but also that the gain of soft decision decoding, with perfect fading amplitude CSI, over that of soft decision decoding, without fading amplitude CSI, increases as the maximum Doppler spread increases. For a Rician factor of $K_i = 9$ dB, this gain is approximately 0.26 dB and 0.4 dB for $B_{D,i} = 33$ Hz and $B_{D,i} = 100$ Hz, respectively.
   - As stated previously, the RS code performs better at $B_{D,i} = 100$ Hz than at $B_{D,i} = 33$ Hz. However, the performance improvement is less dramatic than that observed for the foregoing binary convolutional and linear block codes. This can be attributed to the fact that RS codes are burst error correcting codes, capable of correcting groups of errors. Recall that the RS

$(7, 5, 3)$ code considered here has a $d_{min} = 3$ $GF\left(2^3\right)$ symbols. Hence, each code word is capable of correcting a single error burst, consisting of 3 well-organised (i.e. adjacent) bit errors.

- In flat fading channel conditions, hard decision VA decoding lags soft decision VA decoding by almost 3 dB. For $B_{D,i} = 100$ Hz and $K_i = 9$ dB, this gain is not asymptotic, since it increases non-linearly as the average E_b/N_0 increases.

3. Conclusions and observations from the multi-user multipath fading channel results:

- Investigation of the multi-user multipath fading channel results given in *Fig.* 6.48, *Fig.* 6.49, *Fig.* 6.50 and *Fig.* 6.51 confirms that the VA decoding of non-binary RS $(7, 5, 3)$ linear block codes, implemented on RAKE receiver-based wideband complex DS/SSMA QPSK systems, delivers marked BER performance improvements for all CSS families considered. Although the non-binary RS code effectively combats the bursty errors induced by the multipath fading channel, it is not as efficient at mitigating the effects of MUI as the binary rate $R_c = 1/2$ NSC code, considered in *Section* 6.5.2.1. This is most noticeable for ABC sequences, where hard decision VA decoding in a 10-user system exhibits a cross-over point only at 7 dB. For the other CSS families, this crossover-point is substantially lower, especially for the unfiltered families.
- When soft decision (without fading amplitude CSI) VA decoding is employed in a single user environment, the RS $(7, 5, 3)$ code performs better at high $\overline{E}_b/N_0$ values than an uncoded DS/SSMA system operating in purely AWGN channel conditions. Furthermore, for the single user scenario, soft decision (without fading amplitude CSI) VA decoding of RS code exhibits increasing coding gains over the uncoded system as the average E_b/N_0 increases. For example, at $P_b(e) = 10^{-3}$ a coding gain of $CG_{BC}^{soft} = 3.4$ dB is observed, irrespective of the CSS family used.
- In terms of overall performance, the unfiltered CSSs exhibited the best performances, with QPH CSSs outperforming ZC CSSs by no more than 0.3 dB at high user loads. As was to be expected, ABC sequences demonstrated the poorest BER performances, which is evident from a comparison of the results shown in *Fig.* 6.48, *Fig.* 6.49, *Fig.* 6.50 and *Fig.* 6.51. DSB CE-LI-RU filtered GCL CSSs again delivered BER performances far superior to ABC sequences, coming close to that of the unfiltered CSS families.
- Soft decision (without fading amplitude CSI) VA decoding of the non-binary RS $(7, 5, 3)$ linear block code at low user loads performs approximately 2.7 dB better than hard decision VA decoding, regardless of the CSS family used. This asymptotic gain decreases as the user load increases. For example, for ZC CSSs soft decision decoding (without fading amplitude CSI) exhibits a gain of only 2.5 dB over hard decision decoding at a BER of $P_b(e) = 2/1000$ in a 10-user system. Furthermore, by including perfect fading amplitude CSI during soft decision VA decoding, an additional average improvement of 0.2 dB is attained, regardless of the user load or the CSS family employed in the CDMA system.

6.5.4 REDUCING THE COMPLEXITY OF A BCJR TRELLIS - THE BINARY CYCLIC $(5, 3, 2)$ LINEAR BLOCK CODE

The VA decoding of linear block codes employing reduced trellis structures, obtained using the approach outlined in *Section* 4.3.2, falls under the spotlight in the following subsections. Recall from *Section* 4.3.2 that finding a minimal trellis structure for a (n, k, d_{min}) block code is a tedious process. As such, only the simple binary cyclic $(5, 3, 2)$ block code (see *Section* 3.2.2.2), used as an example to illustrate the trellis reduction technique of *Section* 4.3.2, is used here. This code's original systematic generator matrix is given by *Eq.* (4.22), with its corresponding unreduced BCJR trellis structure

shown in *Fig.* 4.3. After executing the trellis reduction procedure, an equivalent binary cyclic $(5, 3, 2)$ block code with the minimal trellis structure shown in *Fig.* 4.4 was obtained. Note that this equivalent code, defined by *Eq.* (4.22), is non-systematic. Thus, obtaining the simulation results presented in the following subsections required not only VA decoding, but also a mapping of decoded code words to decoded message words. In contrast, obtaining decoded message words for the systematic block codes, presented in the preceding subsections, simply involved stripping the parity symbols from the decoded code words.

Due to time constraints, only AWGN and flat fading channel BER performance simulation tests were performed, using narrowband complex QPSK systems (see *Section* 5.2), on VA decoded (see *Section* 4.4) binary cyclic $(5, 3, 2)$ block codes with reduced complexity trellises. Both hard and soft decision VA decoding approaches were considered. The influence of using perfect fading amplitude CSI (see *Section* 3.3.5 and *Section* 5.2.3) during soft decision decoding (see *Section* 4.4.2.2) was also investigated.

6.5.4.1 AWGN CHANNEL RESULTS

Simulated AWGN channel BER performance results for VA decoded binary cyclic $(5, 3, 2)$ linear block codes, running on narrowband complex QPSK communication systems (see *Section* 5.2), are given in *Fig.* 6.52. Present on this figure are results obtained by performing hard and soft decision VA decoding (see *Section* 4.4) on the original and reduced complexity trellises, shown in *Fig.* 4.3 and *Fig.* 4.4, respectively. Note that the soft decision decoding results were obtained without the use of fading amplitude CSI in the VA metric calculations. For comparative purposes, the theoretical BER performance curve of an uncoded narrowband QPSK system in AWGN channel conditions, defined by *Eq.* (5.20), is also present on this figure.

6.5.4.2 FLAT FADING CHANNEL RESULTS

This subsection is concerned with the simulated BER performance results obtained for binary cyclic $(5, 3, 2)$ codes with VA decoding using original and reduced complexity trellises, tested on narrowband complex QPSK communication systems, operating in flat fading channel conditions. The first set of figures (*Fig.* 6.53 and *Fig.* 6.54) show the simulated BER performance results obtained through hard and soft decision (with and without perfect fading amplitude CSI) VA decoding (see *Section* 4.4) using the original unreduced trellis structure of *Fig.* 4.3 for maximum Doppler spreads (see *Section* 2.4.3.3) of $B_{D,i} = 33$ Hz and $B_{D,i} = 100$ Hz, respectively. Comparable results are respectively contained in *Fig.* 6.55 and *Fig.* 6.56 for VA decoding using the reduced trellis structure of *Fig.* 4.4. For both sets of figures, Rician factors (see *Section* 2.5.2.2) of $K_i = -100$ dB, $K_i = 0$ dB and $K_i = 9$ dB were considered. Also provided on all four figures presented in this subsection, are the theoretical BER performance curve for uncoded QPSK systems in slow Rayleigh flat fading channel conditions (defined by *Eq.* (5.24)), as well as simulated BER performance curves for uncoded QPSK systems in AWGN channel conditions.

6.5.4.3 DISCUSSION OF THE SIMULATION RESULTS

The effects of using reduced trellis structures during the VA decoding of binary cyclic $(5, 3, 2)$ block coded narrowband complex QPSK communication systems, operating in AWGN and flat fading channel conditions, was the focus of the preceding subsections. From the simulated BER performance results obtained, the following conclusions can be drawn:

1. Conclusions and observations for the AWGN channel results:

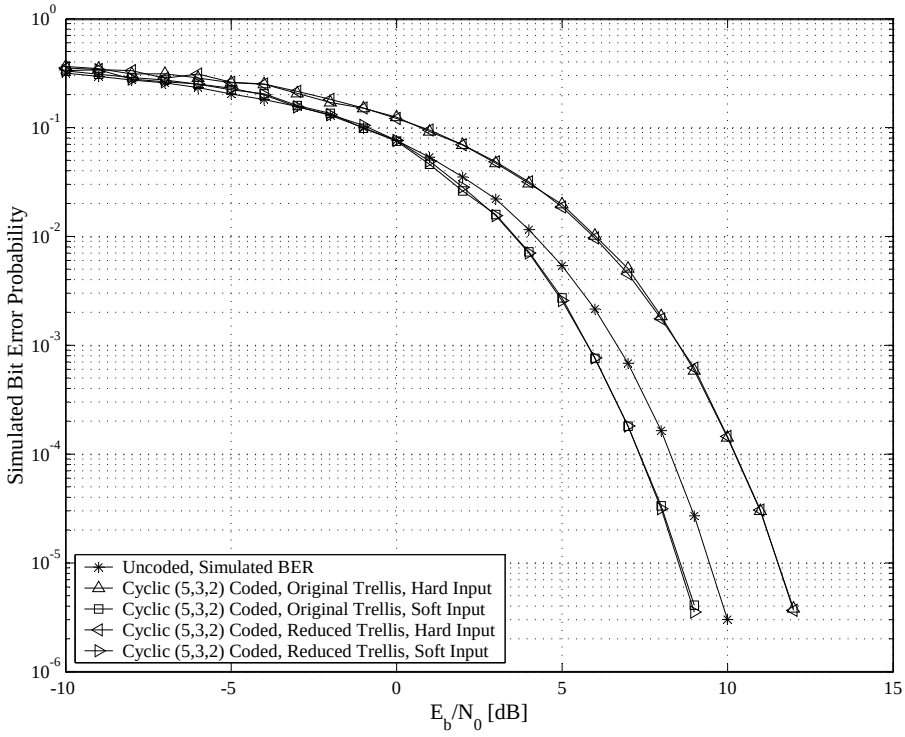

Figure 6.52: AWGN Channel BER Performance Results for Narrowband Complex QPSK Communication Systems Employing Binary Cyclic $(5, 3, 2)$ Linear Block Codes with VA Decoding Using Original and Reduced Trellis Structures

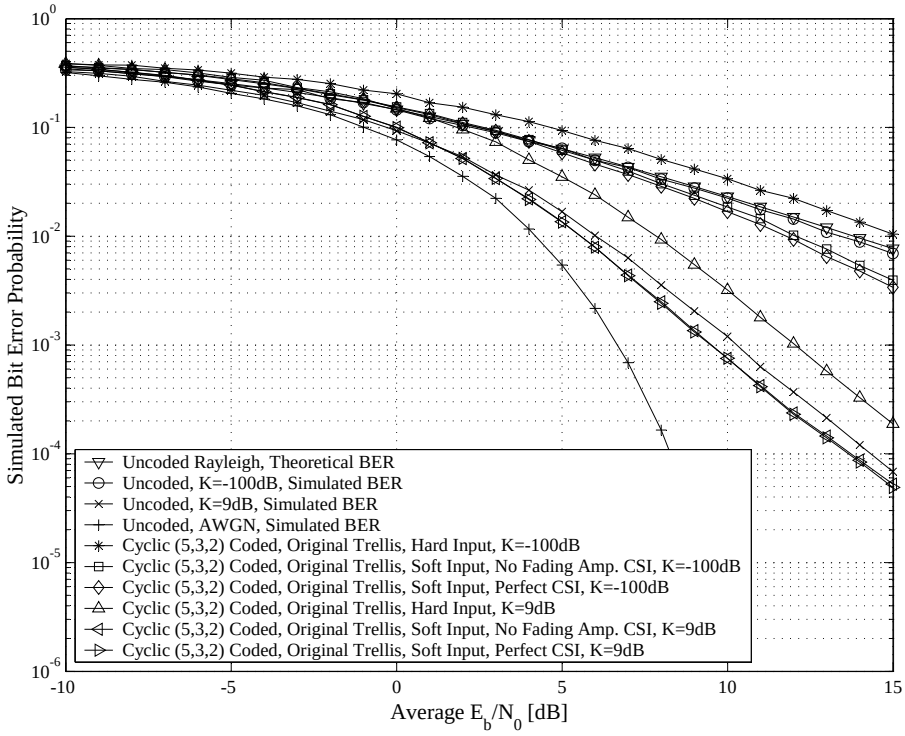

Figure 6.53: BER Performances of Binary Cyclic $(5, 3, 2)$ Block Coded Narrowband Complex QPSK Communication Systems in Flat Fading Channel Conditions ($B_{D,i} = 33$ Hz), VA Decoding Using the Original Trellis Structure of *Fig.* 4.3

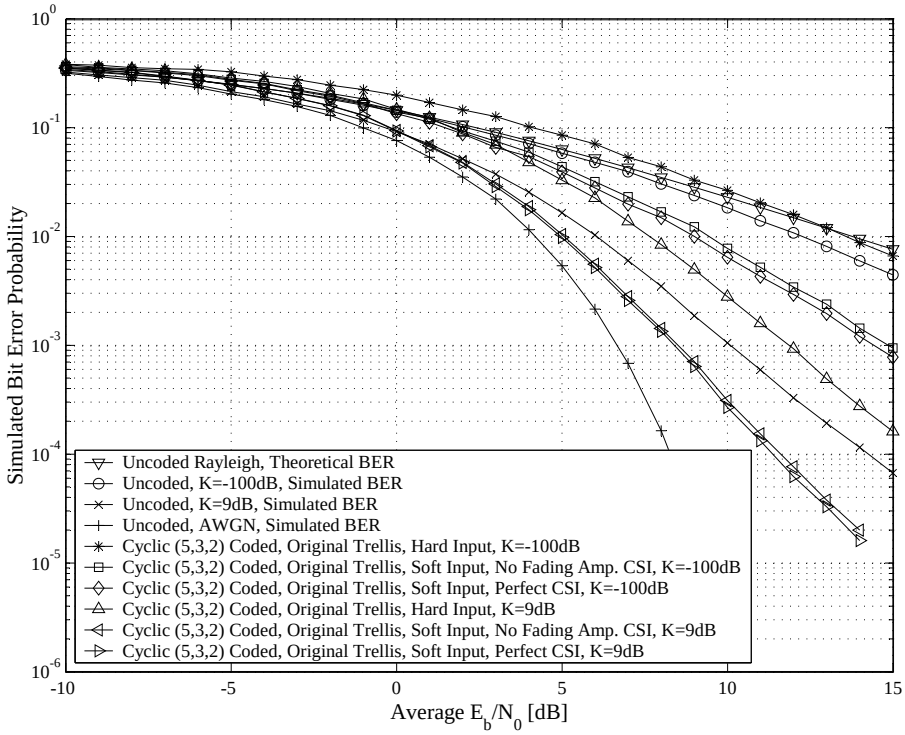

Figure 6.54: BER Performances of Binary Cyclic $(5, 3, 2)$ Block Coded Narrowband Complex QPSK Communication Systems in Flat Fading Channel Conditions ($B_{D,i} = 100$ Hz), VA Decoding Using the Original Trellis Structure of *Fig.* 4.3

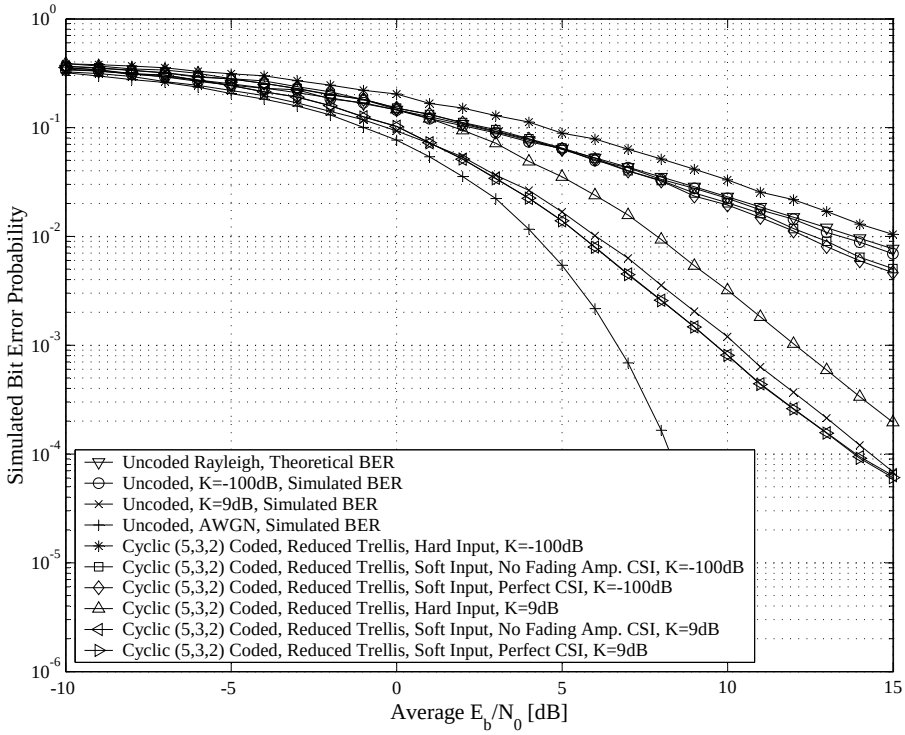

Figure 6.55: BER Performances of Binary Cyclic $(5, 3, 2)$ Block Coded Narrowband Complex QPSK Communication Systems in Flat Fading Channel Conditions ($B_{D,i} = 33$ Hz), VA Decoding Using the Reduced Trellis Structure of *Fig.* 4.4

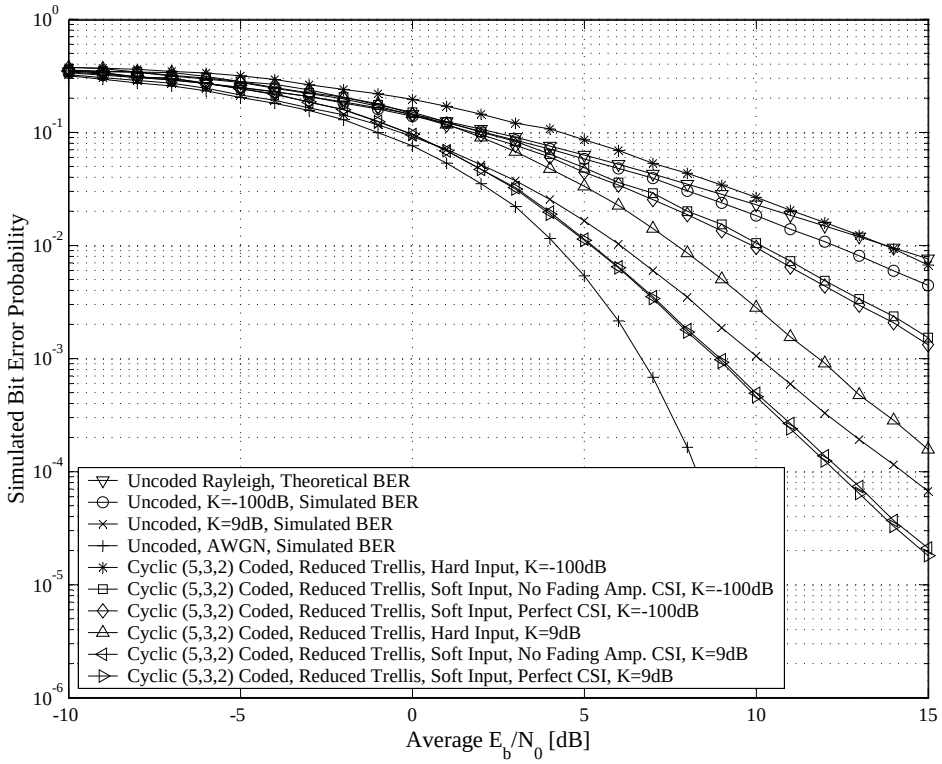

Figure 6.56: BER Performances of Binary Cyclic $(5, 3, 2)$ Block Coded Narrowband Complex QPSK Communication Systems in Flat Fading Channel Conditions ($B_{D,i} = 100$ Hz), VA Decoding Using the Reduced Trellis Structure of *Fig.* 4.4

- From *Fig.* 6.52 it is clear that, in AWGN channel conditions, VA decoding of a simple binary cyclic $(5, 3, 2)$ linear block code using original (see *Section* 4.2) and reduced complexity (see *Section* 4.3.2) BCJR trellis structures deliver almost identical BER performances. This was to be expected, since the reduced complexity trellis was obtained using *Eq.* (4.22)'s generator matrix, which is a non-systematic equivalent of the original generator matrix, given by *Eq.* (4.18).
- In terms of coding gain, soft decision VA decoded binary cyclic $(5, 3, 2)$ linear block codes deliver mediocre BER performances in AWGN channel conditions. Soft decision VA decoding shows a simulated asymptotic coding gain of 0.7 dB over an uncoded narrowband complex QPSK system (comparable with *Eq.* (3.25)'s theoretical gain of $CG_{BC}^{soft} = 0.79$ dB), as well as a cross-over point (see *Section* 6.5.2.1.4) of 1 dB. Since hard decision VA decoding asymptotically lags soft decision decoding by 3 dB (unexpectedly higher than the classic 2 dB) in terms of BER performance, the uncoded system will outperform hard decision VA decoding at any SNR.

2. Conclusions and observations from the flat fading channel results:

- A comparison of *Fig.* 6.53 with *Fig.* 6.54, and *Fig.* 6.55 with *Fig.* 6.56, confirms the following expected observations: For both the $B_{D_i} = 33$ Hz and $B_{D_i} = 100$ Hz flat fading channel scenarios, VA decoding of the binary cyclic $(5, 3, 2)$ linear block code (using the original and reduced complexity trellis structures) delivers increasingly improved BER performances as the channels' Rician factors increase. Furthermore, soft decision VA decoding, with perfect fading amplitude CSI, shows gains of 0.25 dB at $B_{D_i} = 100$ Hz and 0.1 dB at $B_{D_i} = 33$ Hz

over soft decision VA decoding without any fading amplitude CSI. Lastly, on average the VA decoded binary cyclic $(5, 3, 2)$ block code performs better at a faster fading rate, since it is not intended to correct large error bursts.

- Inexplicably, in flat fading channel conditions, the VA decoding of the binary cyclic $(5, 3, 2)$ code, using the reduced complexity trellis structure, performs weaker than when the original trellis is used. For example, with $B_{D,i} = 100$ Hz and $K_i = 9$ dB, VA decoding using the reduced trellis structure lags by 0.75 dB in performance. This difference in BER performance for the different trellis structures is less severe for the slower $B_{D,i} = 33$ Hz channel configuration, measuring only 0.3 dB for $K_i = 9$ dB. Although the author of this dissertation is unable to deliver a bona fide explanation for this phenomenon, it can be conjectured that these inferior performances, obtained using the reduced complexity trellis structure, might be attributed to error propagation: Recall that the equivalent binary cyclic $(5, 3, 2)$ code obtained after executing the trellis reduction procedure described in *Section* 4.3.2, is non-systematic. As such, VA decoding alone will not produce an estimate of the original data input vector $\overline{d}_m$. A second stage ML mapping from decoded code word estimate $\hat{\overline{c}}_m$ to decoded message word estimate $\hat{\overline{d}}_m$ is required. Thus, any errors present in $\hat{\overline{c}}_m$ after VA decoding will not only propagate, but possibly increase in quantity by performing the second stage ML mapping. The end result is reduced BER performances. In [163] *Fossorier et al.* made similar observations when linear block codes with identical dimensions and d_{min}, but with different generator matrices G_{BC} were compared. *Fossorier et al.* went on to show that the systematic encoding of linear block codes not only simplifies decoding, but also minimises the probability of a bit error.

6.5.5 COMMUNICATION SYSTEMS EMPLOYING INTERLEAVED VITERBI DECODED LINEAR BLOCK CODES

The nett result of flat and frequency selective fading on wirelessly transported data streams is the phenomenon of error bursts [60]. Certain types of codes, such as non-binary RS block codes (see *Section* 3.2.2.3.3), are inherently designed to mitigate the detrimental effects of such error bursts [164]. However, using interleaving and de-interleaving (see *Section* 3.2.3) in conjunction with channel coding yields remarkable BER performance improvements for communication systems operating in fading channel conditions, even when burst error correcting codes are already employed [60]. The following subsections investigate the BER performance improvements gained by using interleaved VA decoded (see *Section* 4.4) binary Hamming $(7, 4, 3)$ and non-binary RS $(7, 5, 3)$ linear block codes in narrowband complex QPSK (see *Section* 5.2) and wideband complex DS/SSMA QPSK (see *Section* 5.3) communication systems, operating in flat and multi-user multipath fading channel conditions, respectively. Similar to *Section* 6.5.3, the RAKE receiver-based complex DS/SSMA communication systems employed length $M_{seq} = 63$ CSSs. Again, for all of the CSS families considered, except ABC sequences, sequences were arbitrarily selected from their respective sequence families. For the ABC sequences case, sequences were optimally selected (see *Section* 6.5.1.3.2).

A simple random number generator interleaver (see *Section* C.3.2) of length $N = 105$ bits was employed for both the binary Hamming (7,4,3) (see *Section* 3.2.2.3.1) and non-binary RS $(7, 5, 3)$ (see *Section* 3.2.2.3.3) linear block coded systems. The choice for the length of the interleaver is justified as follows: From the chosen flat fading channel parameters (shown in *Table* 5.1) and multipath fading channel parameters (shown in *Table* 5.5 and *Table* 5.6), the minimum Doppler spread (see *Section* 2.4.3.3) considered in this study is $\min\{B_{D,i}\} = 33$ Hz. Furthermore, both the narrowband complex QPSK and wideband complex DS/SSMA QPSK transmitters are configured for balanced modulation with coded, unspreaded symbol rates of 1000 b/s (see *Table* 5.1 and *Table* 5.4). As such,

a quick rule-of-thumb calculation shows that a slow deep fade can corrupt a maximum of approximately $1000/33 \approx 30$ coded bits. Thus, an interleaver length of $N = 105$ is more than adequate to spread the effects of such a worst case scenario error burst over multiple code words.

6.5.5.1 INTERLEAVED BINARY HAMMING $(7, 4, 3)$ CODED COMMUNICATION SYSTEMS

The binary Hamming $(7, 4, 3)$ code (see *Section* 3.2.2.3.1) considered in *Section* 6.5.3.1 is revisited here again. Since each code word consists of 7 bits, interleaving using the length $N = 105$ random number generator interleaver results in the shuffling of 15 complete code words' code bits. VA decoded interleaved Hamming $(7, 4, 3)$ coded narrowband complex QPSK and wideband complex DS/SSMA systems' simulated BER performances are presented and discussed in the following subsections for flat fading and multi-user multipath fading channel conditions, respectively. Again, hard and soft decision VA decoding (see *Section* 4.4.2) are considered, with varying degrees of fading amplitude CSI (see *Section* 3.3.5) employed during soft decision decoding.

6.5.5.1.1 Flat Fading Channel Results

Fig. 6.57 and *Fig.* 6.58 present the simulation results, obtained during the BER performance tests performed for interleaved binary Hamming $(7, 4, 3)$ coded (see *Section* 3.2.2.3.1) narrowband complex QPSK communication systems (see *Section* 5.2) in flat fading (see *Section* 2.5.1.1) channel conditions, with maximum Doppler spreads (see *Section* 2.4.3.3) of $B_{D,i} = 33$ Hz and $B_{D,i} = 100$ Hz, respectively. Hard and soft decision VA decoding (see *Section* 4.4), following the de-interleaving process, were considered for Rician factors (see *Section* 2.5.2.2) of $K_i = -100$ dB, $K_i = 0$ dB and $K_i = 9$ dB. Results are shown for soft decision decoding without any fading amplitude CSI and soft decision decoding with perfect fading amplitude CSI (see *Section* 3.3.5 and *Section* 5.2.3). Also depicted on these figures are *Eq.* (5.24)'s theoretical BER performance curve for an uncoded QPSK system in slow Rayleigh flat fading channel conditions, as well as simulated BER performance curves for uncoded QPSK systems in the presence of only AWGN.

6.5.5.1.2 Multipath Fading Channel Results

Simulated multi-user multipath fading channel BER performance results for block-wise VA decoded (see *Section* 4.4) interleaved binary Hamming $(7, 4, 3)$ codes (see *Section* 3.2.2.3.1), running on RAKE receiver-based wideband complex DS/SSMA QPSK systems (see *Section* 5.3), are shown in *Fig.* 6.59, *Fig.* 6.60, *Fig.* 6.61 and *Fig.* 6.62 for length $M_{seq} = 63$ ABC (see *Section* D.3.2.2), DSB CE-LI-RU filtered GCL (see *Section* D.3.2.1), ZC (see *Section* D.3.1.1) and QPH (see *Section* D.3.1.2) CSSs, respectively. Both hard and soft decision (with and without fading amplitude CSI (see *Section* 3.3.5 and *Section* 5.3.3)) block-wise VA decoding of the interleaved binary Hamming $(7, 4, 3)$ codes were considered. The simulated uncoded RAKE receiver-based wideband complex DS/SSMA QPSK systems' multi-user multipath fading channel BER performance results, presented in *Section* 6.5.1.3.1, are also present on these figures for comparative purposes, as is the BER performance of an uncoded non-RAKE DS/SSMA system, operating solely in AWGN.

6.5.5.1.3 Discussion of the Simulation Results

The preceding two subsections presented flat and multipath fading BER performance results for interleaved binary Hamming $(7, 4, 3)$ coded narrowband complex QPSK and wideband complex DSSS/MA QPSK systems (with de-interleaving and VA decoding employed in the RAKE receiver), respectively. Listed below are several noteworthy observations and important conclusions drawn from these results:

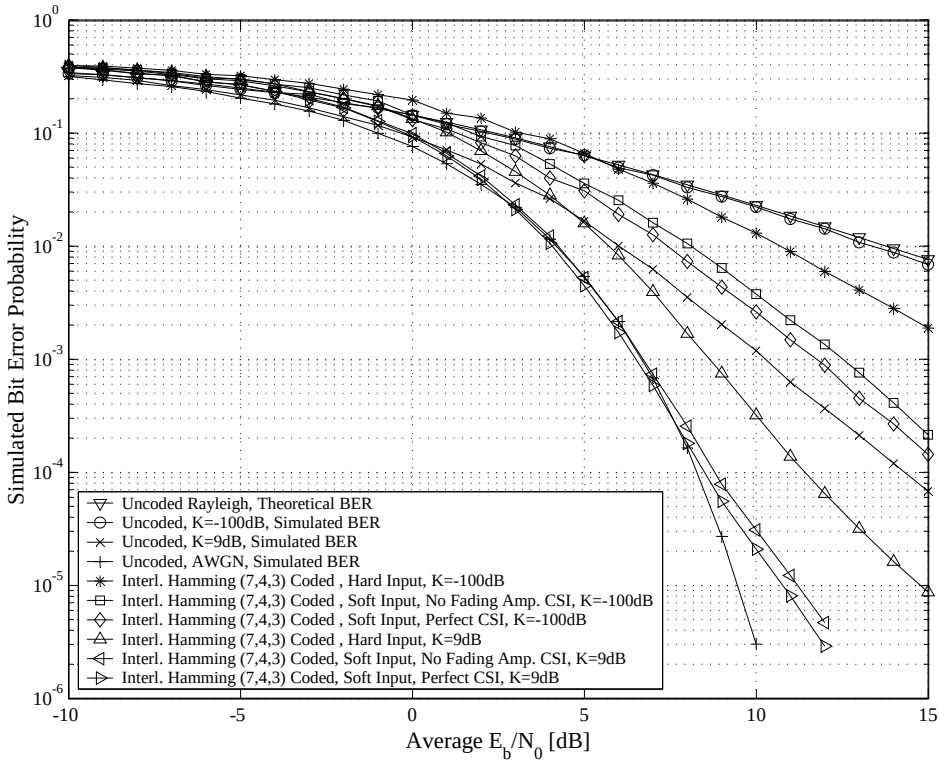

Figure 6.57: BER Performances of Interleaved Binary Hamming $(7, 4, 3)$ Coded Narrowband Complex QPSK Communication Systems in Flat Fading Channel Conditions, $B_{D,i} = 33$ Hz

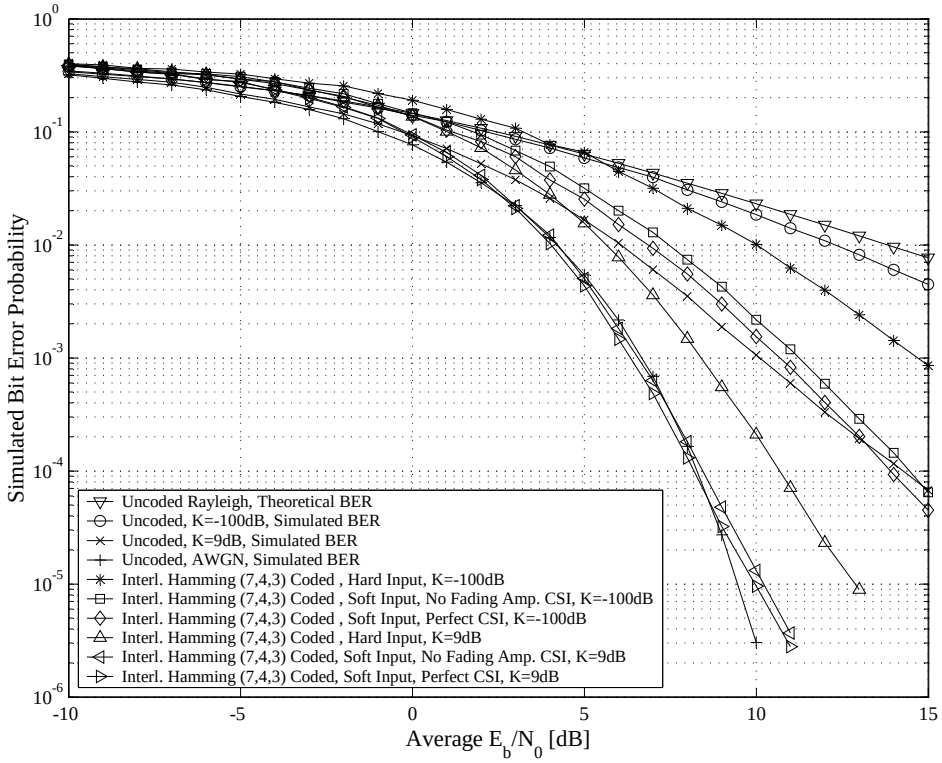

Figure 6.58: BER Performances of Interleaved Binary Hamming $(7, 4, 3)$ Coded Narrowband Complex QPSK Communication Systems in Flat Fading Channel Conditions, $B_{D,i} = 100$ Hz

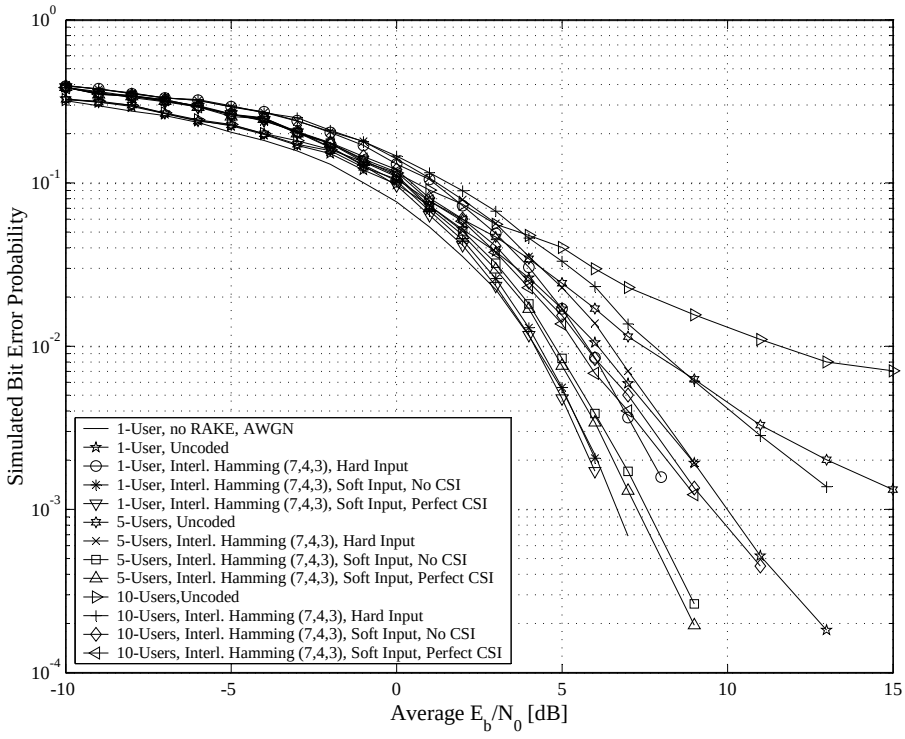

Figure 6.59: BER Performances of Interleaved Binary Hamming $(7, 4, 3)$ Coded Wideband Complex QPSK Communication Systems Employing ABC Sequences in Multi-User Multipath Fading Channel Conditions, $M_{seq} = 63$

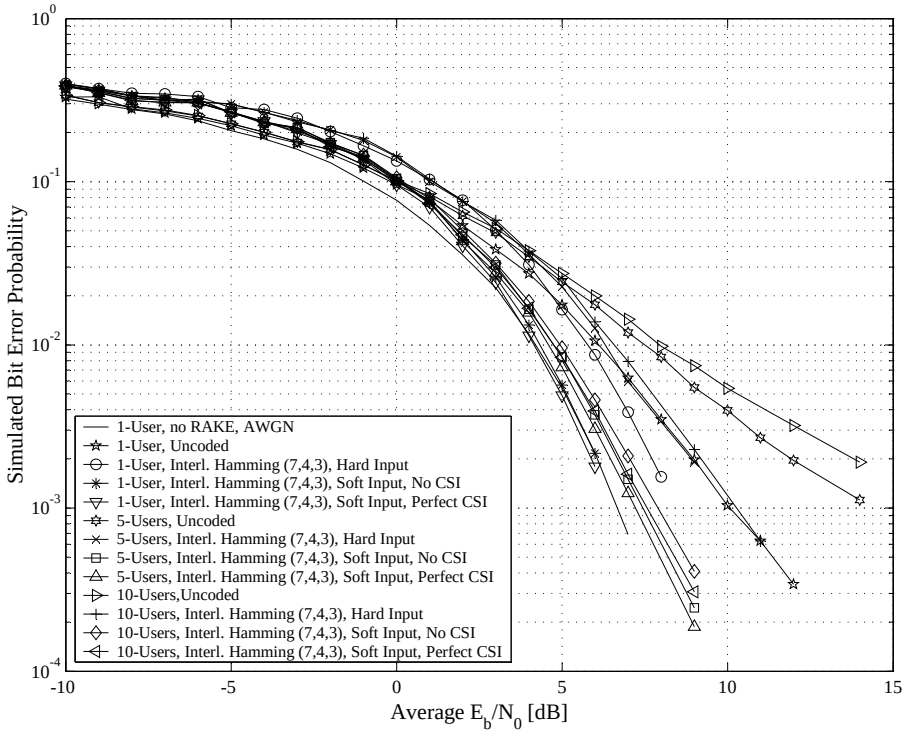

Figure 6.60: BER Performances of Interleaved Binary Hamming $(7, 4, 3)$ Coded Wideband Complex QPSK Communication Systems Employing DSB CE-LI-RU Filtered GCL CSSs in Multi-User Multipath Fading Channel Conditions, $M_{seq} = 63$

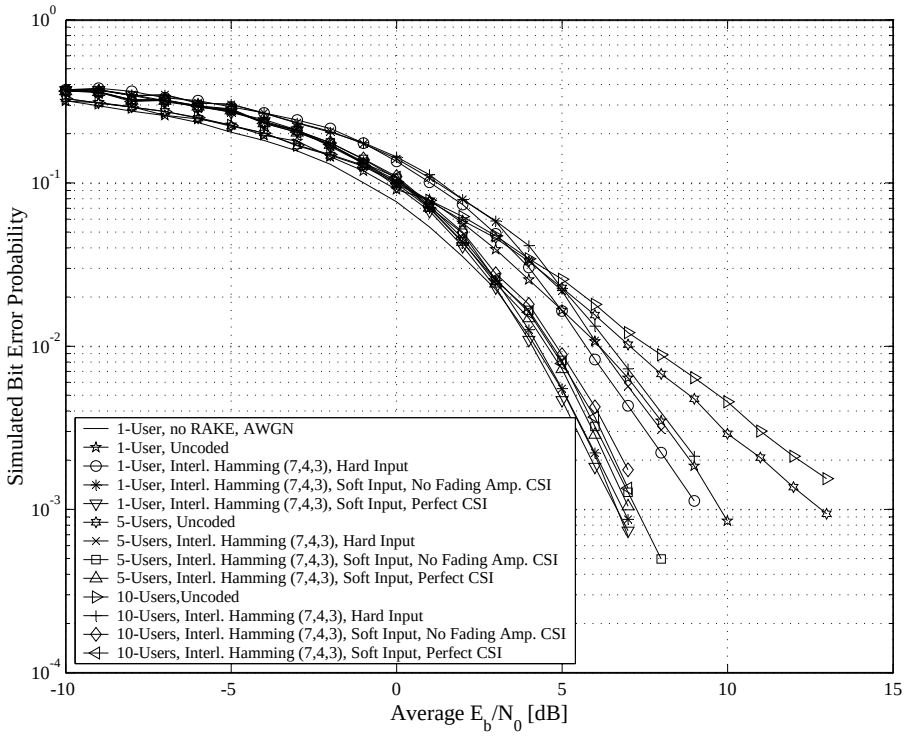

Figure 6.61: BER Performances of Interleaved Binary Hamming $(7, 4, 3)$ Coded Wideband Complex QPSK Communication Systems Employing ZC CSSs in Multi-User Multipath Fading Channel Conditions, $M_{seq} = 63$

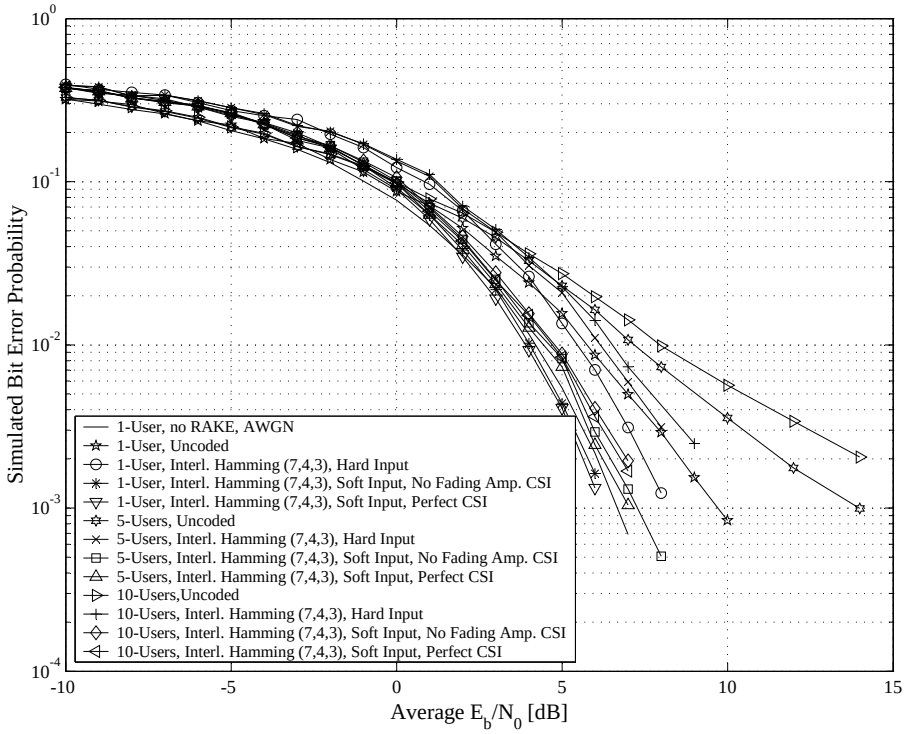

Figure 6.62: BER Performances of Interleaved Binary Hamming $(7, 4, 3)$ Coded Wideband Complex QPSK Communication Systems Employing QPH CSSs in Multi-User Multipath Fading Channel Conditions, $M_{seq} = 63$

1. Conclusions and observations from the flat fading channel results:

   - Contrasting *Fig.* 6.57 with *Fig.* 6.39, and *Fig.* 6.58 with *Fig.* 6.40 reveal that the interleaving process substantially improved the BER performance of hard and soft decision VA decoded binary Hamming $(7, 4, 3)$ codes in flat fading channel conditions (especially for the $B_{D,i} = 33$ Hz case). For example, with $B_{D,i} = 100$ Hz and $K_i = 9$ dB at $P_b(e) = 10^{-4}$, interleaving improved soft decision VA decoding (without any fading amplitude CSI) by approximately 1.75 dB. However, as the Rician factor K_i decreases, the gains obtained using interleaving reduce. Thus, it can be argued that the fading channel's tendency to move from a Gaussian-like to a Rician-like statistical demeanour, starts to overtake the temporal characteristics as the dominating channel effect.
   - A comparison of *Fig.* 6.57 with *Fig.* 6.58 shows that, even after interleaving, VA decoded binary Hamming $(7, 4, 3)$ block codes in flat fading channel conditions with $B_{D,i} = 33$ Hz show inferior BER performances to that obtained for $B_{D,i} = 100$ Hz. However, the performance difference is far less extreme than was the case with the non-interleaved VA decoded binary Hamming $(7, 4, 3)$ block codes (see *Section* 6.5.3.1.2). Thus, it can be concluded that a length $N = 105$ interleaver was not sufficiently capable of decomposing error bursts to obtain IID fading distributions on the received code bits.
   - By incorporating interleaving into the binary Hamming $(7, 4, 3)$ coded narrowband complex QPSK system (operating in flat fading channel conditions), the resultant improvement obtained by employing perfect fading amplitude CSI during soft decision VA decoding, increased. This is particularly evident at $B_{D,i} = 33$ Hz. For example, at $P_b(e) = 10^{-4}$ with $K_i = 9$ dB, fading amplitude CSI improved soft decision VA decoding by approximately 0.25 dB when using interleaving, whereas the non-interleaved scenario showed an almost negligible gain of 0.05 dB.

2. Conclusions and observations from the multi-user multipath fading channel results:

   - Comparing the multi-user multipath fading results presented in *Section* 6.5.3.1.3 and *Section* 6.5.5.1.2 for VA decoded non-interleaved and interleaved binary Hamming $(7, 4, 3)$ linear block codes, respectively, indicates that the use of interleaving improved the BER performance positively. The largest performance improvements were observed at low user loads with hard decision VA decoding. For example, by using interleaving together with hard decision VA decoding, a 1-user system with a BER of $P_b(e) = 2/1000$ obtained a gain of almost 1 dB, irrespective of the CSS family. By employing soft decision decoding (without fading amplitude CSI), this gain diminished to 0.8 dB. However, it was still adequate enough to boost the single user's multipath fading performance results over that of the uncoded DS/SSMA system (without RAKE reception) in AWGN channel conditions for $\overline{E}_b/N_0 > 4$ dB.
   - From *Section* 6.5.5.1.2's BER performance results for the different filtered and unfiltered CSS families considered in this study, it is apparent that, after interleaving, ABC sequences still exhibit the poorest MUI performance, distantly followed by DSB CE-LI-RU filtered GCL CSSs. However, by incorporating interleaving into VA decoded binary Hamming $(7, 4, 3)$ codes, these two pre-filtered CSS families showed the largest BER performance improvements for the 10-user scenario. Thus, it can be speculated that interleaving actually alleviates the detrimental correlative and temporal effects of the MUI caused by the CSSs' poor periodic cross-correlation properties, thereby creating less bursty errors. The unfiltered QPH and ZC CSS families, which performed almost identically, surpassed ABC and DSB CE-LI-RU filtered GCL CSSs for all VA decoder approaches and user load options.
   - Differing from the observations made from *Section* 6.5.5.1.1's flat fading channel results, it was discovered that, in multi-user multipath fading channel conditions, interleaving has no

influence on the performance improvement obtained by incorporating fading amplitude CSI into soft decision VA decoding. The same can also be said of the asymptotic gain of soft decision (without fading amplitude CSI) over hard decision VA decoding, since it remains constant at 2 dB, regardless of the user load or CSS family used.

6.5.5.2 *INTERLEAVED NON-BINARY REED-SOLOMON* $(7, 5, 3)$ *CODED COMMUNICATION SYSTEMS*

Simulated BER performance curves are introduced in the following subsections for interleaved RS $(7, 5, 3)$ block coded (see *Section* 3.2.2.3.3) narrowband complex QPSK (see *Section* 5.2) and wideband complex DS/SSMA QPSK (see *Section* 5.3) communication systems, operating in flat fading and multi-user multipath fading channels, respectively. The non-binary RS (7,5,3) code used throughout these simulations, functions in $GF\left(2^3\right)$ and is defined by *Eq.* (6.5) in *Section* 6.5.3.2. Since each RS code word consists of seven $GF\left(2^3\right)$ code word symbols, with each $GF\left(2^3\right)$ symbol in turn consisting of three bits, it follows that the length $N = 105$ random number generator interleaver shuffles the information of 5 consecutive code words prior to transmission. The following subsections present simulated BER performance results obtained through hard and soft decision (with and without perfect fading amplitude CSI) VA decoding.

6.5.5.2.1 Flat Fading Channel Results

Simulated flat fading channel (see *Section* 2.5.1.1) BER performance results are shown in *Fig.* 6.63 (maximum Doppler spread of $B_{D,i} = 33$ Hz) and *Fig.* 6.64 (maximum Doppler spread of $B_{D,i} = 100$ Hz) for VA decoded (see *Section* 4.4) interleaved non-binary RS $(7, 5, 3)$ coded (see *Section* 3.2.2.3.3) narrowband complex QPSK communication systems (see *Section* 5.2). These figures contain simulation results obtained using flat fading channels configured for Rician factors (see *Section* 2.5.2.2) of $K_i = -100$ dB, $K_i = 0$ dB and $K_i = 9$ dB. Hard and soft decision (with and without perfect fading amplitude CSI (see *Section* 3.3.5 and *Section* 5.2.3)) branch metric calculation approaches were considered for the VA decoding following the de-interleaving process in the receiver. Furthermore, simulated BER performance curves for uncoded QPSK systems in AWGN conditions, as well as *Eq.* (5.24)'s theoretical BER performance curve for an uncoded QPSK system in slow Rayleigh flat fading channel conditions, are also included on *Fig.* 6.63 and *Fig.* 6.64.

6.5.5.2.2 Multipath Fading Channel Results

Simulated multi-user multipath fading channel BER performance results for length $M_{seq} = 63$ ABC (see *Section* D.3.2.2), DSB CE-LI-RU filtered GCL (see *Section* D.3.2.1), ZC (see *Section* D.3.1.1) and QPH (see *Section* D.3.1.2) CSS-based interleaved non-binary RS $(7, 5, 3)$ coded (see *Section* 3.2.2.3.3) wideband complex DS/SSMA QPSK systems (see *Section* 5.3), with VA decoding (see *Section* 4.4) using BCJR trellises, are shown in *Fig.* 6.65, *Fig.* 6.66, *Fig.* 6.67 and *Fig.* 6.68, respectively. Block-wise VA decoding approaches considered include hard and soft decision (with and without fading amplitude CSI (see *Section* 3.3.5 and *Section* 5.3.3)) decoding. Also present on these figures are the simulated uncoded RAKE receiver-based wideband complex DS/SSMA QPSK systems' multi-user multipath fading channel BER performance results, previously presented in *Section* 6.5.1.3.1.

6.5.5.2.3 Discussion of the Simulation Results

Continuing *Section* 6.5.5's investigation into the effects of interleaving on block coded narrowband complex QPSK and wideband complex DSSS/MA QPSK systems (with VA decoding) in flat fading

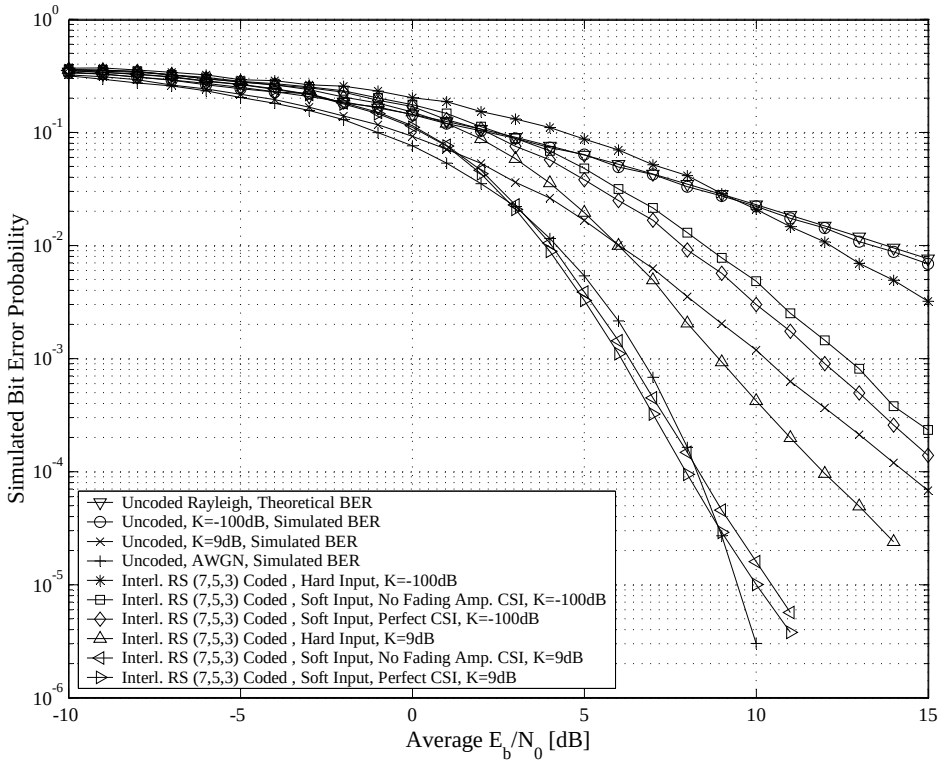

Figure 6.63: BER Performances of Interleaved Non-Binary RS $(7, 5, 3)$ Coded Narrowband Complex QPSK Communication Systems in Flat Fading Channel Conditions, $B_{D,i} = 33$ Hz

and multi-user multipath fading channel conditions, respectively, *Section* 6.5.5.2 brought interleaved non-binary RS $(7, 5, 3)$ codes under the spotlight. Important conclusions and observations from these results are listed below:

1. Conclusions and observations from the flat fading channel results:

   - Coinciding with the findings of *Section* 6.5.5.1, the incorporation of interleaving into non-binary RS $(7, 5, 3)$ coded complex QPSK systems, employing VA decoding, improved the overall BER performances in flat fading channel conditions. However, this improvement is less dramatic for the non-binary RS $(7, 5, 3)$ code than for the binary Hamming $(7, 4, 3)$ code. For example, a comparison between *Fig.* 6.46 and *Fig.* 6.63 indicates that interleaving delivers an additional gain of only 0.2 dB for soft decision decoding (without fading amplitude CSI) at $P_b(e) = 10^{-4}$ with $B_{D,i} = 100$ Hz and $K_i = 9$ dB. This modest gain can be attributed to the fact that RS codes have the inherent capacity to correct bursty errors. It is interesting to note, however, that the gains obtained for both $B_{D,i} = 33$ Hz and $B_{D,i} = 100$ Hz by including interleaving, increase as the Rician factor K_i decreases.
   - Contrasting the flat fading channel results presented in *Section* 6.5.3.2.2 with that given in *Section* 6.5.5.2.1 confirms the observations made in *Section* 6.5.5.1: In general, applying interleaving results in more impressive BER performances at lower maximum Doppler spreads. For the VA decoded non-binary RS $(7, 5, 3)$ code considered here, the resultant improvements obtained through interleaving yield more comparable BER performances between $B_{D,i} = 33$ Hz and $B_{D,i} = 100$ Hz than was the case for the interleaved binary Hamming $(7, 4, 3)$ codes. This can once again be attributed to the RS code's inherent ability to correct any small error bursts still present at the output of the random interleaver.

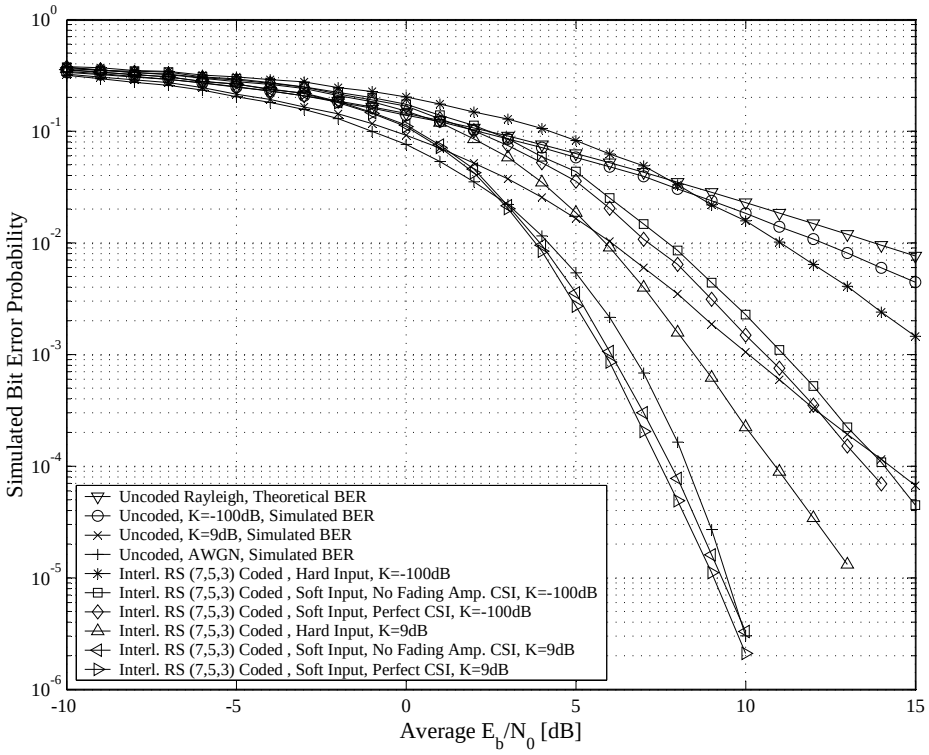

Figure 6.64: BER Performances of Interleaved Non-Binary RS $(7, 5, 3)$ Coded Narrowband Complex QPSK Communication Systems in Flat Fading Channel Conditions, $B_{D,i} = 100$ Hz

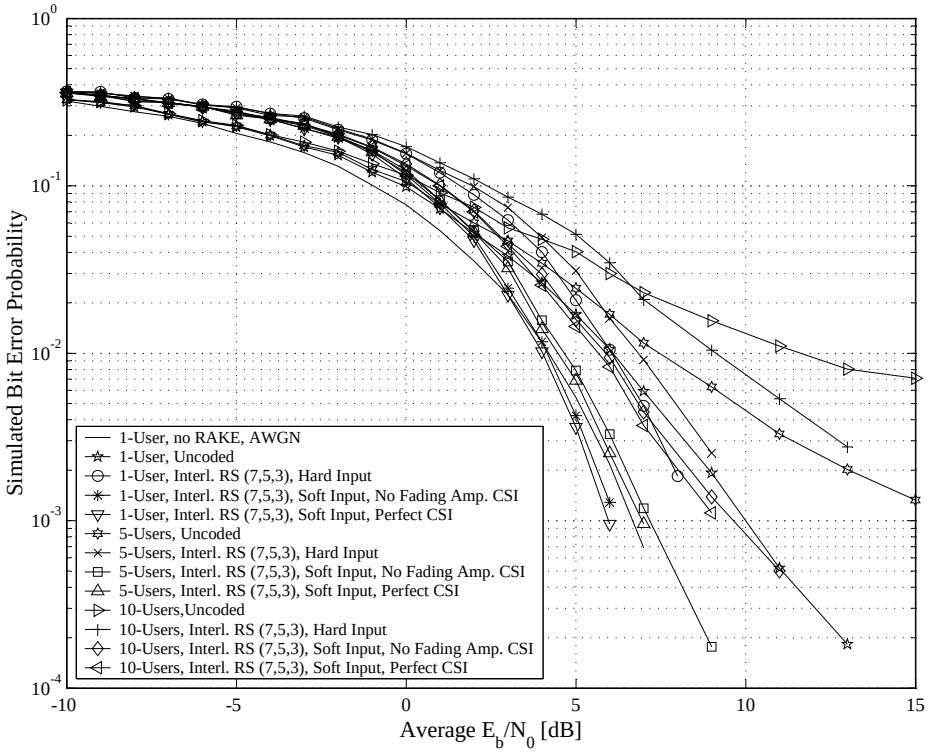

Figure 6.65: BER Performances of Interleaved Non-binary RS $(7, 5, 3)$ Coded Wideband Complex QPSK Communication Systems Employing ABC Sequences in Multi-User Multipath Fading Channel Conditions, $M_{seq} = 63$

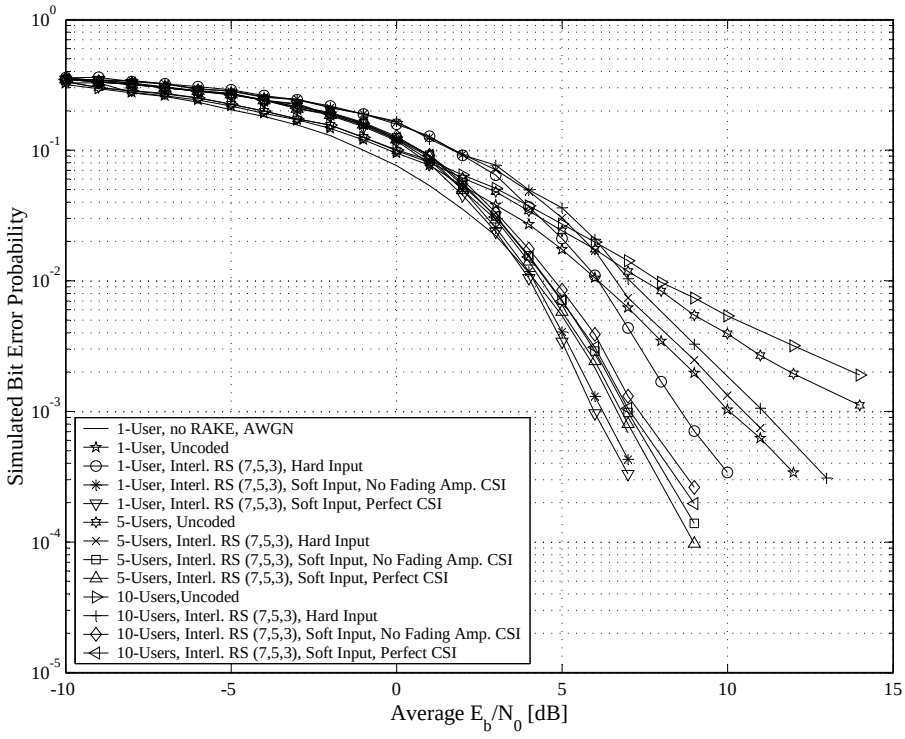

Figure 6.66: BER Performances of Interleaved Non-binary RS $(7, 5, 3)$ Coded Wideband Complex QPSK Communication Systems Employing DSB CE-LI-RU Filtered GCL CSSs in Multi-User Multipath Fading Channel Conditions, $M_{seq} = 63$

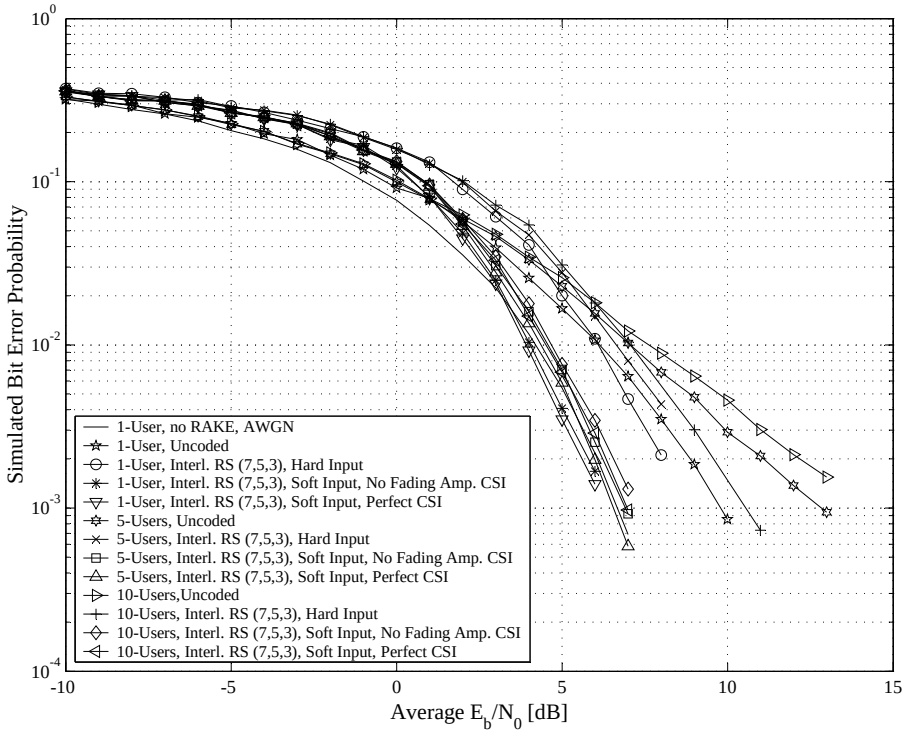

Figure 6.67: BER Performances of Interleaved Non-binary RS $(7, 5, 3)$ Coded Wideband Complex QPSK Communication Systems Employing ZC CSSs in Multi-User Multipath Fading Channel Conditions, $M_{seq} = 63$

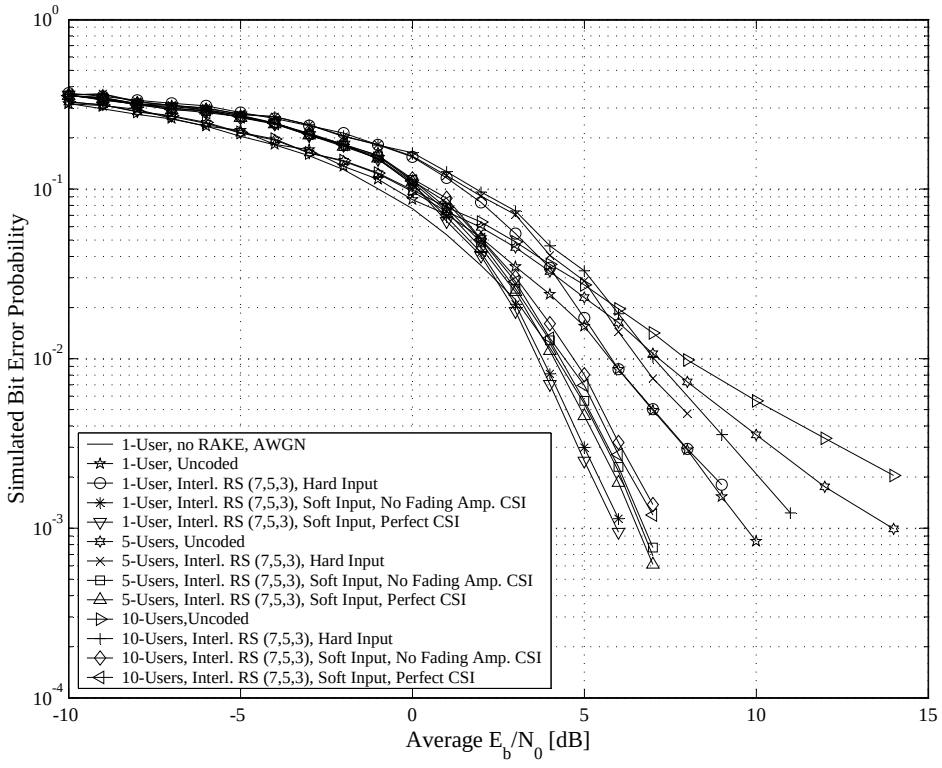

Figure 6.68: BER Performances of Interleaved Non-binary RS $(7, 5, 3)$ Coded Wideband Complex QPSK Communication Systems Employing QPH CSSs in Multi-User Multipath Fading Channel Conditions, $M_{seq} = 63$

- Comparing *Fig.* 6.63 and *Fig.* 6.64 with the results given in *Section* 6.5.3.2.2, it is apparent that, in terms of the BER performance improvement obtained by including perfect fading amplitude CSI into the soft decision VA metric calculations, interleaving proved to be beneficial only for low maximum Doppler spreads. By incorporating interleaving this gain increased from 0.2 dB to 0.4 dB for $B_{D,i} = 33$ Hz, whereas no change was observed for $B_{D,i} = 100$ Hz.

2. Conclusions and observations from the multi-user multipath fading channel results:

- Comparing the results given in *Section* 6.5.3.2.3 and *Section* 6.5.5.2.2, it is apparent that interleaving has little influence on the BER performance of VA decoded non-binary RS $(7, 5, 3)$ block codes in multi-user multipath fading channel conditions. Only the RS $(7, 5, 3)$ coded complex DS/SSMA QPSK systems employing the ABC and DSB CE-LI-RU filtered GCL CSSs showed notable improvements. For example, for $P_b(e) = 3/1000$, the 10-user ABC sequence-based system showed an improvement of 0.2 dB after interleaving. Thus, it can be concluded that the RS code was sufficiently capable of handling the bursty errors created by the multipath fading and MUI, without having to resort to interleaving.
- For all of the CSS families considered, soft decision VA decoding of the interleaved RS $(7, 5, 3)$ block code in a single user CDMA system delivered better performances than an uncoded non-RAKE DS/SSMA QPSK system in AWGN conditions with $\overline{E}_b/N_0 > 4$ dB.
- As was to be expected, ABC sequences exhibited the poorest BER performances, especially at high user loads. QPH and ZC CSSs delivered nearly identical BER performance results, with DSB CE-LI-RU filtered GCL CSSs trailing by no more than 1 dB for the 10-user worst case scenario.

- Coinciding with the observations made from the soft decision VA decoded interleaved binary Hamming $(7, 4, 3)$ block code's multi-user multipath fading BER performance results, it seems that interleaving has no significant influence on the performance improvements obtained by incorporating fading amplitude CSI into the metric calculations.

6.5.6 COMMUNICATION SYSTEMS EMPLOYING VITERBI DECODED PUNCTURED CONVOLUTIONAL AND LINEAR BLOCK CODES

Rate adaptation through code puncturing (see *Section* 3.2.4) has become a standard feature in the channel coding schemes employed by most commercial mobile communication systems (e.g. GSM, GPRS and EDGE). The advantages of using puncturing are twofold: Firstly, puncturing allows for flexible data rates using a single coding scheme, a crucial feature in any communication system that is intended to supply *bandwidth-on-demand*. Secondly, puncturing enables the telecommunications engineer to harness the error correction capabilities of powerful low rate codes, without having to concede considerable transmission bandwidth [102–104].

The following subsections investigate the influence of puncturing on the BER performances of VA decoded RSC codes (see *Section* 3.2.1.3.2) and binary BCH linear block codes (see *Section* 3.2.2.3.2). BER performance results were obtained for these punctured codes on narrowband complex QPSK communication systems (see *Section* 5.2), operating in AWGN and flat fading channel conditions. Multi-user multipath fading simulation results are also presented for the binary BCH $(15, 7, 5)$ code. The RAKE receiver-based complex DS/SSMA communication systems (see *Section* 5.3) employed during these simulations, were configured for length $M_{seq} = 63$ CSSs. The ABC sequences used were optimally selected, as described in *Section* 6.5.1.3.2. CSSs were arbitrarily selected for the other CSS families considered.

6.5.6.1 PUNCTURED BINARY 4-STATE, RATE $R_C = 1/2$ RSC CODED COMMUNICATION SYSTEMS

In the following subsections a punctured [102–104] binary 4-state, rate $R_c = 1/2$ RSC code's BER performances are investigated in AWGN and flat fading channel conditions (multipath fading channel conditions were omitted due to time constraints). From *Table* A.3 the original 4-state, rate $R_c = 1/2$ RSC code is defined by the following generator matrix (see *Section* 3.2.1.3.2):

$$G_{CC}(D) = \left[\begin{array}{cc} 1 & \frac{1+D^2}{1+D+D^2} \end{array} \right] \tag{6.6}$$

As indicated in *Table* A.3, this code has a minimum free distance of $d_{free} = 5$. Code words generated by the encoder structure, defined by *Eq.* (6.6), is punctured according to the following puncturing profile (see *Section* 3.2.4):

$$\Upsilon = \left[\begin{array}{cc} 1 & 1 \\ 1 & 0 \end{array} \right] \tag{6.7}$$

Using *Eq.* (3.46), it readily follows that the resultant punctured code has a rate of $R_p = 2/3$, making it comparable with the RSC code investigated in *Section* 6.5.2.2. Furthermore, note that the systematic information (see *Section* 3.2.1.2) remains intact after puncturing. Hence, this punctured code can still be classified as a binary IIR RSC code (see *Section* 3.2.1.3.2). Furthermore, a equiprobable symbol-generating information source was employed in the transmitter structures used during this subsection's simulations. As such, the receiver-end de-puncturers declare erasure values (see *Eq.* (3.60)) of $\Gamma_{m,i,a} = 0$ in the punctured bit positions, prior to sliding window VA decoding.

6.5.6.1.1 AWGN Channel Results

Fig. 6.69 shows the simulated AWGN channel BER performance results, obtained for narrowband complex QPSK communication systems, employing the punctured 4-state, rate $R_c = 1/2$ RSC code, described in *Section* 6.5.6.1. For comparative purposes the results presented in *Section* 6.5.2.2 for the 8-state, rate $R_c = 2/3$ RSC code are repeated in *Fig.* 6.69. VA decoding using hard and soft decision (without fading amplitude CSI) metric calculations were considered for both the unpunctured rate $R_c = 2/3$ and punctured rate $R_c = 1/2$ RSC codes. *Eq.* (5.20), which defines the theoretical BER performance curve of an uncoded narrowband QPSK system in AWGN channel conditions, is also included in *Fig.* 6.69.

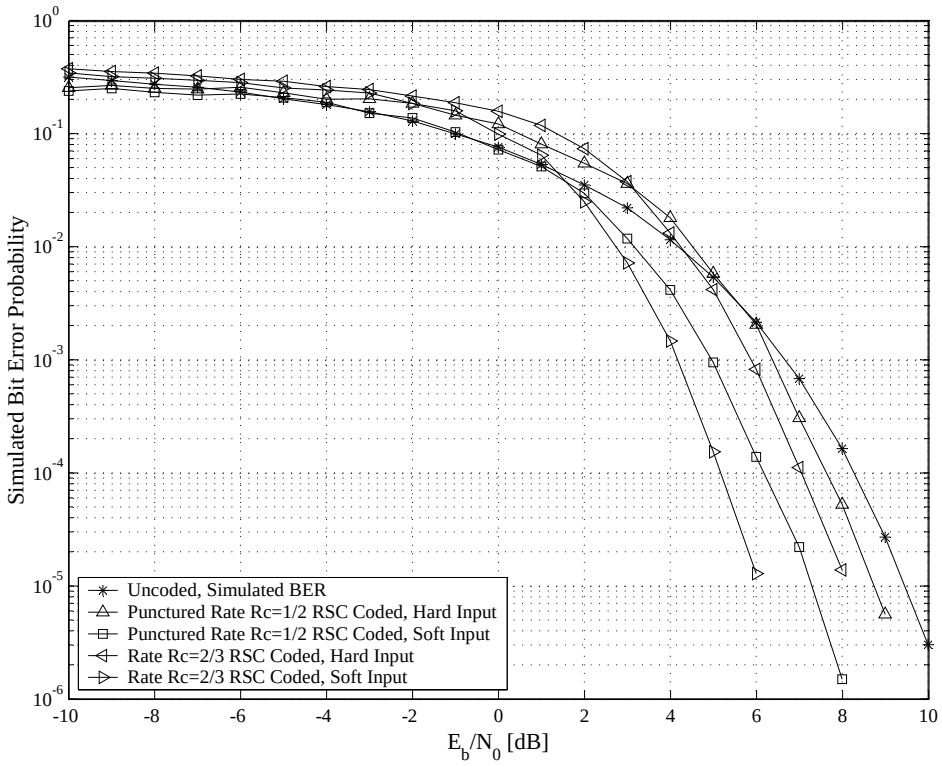

Figure 6.69: BER Performances of Punctured 4-State, Rate $R_c = 1/2$ RSC Coded Narrowband Complex QPSK Communication Systems in AWGN Channel Conditions

6.5.6.1.2 Flat Fading Channel Results

Fig. 6.70 and *Fig.* 6.71 show simulated BER performance results for punctured 4-state, rate $R_c = 1/2$ RSC (see *Section* 3.2.1.3.2) coded narrowband complex QPSK communication systems (see *Section* 5.2) in flat fading channel conditions (see *Section* 2.5.1.1) with maximum Doppler spreads of $B_{D,i} = 33$ Hz and $B_{D,i} = 100$ Hz, respectively. During these simulations the flat fading channel configurations considered included Rician factors (see *Section* 2.5.2.2) of $K_i = -100$ dB, $K_i = 0$ dB and $K_i = 9$ dB. After de-puncturing in the receiver, sliding window VA decoding of the 4-state, rate $R_c = 1/2$ RSC codes were performed. Both hard and soft decision decoding were considered, with either perfect or no fading amplitude CSI (see *Section* 3.3.5 and *Section* 5.2.3) used during soft decision decoding. Simulated BER performance curves for uncoded QPSK systems in AWGN, as well as theoretical BER performance curves for uncoded QPSK systems in slow Rayleigh flat fading channel conditions (defined by *Eq.* (5.24)) are present on *Fig.* 6.70 and *Fig.* 6.71.

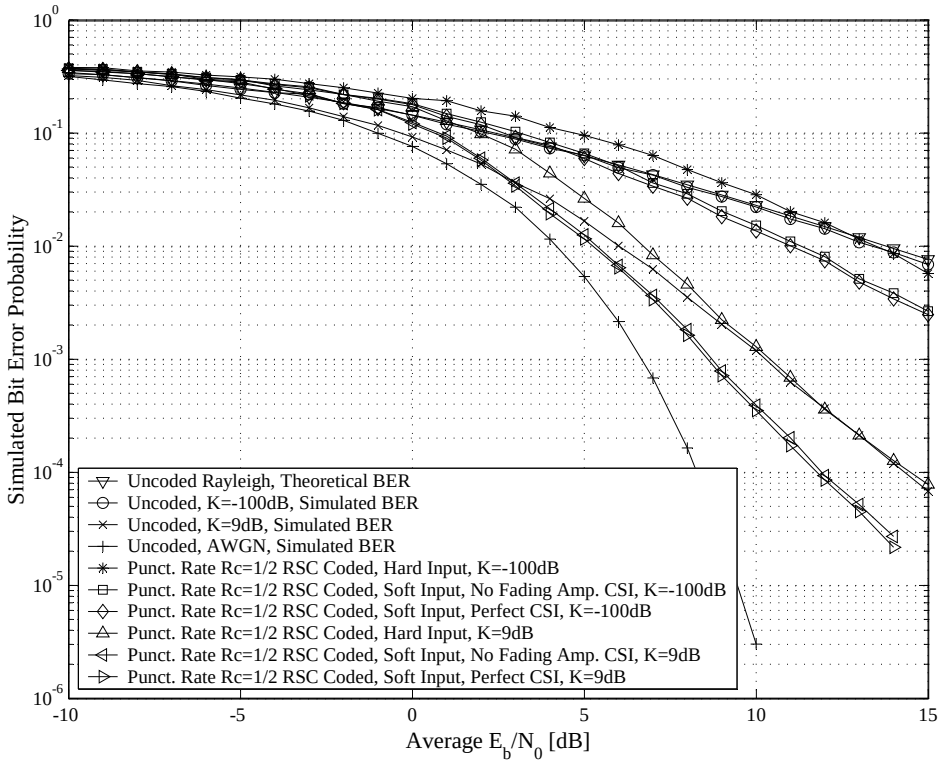

Figure 6.70: BER Performances of Punctured 4-State, Rate $R_c = 1/2$ RSC Coded Narrowband Complex QPSK Communication Systems in Flat Fading Channel Conditions, $B_{D,i} = 33$ Hz

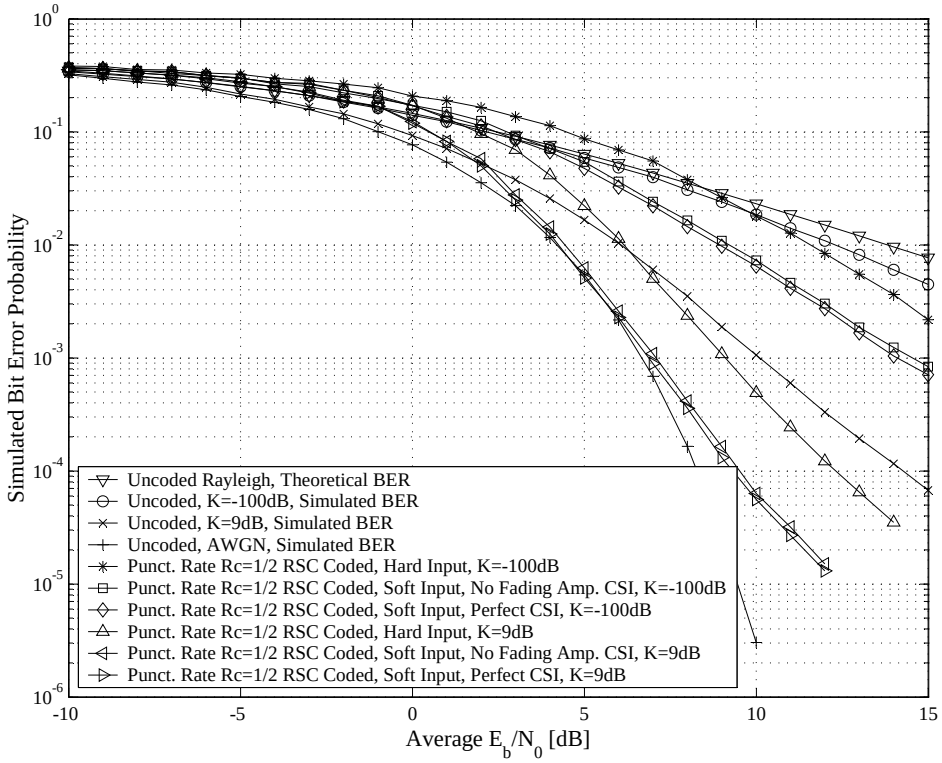

Figure 6.71: BER Performances of Punctured 4-State, Rate $R_c = 1/2$ RSC Coded Narrowband Complex QPSK Communication Systems in Flat Fading Channel Conditions, $B_{D,i} = 100$ Hz

6.5.6.1.3 Discussion of the Simulation Results

Punctured binary 4-state, rate $R_c = 1/2$ RSC coded narrowband complex QPSK systems were evaluated in *Section* 6.5.6.1.1 and *Section* 6.5.6.1.2. The narrowband systems were tested in AWGN and flat fading channel conditions. From the simulated BER performance results presented in the two preceding subsections, the following is evident:

1. Conclusions and observations from the AWGN channel results:

   - The simulated AWGN channel results of *Fig.* 6.69 show that the punctured 4-state, rate $R_c = 1/2$ RSC code does not perform as well as the unpunctured 8-state, rate $R_c = 2/3$ RSC code of *Section* 6.5.2.2, even though both codes have the same minimum free distance. This can be attributed to the fact puncturing decreased the effective minimum free distance of the rate $R_c = 1/2$ RSC code. Exact calculation of the punctured code's overall minimum free distance is a cumbersome process. However, reverse engineering *Eq.* (3.8), using a measured asymptotic coding gain of $GC_{CC}^{soft} = 2.2$ dB for soft decision VA decoding over an uncoded system, the effective minimum free distance for the punctured RSC code can be estimated as $d_{free} = 3$.
   - It is interesting to note from *Fig.* 6.69's AWGN channel results that, although the cross-over point (see *Section* 6.5.2.1.4) for hard decision VA decoding of the punctured rate $R_c = 1/2$ RSC code is higher than that of the unpunctured rate $R_c = 2/3$ RSC code, these two codes have similar cross-over points for soft decision VA decoding.
   - In AWGN channel conditions (see *Fig.* 6.69), soft decision VA decoding of the punctured rate $R_c = 1/2$ RSC code shows an improvement of 1.7 dB, which is less than the expected 2 dB.

2. Conclusions and observations from the flat fading channel results:

   - *Fig.* 6.70 and *Fig.* 6.71 not only show that the punctured rate $R_c = 1/2$ RSC code's performance in flat fading channel conditions improve as the Rician factor K_i increases, but also that the punctured RSC code is presented with more adverse temporal distortions to overcome when $B_{D,i} = 33$ Hz. In general, the BER performances of hard and soft decision VA decoded punctured rate $R_c = 1/2$ RSC codes deteriorate as the maximum Doppler spread decreases, regardless of the Rician factor K_i.
   - From the $B_{D,i} = 33$ Hz and $B_{D,i} = 100$ Hz flat fading channel results, shown in *Fig.* 6.70 and *Fig.* 6.71, respectively, it is clear that the use of perfect fading amplitude CSI during soft decision VA decoding resulted in minor BER performance improvements. For the $B_{D,i} = 100$ Hz the improvement was most noticeable, measuring approximately 0.25 dB for $K_i = 9$ dB. Furthermore, it is interesting to note that the asymptotic gain of soft decision decoding (without any fading amplitude CSI) over hard decision decoding is an impressive 2.5 dB for the $B_{D,i} = 100$ Hz scenario, but only 2 dB for $B_{D,i} = 33$ Hz.
   - The flat fading channel BER performance results, given in *Section* 6.5.2.2.2, for the unpunctured 8-state, rate $R_c = 2/3$ RSC code, are superior to the results obtained here for the punctured rate $R_c = 1/2$ RSC code. Although practical implementation of both codes result in identical bandwidth enlargements, the punctured RSC code has a smaller number of states in its trellis (see *Section* 3.3.1.1), resulting in an inferior minimum free Hamming property (see *Section* 3.2.1.2). This, in turn, produces weaker BER performances.

6.5.6.2 *PUNCTURED BINARY BCH* $(15, 7, 5)$ *CODED COMMUNICATION SYSTEMS*

The effects of puncturing on the BER performances of a VA decoded binary BCH $(15, 7, 5)$ code (see *Section* 3.2.2.3.2), operating in varying channel conditions, are considered in the following subsections. The code under investigation is defined by the following generator polynomial [47]:

$$g_{BC}(p) = p^8 + p^7 + p^6 + p^4 + 1 \tag{6.8}$$

which can be used to construct the following equivalent systematic generator matrix (see *Section* 3.2.2.2):

$$G_{BC} = \begin{bmatrix} 1 & 0 & 0 & 0 & 0 & 0 & 0 & 1 & 1 & 1 & 0 & 1 & 0 & 0 & 0 \\ 0 & 1 & 0 & 0 & 0 & 0 & 0 & 0 & 1 & 1 & 1 & 0 & 1 & 0 & 0 \\ 0 & 0 & 1 & 0 & 0 & 0 & 0 & 0 & 0 & 1 & 1 & 1 & 0 & 1 & 0 \\ 0 & 0 & 0 & 1 & 0 & 0 & 0 & 0 & 0 & 0 & 1 & 1 & 1 & 0 & 1 \\ 0 & 0 & 0 & 0 & 1 & 0 & 0 & 1 & 1 & 1 & 0 & 0 & 1 & 1 & 0 \\ 0 & 0 & 0 & 0 & 0 & 1 & 0 & 0 & 1 & 1 & 1 & 0 & 0 & 1 & 1 \\ 0 & 0 & 0 & 0 & 0 & 0 & 1 & 1 & 1 & 0 & 1 & 0 & 0 & 0 & 1 \end{bmatrix} \tag{6.9}$$

From [47] this BCH code has a minimum Hamming distance (see *Section* 3.2.2.2) of $d_{min} = 5$ bits. Furthermore, since it has a code rate of $R_c = 7/15$, incorporating it into a communication system will come at the expense of a 114.29% inflation in transmission bandwidth. This bandwidth expansion can be alleviated by incorporating the following puncturing profile (see *Section* 3.2.4) into the communication system's channel coding subsystem:

$$\Upsilon = \begin{bmatrix} 0 & 1 & 1 & 1 \\ 1 & 0 & 1 & 1 \\ 1 & 1 & 0 & 1 \\ 1 & 1 & 1 & 1 \\ 1 & 1 & 1 & 0 \\ 1 & 1 & 1 & 1 \\ 0 & 1 & 1 & 1 \\ 1 & 0 & 1 & 1 \\ 1 & 1 & 0 & 1 \\ 1 & 1 & 1 & 1 \\ 1 & 1 & 1 & 0 \\ 1 & 1 & 1 & 1 \\ 0 & 1 & 1 & 1 \\ 1 & 0 & 1 & 1 \\ 1 & 1 & 0 & 1 \end{bmatrix} \tag{6.10}$$

From *Eq.* (3.46) it follows that, when using this puncturing profile in conjunction with the binary BCH $(15, 7, 5)$ block code, a punctured code rate of $R_p = 4/7$ is obtained. Thus, the resultant punctured binary BCH code is comparable with the binary Hamming $(7, 4, 3)$ code, examined in *Section* 6.5.3.1 and *Section* 6.5.5.1. Although this puncturing profile was arbitrarily chosen to deliver an overall code rate of $R_c = 4/7$, the author did attempt to uniformly distribute the deletion of code bits from consecutive BCH code words. However, at no point can it be claimed that the puncturing profile of *Eq.* (6.10) is in any sense optimal.

The following subsections present AWGN and flat fading channel BER performance results, obtained using narrowband complex QPSK communication systems (see *Section* 5.2) employing the punctured binary BCH $(15, 7, 5)$ block code. Also given here are multi-user multipath fading channel BER performance results for punctured binary BCH $(15, 7, 5)$ block codes, running on wideband

complex DS/SSMA QPSK communication systems (see *Section* 5.3). Hard decision VA decoding, as well soft decision VA decoding, with varying degrees of fading amplitude CSI (see *Section* 3.3.5), are considered. The punctured binary BCH $(15, 7, 5)$ code BER performance results are compared with that obtained for the binary Hamming $(7, 4, 3)$ code.

6.5.6.2.1 AWGN Channel Results

Simulated AWGN channel BER performance results are depicted in *Fig.* 6.72 for narrowband complex QPSK communication systems, employing the punctured binary BCH $(15, 7, 5)$ block code detailed in *Section* 6.5.6.2. As is clear from this figure, hard and soft decision (without fading amplitude CSI) VA decoding results were obtained. Since the punctured binary BCH $(15, 7, 5)$ code is comparable with the binary Hamming $(7, 4, 3)$ block code of *Section* 6.5.3.1, the hard and soft decision VA decoding AWGN channel results provided in *Fig.* 6.36 are included in *Fig.* 6.72. Also depicted on this figure is the BER performance curve of an uncoded narrowband QPSK system in AWGN, theoretically defined by *Eq.* (5.20).

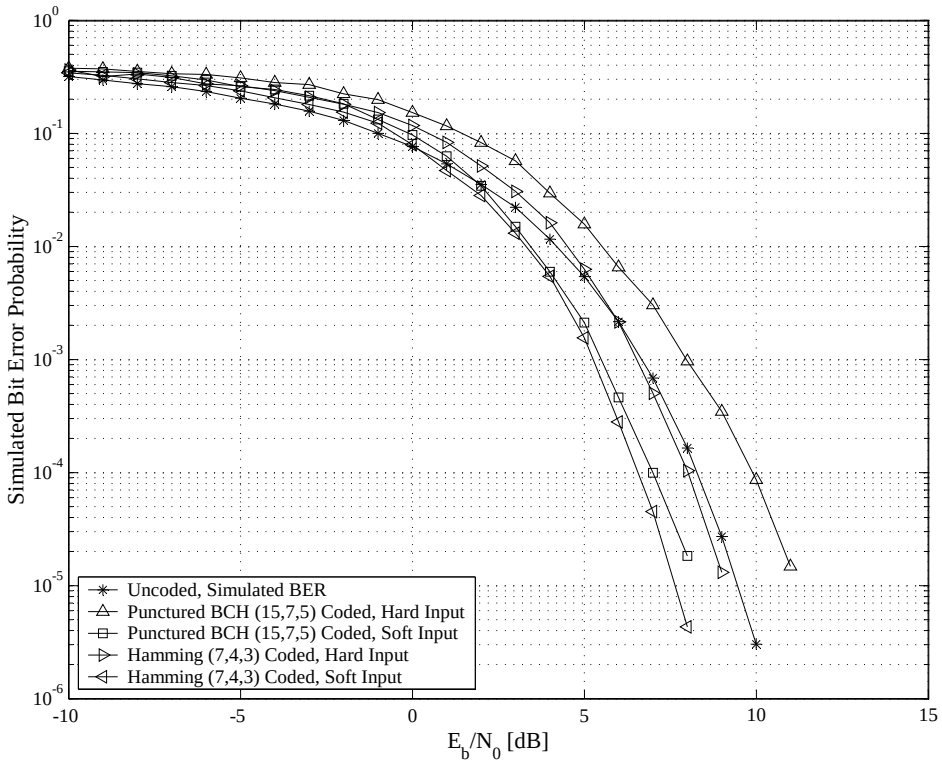

Figure 6.72: BER Performances of Punctured Binary BCH $(15, 7, 5)$ Coded Narrowband Complex QPSK Communication Systems in AWGN Channel Conditions

6.5.6.2.2 Flat Fading Channel Results

Flat fading channel (see *Section* 2.5.1.1) simulated BER performance results are depicted in *Fig.* 6.63 (maximum Doppler spread of $B_{D,i} = 33$ Hz) and *Fig.* 6.64 (maximum Doppler spread of $B_{D,i} = 100$ Hz) for VA decoded (see *Section* 4.4) punctured binary BCH $(15, 7, 5)$ coded (see *Section* 3.2.2.3.2) narrowband complex QPSK communication systems (see *Section* 5.2). Simulation results are included for flat fading channels configured with Rician factors (see *Section* 2.5.2.2) of $K_i = -100$ dB, $K_i = 0$ dB and $K_i = 9$ dB. After de-puncturing in the narrowband complex QPSK

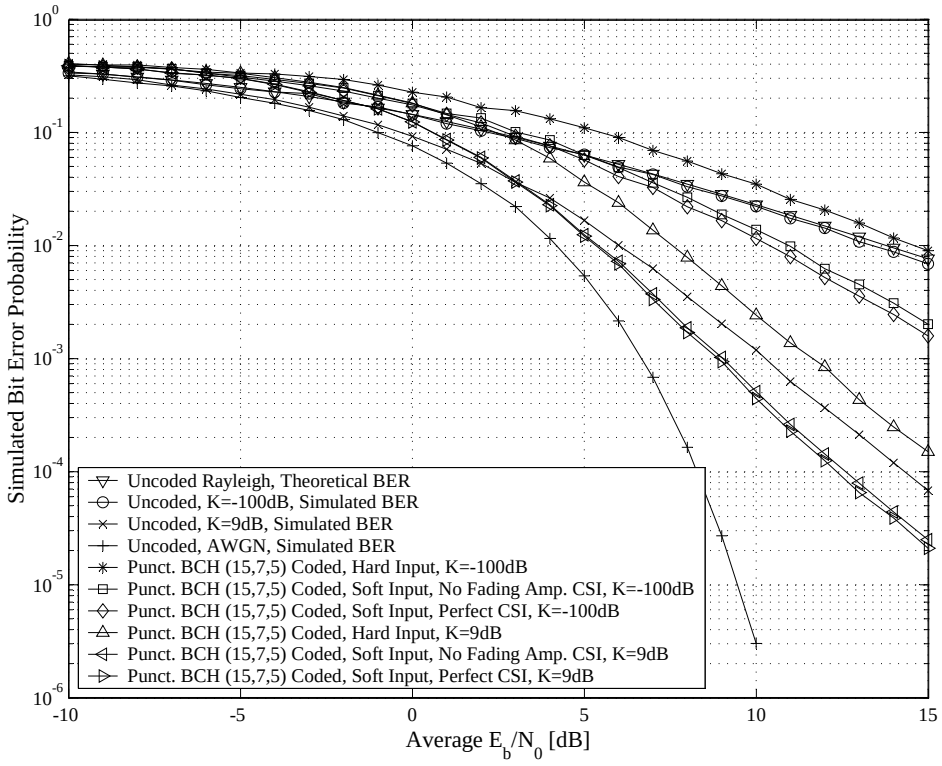

Figure 6.73: BER Performances of Punctured Binary BCH $(15, 7, 5)$ Coded Narrowband Complex QPSK Communication Systems in Flat Fading Channel Conditions, $B_{D,i} = 33$ Hz

receiver, VA decoding using either hard or soft decisions (with and without perfect fading amplitude CSI (see *Section* 3.3.5 and *Section* 5.2.3)) were performed. For comparative purposes, simulated BER performance curves for uncoded QPSK systems in AWGN, as well as the theoretical BER performance curve for uncoded QPSK systems in slow Rayleigh flat fading channel conditions (given in *Eq.* (5.24)), are also included on *Fig.* 6.73 and *Fig.* 6.74.

6.5.6.2.3 Multipath Fading Channel Results

Fig. 6.75, *Fig.* 6.76, *Fig.* 6.77 and *Fig.* 6.78 respectively show simulated multi-user multipath fading channel BER performance results for length-63 ABC (see *Section* D.3.2.2), DSB CE-LI-RU filtered GCL (see *Section* D.3.2.1), ZC (see *Section* D.3.1.1) and QPH (see *Section* D.3.1.2) CSS-based punctured binary BCH $(15, 7, 5)$ coded (see *Section* 3.2.2.3.2) wideband complex DS/SSMA QPSK systems (see *Section* 5.3). Following the de-puncturing process (see *Section* 3.3.4) at the RAKE receiver, block-wise VA decoding, using the binary BCH $(15, 7, 5)$ code's BCJR trellis, which consists of 16 layers with 64 nodes each, was employed. Simulation results are given for hard and soft decision (with and without fading amplitude CSI (see *Section* 3.3.5 and *Section* 5.3.3)) VA decoding approaches. The multi-user multipath fading and AWGN channel BER performance results for uncoded RAKE receiver-based and non-RAKE receiver-based wideband complex DS/SSMA QPSK systems, respectively, are also included on these four figures.

6.5.6.2.4 Discussion of the Simulation Results

The focus of the preceding three subsections were the effects of using puncturing in conjunction with VA decoded binary BCH $(15, 7, 5)$ codes. Simulated BER performance results were presented for

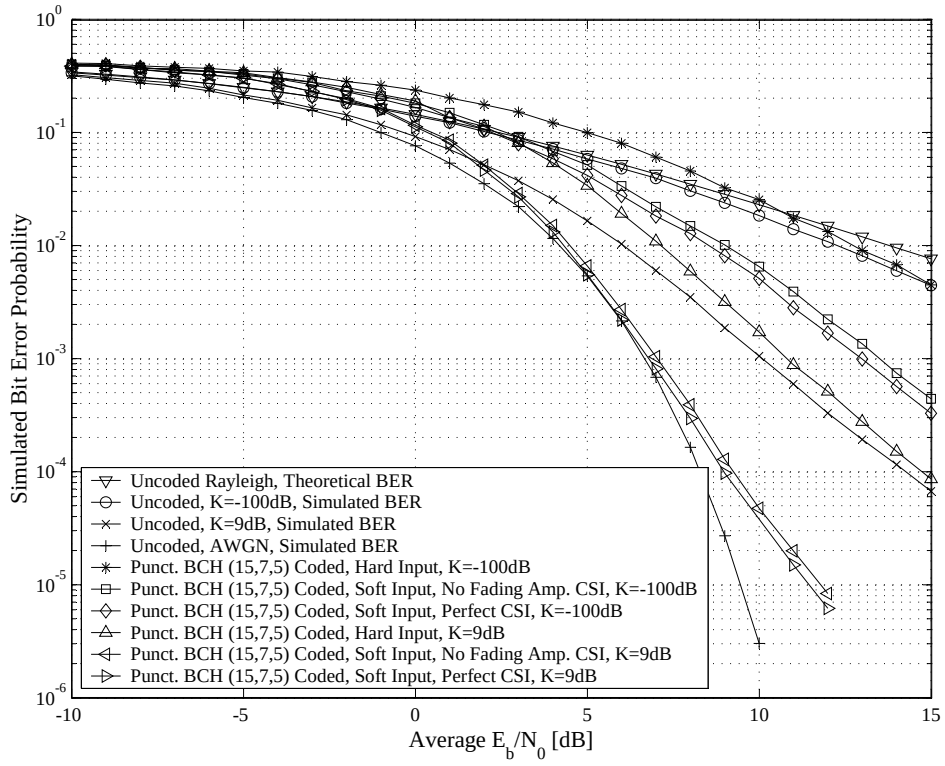

Figure 6.74: BER Performances of Punctured Binary BCH $(15, 7, 5)$ Coded Narrowband Complex QPSK Communication Systems in Flat Fading Channel Conditions, $B_{D,i} = 100$ Hz

punctured binary BCH $(15, 7, 5)$ coded narrowband complex QPSK communication systems (operating in AWGN and flat fading channel conditions) and multi-user wideband complex DSSS/MA QPSK systems (operating in multipath fading channel conditions). The following observations were made from these results:

1. Conclusions and observations from the AWGN channel results:

   - Investigation of the AWGN channel BER performance results for the VA decoded punctured binary BCH $(15, 7, 5)$ codes, implemented on narrowband complex QPSK systems (see *Fig.* 6.72), indicates that the puncturing process not only decreased the strain on the transmission bandwidth, but also decreased the binary BCH $(15, 7, 5)$ code's error correcting capabilities. For soft decision VA decoding of the punctured binary BCH $(15, 7, 5)$ code a mundane asymptotic coding gain of 1.8 dB is achieved, whereas hard decision decoding shows a coding loss of 1.9 dB. Thus, reverse engineering *Eq.* (3.25) shows that puncturing (using the profile given by *Eq.* (6.10)) has effectively decreased the BCH code's minimum Hamming distance (see *Section* 3.2.2.2) from $d_{min} = 5$ to approximately $d_{min} = 3$.
   - Comparing the AWGN channel BER performance results for VA decoded binary Hamming $(7, 4, 3)$ and punctured binary BCH $(15, 7, 5)$ codes on narrowband complex QPSK systems (shown in *Fig.* 6.36 and *Fig.* 6.72, respectively), establishes that the soft decision decoding (with or without fading amplitude CSI) of both codes deliver comparable results. However, hard decision VA decoding of the binary BCH $(15, 7, 5)$ code failed to perform at the same level as hard decision VA decoded binary Hamming $(7, 4, 3)$ codes. Specifically, for high average E_b/N_0 values, hard decision VA decoded BCH $(15, 7, 5)$ codes showed an asymptotic performance loss of 2 dB when compared to the hard decision VA decoded binary Hamming $(7, 4, 3)$ code.

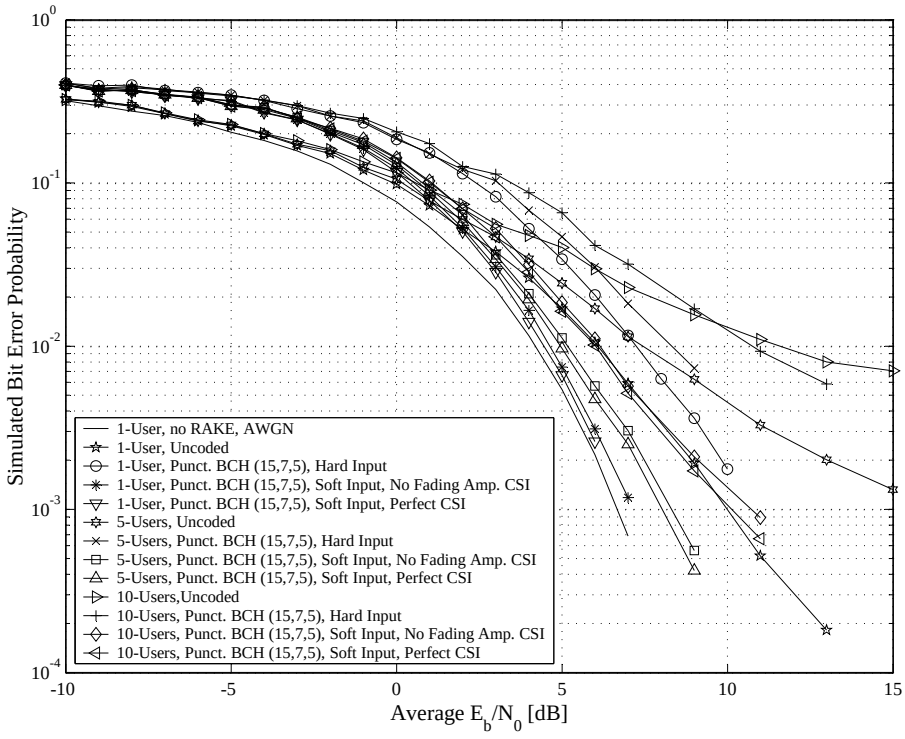

Figure 6.75: BER Performances of Punctured Binary BCH $(15, 7, 5)$ Coded Wideband Complex QPSK Communication Systems Employing ABC Sequences in Multi-User Multipath Fading Channel Conditions, $M_{seq} = 63$

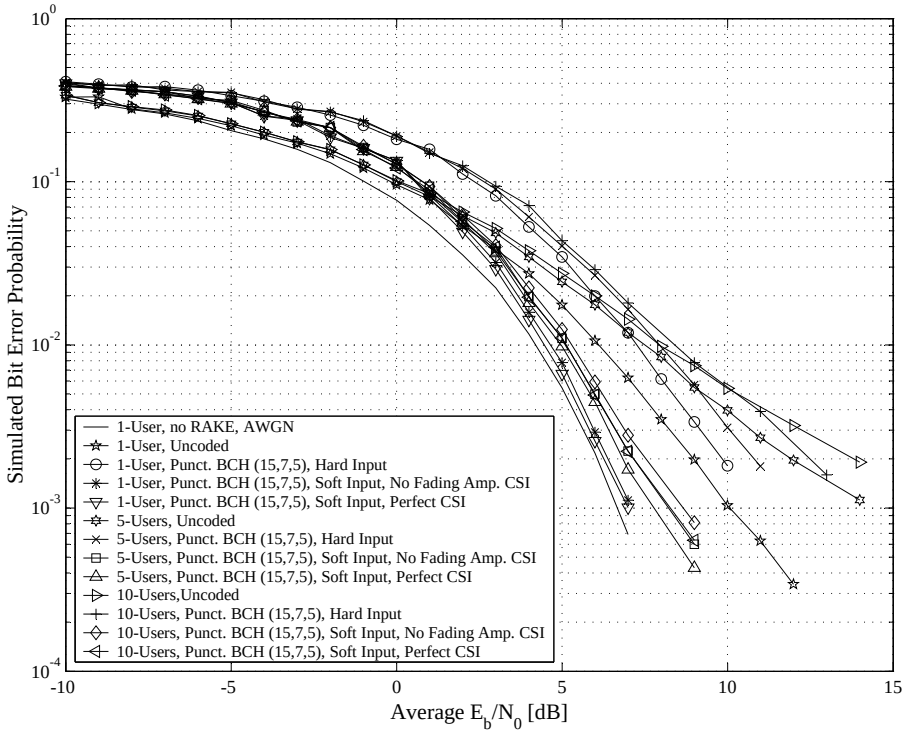

Figure 6.76: BER Performances of Punctured Binary BCH $(15, 7, 5)$ Coded Wideband Complex QPSK Communication Systems Employing DSB CE-LI-RU Filtered GCL CSSs in Multi-User Multipath Fading Channel Conditions, $M_{seq} = 63$

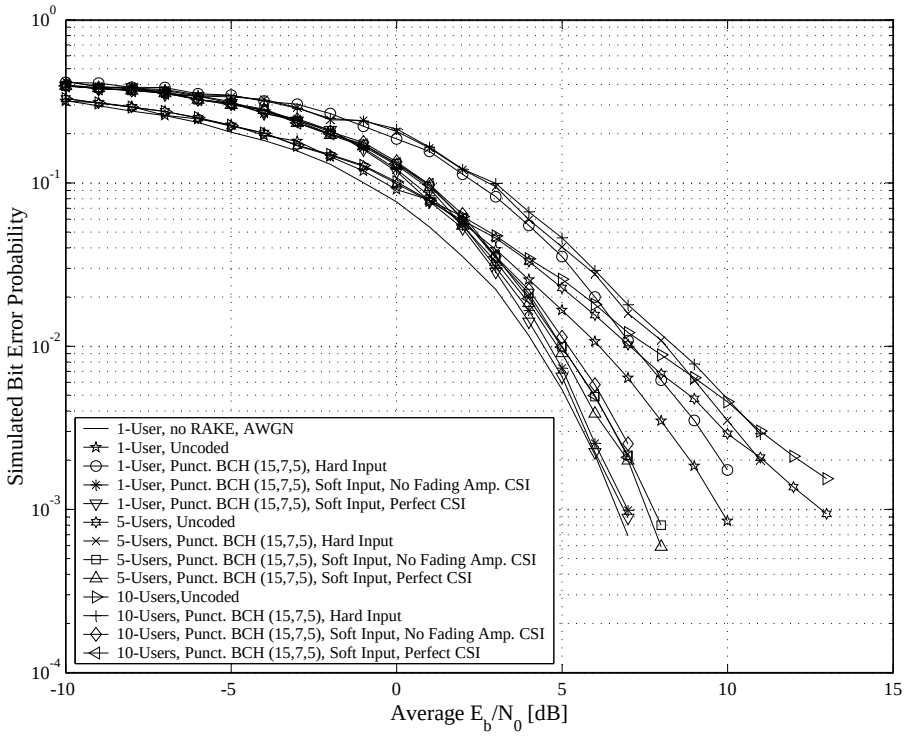

Figure 6.77: BER Performances of Punctured Binary BCH $(15, 7, 5)$ Coded Wideband Complex QPSK Communication Systems Employing ZC CSSs in Multi-User Multipath Fading Channel Conditions, $M_{seq} = 63$

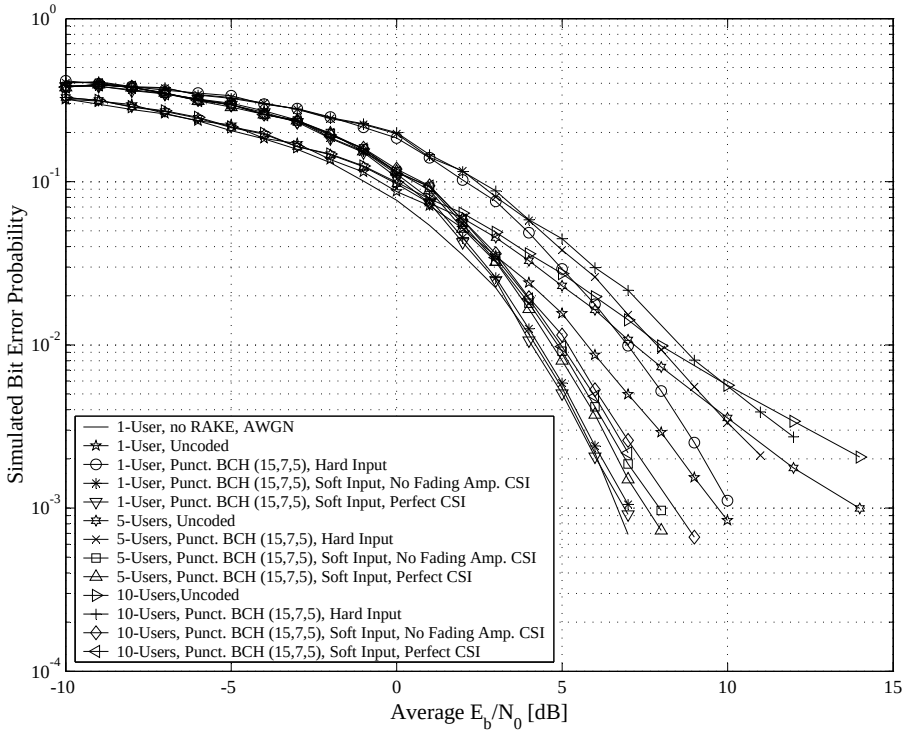

Figure 6.78: BER Performances of Punctured Binary BCH $(15, 7, 5)$ Coded Wideband Complex QPSK Communication Systems Employing QPH CSSs in Multi-User Multipath Fading Channel Conditions, $M_{seq} = 63$

- *Fig.* 6.72 demonstrates that soft decision VA decoding of the punctured binary BCH $(15, 7, 5)$ code outperforms hard decision decoding with approximately 3 dB. This result far exceeds the characteristic 2 dB gain for hard over soft decision ML decoding, characteristic with non-punctured linear block codes [47].

2. Conclusions and observations from the flat fading channel results:

   - The punctured binary BCH $(15, 7, 5)$ code exhibits an increase in flat fading channel BER performance as the Rician factor K_i increases (refer to *Fig.* 6.73 and *Fig.* 6.74). This is true for both $B_{D,i} = 33$ Hz and $B_{D,i} = 100$ Hz. On average, the punctured code performs best at the maximum Doppler spread, i.e. $B_{D,i} = 100$ Hz. Since the flat fading channel creates shorter error bursts at higher maximum Doppler spreads, the VA decoding of the punctured binary BCH $(15, 7, 5)$ code (which is not intended for burst error correction) produces better BER performance results, irrespective of the channel's Rician factor K_i.
   - Referring to *Fig.* 6.73 and *Fig.* 6.74 it is clear that the use of perfect fading amplitude CSI during the soft decision VA decoding of the punctured BCH $(15, 7, 5)$ codes resulted in relatively small gains over soft decision decoding (without any fading amplitude CSI). For both $B_{D,i} = 33$ Hz and $B_{D,i} = 100$ Hz this gain was approximately 0.15 dB when $K_i = 9$ dB. Moreover, hard decision VA decoding asymptotically lags soft decision decoding (without any fading amplitude CSI) by 1.75 dB for $B_{D,i} = 33$ Hz, and 2.25 dB for $B_{D,i} = 100$ Hz.
   - Recall from *Section* 6.5.6.2 that the puncturing profile defined by *Eq.* (6.10) was designed with the singular intention to reduce the binary BCH $(15, 7, 5)$ code's rate to that of the binary Hamming $(7, 4, 3)$ code, but still preserve its superior error correction capabilities. As was observed from the AWGN channel results, puncturing unfortunately reduced the code's effectively minimum Hamming distance, resulting in poorer BER performances. Corresponding to the observations made for AWGN channel conditions, a comparison of the simulated results presented in *Section* 6.5.3.1.2 and *Section* 6.5.6.2.2 shows that, in flat fading channel conditions, soft decision VA decoding of the two codes performed similarly. With hard decision VA decoding, however, the binary BCH $(15, 7, 5)$ codes proved to be inferior to the binary Hamming $(7, 4, 3)$ codes.

3. Conclusions and observations from the multi-user multipath fading channel results:

   - Matching *Section* 6.5.6.2.3's multi-user multipath fading BER results with that presented in *Section* 6.5.3.1.3 for VA decoded binary Hamming $(7, 4, 3)$ codes, it is clear that soft decision decoding of the binary Hamming $(7, 4, 3)$ code and the punctured binary BCH $(15, 7, 5)$ code deliver nearly the same performances, irrespective of the quality of the fading amplitude CSI employed in the metric calculations. Unfortunately, the BER performances obtained using hard decision VA decoding of the punctured binary BCH $(15, 7, 5)$ code follows the pattern observed for the AWGN and flat fading channels. At a BER of $P_b(e) = 2/1000$, for example, hard decision decoding of the punctured binary BCH $(15, 7, 5)$ code exhibits a loss of 1.5 dB in a single user CDMA system, employing DSB CE-LI-RU filtered GCL CSSs. This poor BER performance trend, observed for the hard decision VA decoding of the punctured binary BCH $(15, 7, 5)$ code, increases in severity as the user load increases, regardless of the CSS family employed.
   - On the whole, VA decoded punctured binary BCH $(15, 7, 5)$ codes, implemented on RAKE receiver-based DS/SSMA QPSK systems using ABC sequences, delivered the poorest BER performances at high user loads. QPH CSSs produced the best results, with ZC CSSs a close second. Furthermore, for the single user scenario at high $\overline{E}_b/N_0$ values, only the unfiltered

CSS families were capable of performing better or equivalent to the single user uncoded non-RAKE receiver-based DS/SSMA QPSK system, operating purely in AWGN. However, the unfiltered CSS families did come close to this AWGN curve, lagging by no more than 0.2 dB behind the unfiltered CSS families.

- Contrasting the hard and soft decision VA decoding results of *Fig.* 6.75, *Fig.* 6.76, *Fig.* 6.77 and *Fig.* 6.78, soft decision decoding (without fading amplitude CSI) gains, ranging between approximately 2.4 dB and 2.8 dB, can be observed for user loads ranging from low to high, irrespective of the CSS family. Furthermore, the inclusion of perfect fading amplitude CSI during soft decision VA decoding produces an average gain of 0.2 dB for all user loads and CSS families.

6.6 CONCLUDING REMARKS

Chapter 6 presented a culmination of simulation results that investigated, evaluated and verified the theories, algorithms, communication system building blocks, simulation platforms and VA decoded coding schemes covered in the previous chapters. Firstly, it examined the operation of the novel complex flat fading and multipath fading channel simulators, presented in *Section* 2.6.2.3 and *Section* 2.6.3.2, respectively. Next, attention shifted to the verification of the narrowband complex QPSK (see *Section* 5.2) and wideband complex DSSS/MA QPSK communication systems (see *Section* 5.3). Lastly, numerous simulated AWGN, flat fading and multi-user multipath fading channel BER performance results, obtained using *Section* 5.4's comprehensive simulation platforms, were presented and assessed for uncoded, as well as VA decoded convolutional and linear block coded narrowband and wideband communication systems. This chapter not only documents several interesting and important findings from the simulation results presented here, but it also makes a number of unique contributions. Important results presented and novel contributions made by this chapter, are listed below:

1. Measured phase and fading amplitude PDFs, as well as measured Doppler spectra, are presented in *Section* 6.2.1 for the novel complex fading channel simulator, featured in *Section* 2.6.2.3. These simulation results not only certifies the accuracy of the proposed complex flat fading channel simulator's operation, but also serves as proof of its flexibility in terms of supported fading distributions and fading rates.

2. The functioning and configurability of the unique complex multipath fading channel simulator, proposed in *Section* 2.6.3.2, are authenticated in *Section* 6.2.2 via simulated power delay profile and Doppler spread PSD measurements.

3. Simulated time signals, PSDs and eye diagrams are given in *Section* 6.3 for the unique complex QPSK transmitter and receiver models, presented in *Section* 5.2. The PSD and eye diagram results were obtained in perfect, noiseless channel conditions, whereas the simulated time signals were measured in noiseless, flat fading channel conditions. These results not only prove the optimal operation of the proposed complex QPSK system, but also validates the average fading amplitude calculation method, detailed in *Section* 5.2.3.

4. The functioning of the proposed RAKE receiver-based wideband complex DS/SSMA QPSK system, described in *Section* 5.3, is scrutinised in *Section* 6.4. Simulated PSDs for the ABC, DSB CE-LI-RU filtered GCL, ZC and QPH CSS families considered in this study (see *Appendix D*), were obtained in perfect noiseless channel conditions. These PSDs illustrate the perfect single sideband and Nyquist bandwidth-like spectral characteristics of the ABC and DSB CE-LI-RU filtered GCL CSSs, respectively. Eye diagram results (also obtained in perfect noiseless channel

conditions) for the complex DS/SSMA QPSK system, employing QPH CSSs, verify the acceptable operation of the square-root Nyquist chip-level pulse shaping filters, used at the wideband transmitter and RAKE receiver for the unfiltered CSS families. Time signal measurements, procured in noiseless multipath fading channel conditions, certify the usefulness of the average fading amplitude calculation method, proposed in *Section* 5.3.3.

5. *Chapter* 6 presented numerous simulated AWGN, flat fading and multi-user multipath fading channel BER performance results for binary NSC (see *Section* 3.2.1.3.1) and RSC (see *Section* 3.2.1.3.2) codes. These results acted mostly as baseline references for the VA decoded binary and non-binary linear block codes considered in this study. However, a number of unique contributions were made to the discipline of convolutional coding, including an investigation into the effects of perfect fading amplitude CSI on the soft decision VA decoding of convolutional codes, as well as the influence of puncturing on binary RSC codes' BER performances. The most significant contribution, however, is the BER performance results obtained for VA decoded binary convolutional codes, implemented on RAKE receiver-based wideband complex DS/SSMA systems. These results substantiate convolutional codes' effectiveness in combatting the effects of MUI and multipath fading.

6. Simulated AWGN and flat fading channel BER performance results, acquired for narrowband complex QPSK systems employing VA decoded binary Hamming $(7, 4, 3)$ and non-binary RS $(7, 5, 3)$ linear block codes (see *Section* 6.5.3.1 and *Section* 6.5.3.2, respectively), are some of the major contributions of this chapter. Even more pivotal are the simulated BER performance results obtained for these VA decoded linear block codes, running on RAKE receiver-based wideband complex DS/SSMA QPSK systems (employing the unfiltered and filtered CSS families presented in *Appendix D*) in multi-user multipath fading channel conditions. From the results obtained for the various mobile communication channel environments considered, it is evident that the application of the VA to the BCJR trellis structures of linear block codes deliver optimal ML decoding BER performances.

7. Novel simulated AWGN and flat fading channel BER performance results are presented in *Section* 6.5.4 for binary cyclic $(5, 3, 2)$ linear block codes, VA decoded using original and reduced complexity trellis structures. These results show that BCJR trellis complexity has no influence on the BER performance results obtained in AWGN conditions. However, for flat fading channel conditions, usage of the reduced complexity BCJR trellis delivered slightly weaker BER performances.

8. *Section* 6.5.5's investigation into the BER performance improvements obtained by interleaving the VA decoded binary Hamming $(7, 4, 3)$ and non-binary RS $(7, 5, 3)$ linear block codes in flat fading and multi-user multipath fading channel conditions, produced unique and valuable simulation results. From these results it can be surmised that interleaving improves the BER performances of both the binary Hamming $(7, 4, 3)$ and non-binary RS $(7, 5, 3)$ linear block codes. However, the improvements observed for the non-binary RS $(7, 5, 3)$ linear block codes were less impressive, due their inherent ability to mitigate the bursty errors typically created by fading effects in mobile communication channels.

9. *Section* 6.5.6.2 focused on the VA decoding of punctured binary BCH $(15, 7, 5)$ linear block codes in AWGN, flat fading and multi-user multipath fading channel conditions. Soft decision VA decoding of this punctured code delivered novel BER performance results comparable to the binary Hamming $(7, 4, 3)$ code (which also has a code rate of $R_c = 4/7$), irrespective of the quality of the fading amplitude CSI used during the metric calculations. Hard decision VA decoding of the punctured binary BCH $(15, 7, 5)$ code, however, did not only performed inferior to soft decision decoding, but also to hard decision VA decoding of the binary Hamming $(7, 4, 3)$ code.

10. This chapter's simulated BER performance results for binary convolutional codes, as well as binary and non-binary linear block codes, tested on narrowband and wideband communication systems in flat fading and multi-user multipath fading channel conditions, respectively, are instrumental in the determination of the influence of fading amplitude CSI during VA decoding. Of particular interest in this study, were the underlying effects of code complexity, fading rates, Rician factors, interleaving, puncturing, CDMA user loads and CSS families on the performance gains achieved through soft decision VA decoding with fading amplitude CSI.

11. Although this chapter's major contribution is undoubtable the simulated BER performances of VA decoded binary and non-binary linear block codes, operating in a wide variety of mobile channel conditions, the respective investigations of *Section* 6.5.1.3.2 and *Section* 6.5.1.3.3 into the influence of CSS selection and length on the multi-user multipath fading channel BER performances of uncoded complex DS/SSMA QPSK systems, are also pivotal. Not only was the concept of SSLD introduced (mathematically defined in *Section* D.2.6), but also a simple GCL CSS selection scheme, proposed by *Staphorst* and*Linde* in [162]. From the simulation results it is apparent that, when used in RAKE receiver-based DS/SSMA systems, ABC sequences deliver mediocre BER performances. However, for a fixed BEF (see *Section* D.2.5), ABC sequences support much higher user loads than the other CSS families considered in this study. Furthermore, it was shown that care must be taken in the selection of sequences from a ABC sequence family, since the assignment of CSSs to CDMA users has a definite impact of the overall BER performance of the system due to MUI.